CONDITION ASSESSMENT OF NATURAL ESTER OIL AND ITS NANOFLUID FILLED TRANSFORMER

A Thesis
Submitted in Partial Fulfillment of the Requirements for the Award of the Degree of

Doctor of Philosophy (PhD)

By

Niharika Baruah

Department of Electronics and Electrical Engineering
Indian Institute of Technology Guwahati
Guwahati, Assam-781039 India

July, 2021

TH-2868_156302003

Dedicated

To

my Supervisor

Dr. Sisir Kumar Nayak

for his guidance and support

My Parents

Dipti Kumar Baruah *and* ***Mirdula Kakoti Baruah***

and ***my husband Istiaque Haque***

for their Support and Love

TH-2868_156302003

Declaration

I hereby certify that the work presented in this thesis entitled '**CONDITION ASSESSMENT OF NATURAL ESTER OIL AND ITS NANOFLUID FILLED TRANSFORMER**' is entirely my own account of research performed under the guidance of Dr. Sisir Kumar Nayak. Any part of this work has not earlier been submitted for the award of any degree, diploma, associate-ship, fellowship or its equivalent to any University or Institution.

Niharika Baruah

Date: 22.07.2021

(Niharika Baruah)
Registration No. 156302003
Department of Electronics and Electrical Engineering
Indian Institute of Technology Guwahati
Guwahati – 781039, India

TH-2868_156302003

Department of Electronics and Electrical Engineering
Indian Institute of Technology Guwahati
Guwahati – 781039, India

Certificate

This is to certify that the thesis entitled "***Condition Assessment of Natural Ester Oil and its Nanofluid filled Transformer***", submitted by ***Niharika Baruah*** (156302003), a research scholar in the Department of Electronics and Electrical Engineering, Indian Institute of Technology Guwahati, for the award of the degree of Doctor of Philosophy, is a record of an original research work carried out by her under my supervision and guidance. The thesis has fulfilled all the requirements as per the regulations of the institute and in my opinion has reached the standard needed for submission. The results embodied in this thesis have not been submitted to any other University or Institute for the award of any degree or diploma.

Date: 22.07.2021

Place: Guwahati

Dr. Sisir Kumar Nayak

Associate Professor
Dept. of EEE
IIT Guwahati
Guwahati - 781 039,
Assam, India.

TH-2868_156302003

Acknowledgements

The first and foremost gratitude goes to my supervisor **Dr. Sisir Kumar Nayak** for his valuable guidance throughout the research work. I thank him for his encouragement, patience towards research and support, which enabled me to develop a better understanding of the subject leading to the presentation of this thesis. I would like to thank him for spending his precious time to discuss thoroughly on the topic and make me what I am today. I would also like to acknowledge my sincere gratitude to my doctoral committee members, **Prof. Harshal B. Nemade, Dr. Praveen Tripathy** and **Dr. Ravindranath Adda** for their advice and suggestions throughout my research work.

I also like to extend my gratitude towards the members of the Regional Testing Laboratory (RTL), Central Power Research Institute (CPRI) Guwahati especially Mr. Manas Chakraborty for the support in availing the testing facility. I also like to acknowledge Mr. Das and the members of Power Maker, EPIP, Amingaon, Guwahati Assam for providing us the raw material for the experiments failing which the experimental analysis couldn't be performed.

I am grateful to my research group members Dr. Mrutyunjay Maharana, Ms. Moon Moon Bordeori, Ms. Sujita S. Dey, Mr Rohith Sangineni, Mr. Deepak Kanumuri, Ms. Chandrima Saha, and Mr. Ambuj Kumar for their co-operative assistance and suggestions in performing experiments. I am thankful to the most important support system during my research, my friends Ms. Nupur, Mr. Abhishek Paikray, Mr. Amit Baghel, Mr. Shashank Kulkarni for their encouragement. I would also like to thank my friends Ms. Aparajita Dutta and Ms. Tanushree Paul for their support and motivation outside the lab activities and inside hostel.

I would like to thank all the faculty members, and staffs of Electronics and Electrical Engineering Department for rendering their whole hearted cooperation and support in the entire course of work. A word of appreciation goes to the senior technician and technical support staff of Mechanical Engineering Department Mr. Saiffuddin Ahmed. I am thankful to Prof. V. S. Moholkar, Head, Centre for Energy and Scientific Officer Dr. Lepakshi Barbora, Centre for Energy for their enthusiastic support for using the various apparatus.

I am grateful to SERB, DST, for providing me financial support to attend and present a technical paper in 99th Conference on Electrical Insulation and Dielectric Phenomena (CEIDP) held at Richland, Washington, USA during 20-23 October 2019. I am also thankful

TH-2868_156302003

to IEEE PES for the funding support to attend the 10th IEEE PES Asia-Pacific Power and Energy Engineering Conference 2018 (APPEEC) held at Hilton, Kota Kinabalu, Sabah, Malaysia during 7-10 October 2018.

I would like to thank my parents, Mrs. Mirdula Kakoti Baruah and Dr. Dipti Kumar Baruah for all their love, support and encouragement. I would also like to thank my husband Mr. Istiaque Haque for understanding my work schedule and encouraging me throughout the PhD journey and bearing with me during my phases of mental breakdown. I feel proud of their patience in times when I was unable to spend much time at a stretch with them during the last few years. I would like to express appreciation to my in-laws Mrs. Musfia Begum, Mr. Ohidul Haque and Ms. Tanjum Haque for their constant support and encouragement.

Lastly, I am and will always be thankful to God for guiding me through this testing period of my life. I will be grateful to Him who has destined my life to be a part of Indian Institute of Technology Guwahati.

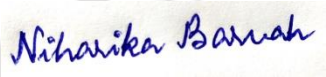

(Niharika Baruah)
Registration No. 156302003
Department of Electronics and Electrical Engineering
Indian Institute of Technology Guwahati
Guwahati – 781039, India

TH-2868_156302003

Abstract

This thesis presents the condition assessment of transformers filled with alternative dielectric fluids such as natural ester oil by evaluating the oil properties. It also presents the development of a non-edible natural ester oil (NEO) modified with nanoparticles (NPs) with enhanced physicochemical, thermal and electrical performance for transformer application.

Considering the enhanced properties of NEOs, two kinds of NEO are analyzed for the evaluation of the dissolved gases in this work, one is the Environtemp (FR3) and the other is the jatropha curcas oil (JAT). The purpose of considering JAT is its non-edible nature, thus it poses as an added advantage of using a biodegradable substitute to the conventional mineral oil (MO). The ageing study is essential to understand the behaviour of insulating oil under thermal stress. The dissolved gas analysis (DGA) helps in monitoring the emission pattern of gases when the oil is subjected to stress for a longer duration. Both the oils were subjected to thermal stress in a sealed beaker setup at 150^{o}C for 500, 1000, 1500 and 2000 hours. The different gases generated, such as methane (CH_4), hydrogen (H_2), ethane (C_2H_6), ethylene (C_2H_4), carbon monoxide (CO), carbon dioxide (CO_2) and acetylene (C_2H_2) are analyzed and compared for both types of oils. Fourier-transform infrared spectroscopy (FTIR) and Nuclear magnetic resonance (NMR) analyses are implemented before and after ageing, to observe the alterations in the chemical structure. The classic Duval triangle, Dornenburg ratio, Rogers ratio and IEC method were applied to ascertain the type of incipient faults. A comparative analysis is done between the two oils to understand the behaviour of the oils at accelerated thermal ageing for longer durations. The total dissolved combustible gases (TDCG) of the oils are done to examine the composition of combustible gases evolved after 2000 hours of ageing. Thus, the investigation of the dissolved gases in the NEOs will establish a good indicator of the types of faults the oils can sustain.

Further, continuing with the analyses, study of the ageing characteristics of the NEO is done by the frequency domain spectroscopy (FDS), which is a non-invasive offline measurement technique. The NEO considered is the JAT from the earlier study. The FDS method is used to analyze the characteristics of the oil by obtaining the complex permittivity and dielectric dissipation factor (tan δ) over a wide range of frequencies. The JAT is reported to possess superior dielectric properties. However, the ageing behaviour of this oil with open beaker under thermal stress is not reported. The oil is subjected to thermal stress in an open beaker ageing test setup at 115^{o}C for up to 500 hours, and samples are taken out at intervals

TH-2868_156302003

of 100 hours for testing. The FTIR and ultraviolet visible (UV-Vis) spectroscopy analyses are implemented to observe the alterations in the structure of the oil samples. The FTIR results showed the composition of the oil to be intact even after 500 hours of ageing, as there is no significant change in the spectra. By analyzing the UV spectra, it is observed that the oil samples showed a red shift in the spectra with increasing ageing duration and thus the samples are identified accordingly. The FDS results show how the permittivity and tan δ of the JAT increases with ageing duration towards the lower frequency range. This shows the formation of polar contaminants which hampers the condition of the oil. The statistical technique of regression modeling is used to determine the variation of the dielectric parameters with respect to ageing duration at different decades of the frequency range and an expression relating all three parameters such as frequency, ageing duration and dielectric parameters is developed.

The temperature dependence on the FDS characteristics of the dielectric liquids is also an important aspect to be studied; hence a comparative analysis is carried out to understand how the dielectric properties vary with changing temperature and frequencies. In this case, the semi-conductive titanium oxide (TiO_2) nanoparticle (NP) is considered along with MO and FR3 as base fluids. The FDS response of TiO_2 based NFs is studied in the frequency range of 10^{-3} to 10^{4} Hz and the temperature range varies from 30 to 90^{o}C with an interval of 15^{o}C between two successive temperatures. The Cole-Cole double relaxation model is used to ascertain the number of relaxations in the samples. The parameters of the Cole-Cole model are estimated by means of the least square technique to obtain the best fit of the measured real and imaginary parts of relative permittivity (ε_r' and ε_r''). The ε_r', ε_r'' and tan δ obtained from the FDS are compared for all the oil samples-MO, FR3, MO-NF and FR3-NF. Based on the experimental results, low frequency dispersion of the oils is investigated to obtain an insight into the integrity of the oil samples. It is observed that the conductivity increases with increase in temperature for all the oil samples. A predictive analysis model is proposed using ML algorithms DTR and KNN, to predict the dielectric properties like ε_r', ε_r'' and tan δ of all the oil samples considering its dielectric response using the FDS.

Further to understand the breakdown probability of the fresh and aged NEO and NEO-NFs, statistical analysis is carried out in this work. The open beaker oxidative ageing technique is considered to comprehend the process of degradation. The information of AC breakdown voltage (ACBDV) is very essential for any insulation system, which depends on many attributes like moisture content, contaminations present as well as on the electrodes

TH-2868_156302003

arrangement. Since the breakdown is a random occurrence, it is required to examine the reproducibility of experimental data on an adequate number of tests. In this work ACBDV tests are performed for all the samples: NEO, NEO-NF, aged NEO and aged NEO-NF and a comparative examination is done among them to estimate the behaviour of the new and aged oils. A concentration of 0.01wt% of TiO_2 is selected to prepare the NFs for ageing. To understand the statistical behaviour of the ACBDV of the oil samples, normal, 2-parameter Weibull and 3-parameter Weibull distributions are considered. To confirm whether these distributions really belong to a specific distribution, hypothesis testing with Shapiro-Wilk test and Anderson-Darling test is used. This is a powerful technique to ascertain if the distribution of experimental data follows a theoretical distribution. The goodness of fit is used to measure how well the data fits a specified distribution. The correlation coefficients are chosen to analyze the goodness of fit which shows that all the 4 datasets follow a 3-parameter Weibull distribution quite well.

As NEOs are being advocated for usage in transformer applications, a new NEO is developed in this work known as the Pongamia pinnata oil (PPO). The crude PPO is modified by the transesterification process and converted to pongamia oil methyl ester (POME) as the crude oil is not suitable for direct use because of its high viscosity, high pour point and acid number. To enhance the properties further, a part of the study is also done considering the NFs prepared with the base fluids using an insulating NP. Due to the extraordinary thermal and insulating properties of the hexagonal boron nitride (h-BN) NP, it is selected as the NP to be dispersed in the oils to prepare the NFs. The bulk h-BN NP of size 1 μm is exfoliated into 2-D nanosheets of size 50-100 nm subsequently enhancing the surface area of exfoliated h-BN (Eh-BN). The Eh-BN nanosheets are homogeneously dispersed in both MO and POME at 30^{o}C using probe sonication for an hour. A dispersion stability of 0.01wt.% Eh-BN in base fluid is observed from previous studies and hence this concentration is chosen for further analysis. The charging dynamics study has also been investigated to understand the phenomenon underlying the enhanced breakdown voltages of NEO based NFs. This work also explores the various thermophysical properties such as viscosity, thermal conductivity, interfacial tension (IFT), flash point, pour point, and electrical properties such as ACBDV, tan δ, permittivity of NFs and compared them to the base fluids and they are observed to be superior. The results of the POME are also compared with two more NEOs, one is the FR3 and the other is JAT and the POME shows comparable results and thus may be used as a potential substitute to MO for transformer application.

TH-2868_156302003

Table of Contents

TH-2868_156302003

TH-2868_156302003

TH-2868_156302003

TH-2868_156302003

List of Figures

TH-2868_156302003

TH-2868_156302003

भारतीय प्रौद्योगिकी संस्थान गुवाहाटी • Indian Institute of Technology Guwahati •

TH-2868_156302003

List of Tables

TH-2868_156302003

TH-2868_156302003

List of Acronyms

ACBDV	AC breakdown voltage
AlN	Aluminium nitride
Al_2O_3	Aluminium oxide
CC	Correlation coefficient
$CDCl_3$	Deuterated chloroform
CH_4	Methane
C_2H_6	Ethane
C_2H_4	Ethylene
C_2H_2	Acetylene
C_3H_6	Propylene
C_3H_8	Propane
CM	Clausius-Mossotti
CO	Carbon dioxide
CO_2	Carbon monoxide
COD	Coefficient of determination
CTAB	Cetyltrimethylammonium bromide
CuO	Copper oxide
DDF	Dielectric dissipation factor
DGA	Dissolved gas analysis
DTR	Decision tree regression
EDL	Electrical double layer
Eh-BN	Exfoliated hexagonal boron nitride
FAME	Fatty acid methyl ester

TH-2868_156302003

FDS	Frequency domain spectroscopy
Fe_3O_4	Iron oxide
FFA	Free fatty acid
FR3	Environtemp FR3 fluid
FTIR	Fourier transform infrared
GA	Genetic algorithm
GC	Gas chromatograph
GCMS	Gas chromatography and mass spectrometry
H_2	Hydrogen
h-BN	Hexagonal boron nitride
HV	High voltage
IFT	Interfacial tension
JAT	Jatropha Curcas Oil
KNN	K-nearest neighbour
KOH	Potassium hydroxide
kV	Kilovolts
MG	Maxwell-Garnett
ML	Machine learning
MO	Mineral oil
MOR	Multi-output regression
ND	Not determined
NEO	Non-edible ester oil
NF	Nanofluid
NMR	Nuclear magnetic resonance
NP	Nanoparticle

TH-2868_156302003

PD	Partial discharge
PDC	Polarization and depolarization current
PDIV	Partial discharge inception voltage
PPO	Pongamia pinnata oil
POME	Pongamia oil methyl ester
ppm	Parts per million
RSS	Residual sum of squares
RVM	Return voltage measurement
SE	Synthetic ester
SiO_2	Silica
SGO	Stray gassing of oil
SNN	Supervised neural network
SVM	Support vector machine
TAN	Total acid number
TDCG	Total dissolved combustible gases
TDS	Time domain spectroscopy
TEM	Transmission electron microscopy
TGC	Total gas content
TiO_2	Titanium oxide
TO	Transformer oil
UV-Vis	Ultra violet visible
VO	Vegetable oil
VO-NF	Vegetable oil nanofluid

TH-2868_156302003

List of Symbols

q	*Charge*
d	*Distance between charges in a dipole*
α_0	*Polarizability*
$\boldsymbol{P}$	*Polarization vector*
$\boldsymbol{E}$	*Electric field vector*
$\boldsymbol{D}$	*Electric displacement vector*
χ	*Electric susceptibility*
ε_0	*Permittivity of free space*
ε_r	*Relative permittivity*
ε'_r	*Real part of relative permittivity*
ε''_r	*Imaginary part of relative permittivity*
ω	*Angular frequency*
$\tan\delta$	*Dielectric dissipation factor*
Ak	*Percentage concentration of CH_4, C_2H_4, C_2H_2 in Duval's triangle*
m_k	*Gas concentration in ppm*
b_0	*Intercept of a polynomial equation*
b_1	*1^{st} coefficient of a polynomial equation*
b_2	*2^{nd} coefficient of a polynomial equation*
b_3	*3^{rd} coefficient of a polynomial equation*
b_4	*4^{th} coefficient of a polynomial equation*
x	*Independent variable*
y	*Dependent variable*
R^2	*Coefficient of determination*
I_c	*Conduction current*
I_d	*Displacement current*
V	*Voltage*
Abs	*Absorbance*
I_0	*Incident light intensity*
I_t	*Transmitted light intensity*

TH-2868_156302003

c	*Concentration of the sample*
L	*Length of the cuvette*
ε_{abs}	*Molar absorptivity*
A_k	*Constant*
p_k	*Constant*
q_k	*Constant*
C_k	*Constant*
f	*Frequency*
ε_∞	*High frequency permittivity*
A	*Parameter of inverse power law*
n	*Parameter of inverse power law*
$\Delta\varepsilon_1$	*Relaxation amplitude of first relaxation*
$\Delta\varepsilon_2$	*Relaxation amplitude of second relaxation*
τ_1	*Time constant of first relaxation*
τ_2	*Time constant of second relaxation*
α_1	*Spread of first relaxation*
α_2	*Spread of second relaxation*
σ_{dc}	*DC conductivity*
σ_0	*Conductivity constant*
E_a	*Activation energy*
T	*Temperature in kelvin*
N_{ML}	*Number of classes in decision tree*
E_n	*Entropy*
p_i	*Probability of class i*
IG	*Information gain*
w_i	*Weights attached to each class*
Var	*Variance of a dataset*
$d(u, v)$	*Euclidean distance between two points*
W	*Shapiro-Wilk test statistic*
c_i	*Constant in Shapiro-Wilk equation*
y_i	*Data values in Shapiro-Wilk equation*
H_o	*Null hypothesis*
H_A	*Alternate hypothesis*

TH-2868_156302003

AD	*Anderson-Darling test statistic*
x_i	*i^{th} value in a dataset*
N	*Number of sample size*
$F(x)$	*Cumulative distribution function*
S	*Skewness*
K	*Kurtosis*
$\bar{x}$	*Average value*
s	*Sample standard deviation*
α	*Scale parameter in Weibull distribution*
β	*Shape parameter in Weibull distribution*
γ	*Location parameter in Weibull distribution*
ρ	*Correlation coefficient*
α_s	*Significance level*
E_r	*Radial component of electric field in the oil outside the NP*
R	*Radius of NP*
$Q(t)$	*Deposited charge on the NP w.r.t time*
Q_s	*Saturation charge*
ε_1	*Permittivity of base oil*
ε_2	*Permittivity of NP*
ε_{r1}	*Relative permittivity of base oil*
ε_{r2}	*Relative permittivity of NP*
σ_1	*Conductivity of oil*
σ_2	*Conductivity of NP*
τ_r	*Relaxation time constant of NP*
τ_{pc}	*Charging time constant of NP*
ρ_e	*Electron charge density*
μ_e	*Electron mobility*
ε_{nf}	*Permittivity of NF*
φ	*Volume fraction of the dispersed nanoparticles*
K	*Thermal conductivity*
q_t	*Heat flow per unit length*
θ_c	*Critical angle*
J_r	*Current density*

TH-2868_156302003

N_e	*Number of electrons*
N_{np}	*Number of NPs*
α_{01}	*Polarizability of the oil molecule*
α_{02}	*Polarizability caused by inner polarization of the NP*
α_{03}	*Orientational polarizability of the NP*
N_1	*Number of oil molecules*
N_2	*Number of polarized NPs in oil*
Q_+	*Positive charge in a dipole*
μ_c	*Electric dipole moment*
E_i	*Electric field inside NP*
P_i	*Polarization vector inside NP*
μ_i	*Vector sum of electric dipole moment inside the NP*
Vol	*Volume of NP*
k	*Boltzmann constant*
T_1	*Temperature of heat source at time* t_1
T_2	*Temperature of heat source at time* t_2
U_{c1}	*Measurement uncertainty of ACBDV and thermal conductivity*
U_{c2}	*Measurement uncertainty of dielectric constant*

TH-2868_156302003

TH-2868_156302003

1

Introduction

Contents

TH-2868_156302003

1.1 Introduction

Transformer is a critical high voltage (HV) apparatus in a power system network and its reliability is crucial to the continuity of the power supply. Among the various functional systems in a transformer, the insulation system is the weakest. During its operational lifetime, the insulation system is subjected to multiple stresses such as electrical, mechanical, chemical and thermal stresses simultaneously. The insulation system comprises both solid and liquid insulation and is susceptible to degradation due to factors such as hot spots, moisture, partial discharge, arcing and electromechanical forces on the winding. A transformer shutdown process for the repair and replacement of the solid insulation system is highly undesirable as it causes major disruption to the power supply and should therefore be minimized. Hence, efforts are needed to identify the factors that cause the ageing of the insulation system and initiate corrective actions without needing a shutdown.

Solid insulation, which is mainly composed of cellulose ages fast in the presence of heat and moisture. The liquid insulation, which mainly comprises of mineral oil (MO), is used as coolant, impregnant and insulant and it plays a crucial role in the proper functioning of the whole transformer. The higher the thermal conductivity of oil, the lower will be the temperature rise on cellulose. Cellulose is hygroscopic and holds much more water than oil. The moisture equilibrium between oil and cellulose needs to be altered such that the oil can take away more moisture from the cellulose during a temperature rise, and thus the cellulose ageing will be lower [1]. The degradation of the oil not only affects its insulation strength but also that of cellulose. MO impregnated cellulosic kraft paper, in the presence of heat for a certain period of time generates aged byproducts such as dangerous acids, oxides, and peroxides in the oil. These ageing byproducts actively take part in the formation of sludge and solid wax which deposits in the winding and bottom of the transformer tank which is highly undesirable.

The MO which is used conventionally as an insulating liquid in transformer has a few drawbacks like low flash point, poor biodegradability and lower breakdown strength. Also, the moisture retention capacity of MO is lower, so it is difficult to keep the solid insulation dry as MO is not able to capture much moisture from the solid insulation. To mitigate the drawbacks of the MO, an alternative with improved thermal conductivity, moisture absorption from cellulose, high dielectric strength and flash point needs to be explored and developed. The use of natural ester oil (NEO) as an insulating fluid in transformers is gaining much significance, owing to many advantages, like, higher biodegradability, flash point and

TH-2868_156302003

breakdown voltage [2, 3, 4]. Studies are conducted to use vegetable seed-based NEOs as they are environment-friendly and have enhanced dielectric properties. The observed thermal, physicochemical and electrical properties of the MO-based TO are inferior to other alternatives [5-7]. Hence, oils with higher flash point and breakdown voltage are required to be developed in order to avoid any accidental fire or electrical breakdown. This leads researchers to make more developments to use NEO in high voltage apparatus. The timeline in the evolution of transformer insulating fluids is given in Figure 1.1.

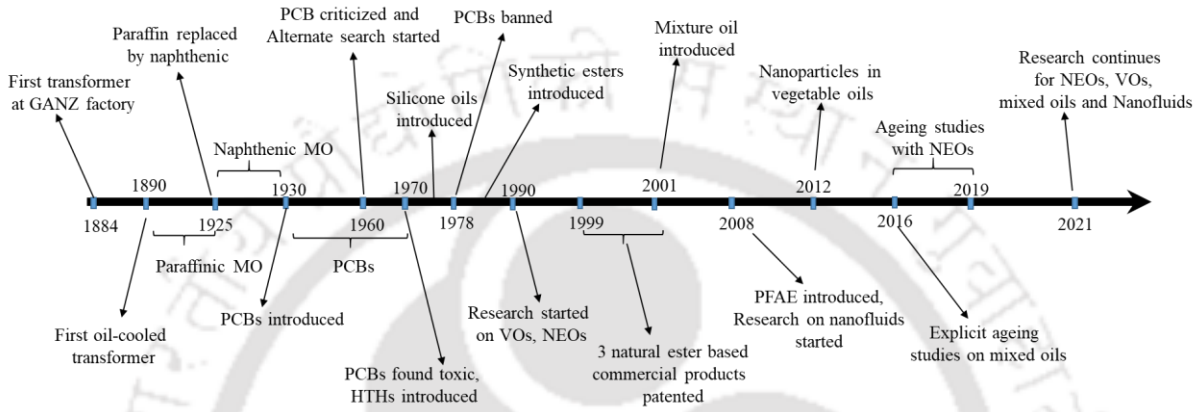

Figure 1.1: Evolution of transformer insulating fluids.

1.2 Literature survey

1.2.1 Alternative dielectric liquids

Since the ever-growing alertness on environmental safety and biodegradability, it has become necessary to look for a sustainable and environment-friendly dielectric fluid with higher heat transfer, fire resistance and insulating characteristics. Low biodegradability, low fire resistance and the limited available resources of petroleum crude have motivated the researchers to explore sustainable alternative transformer oil (TO) with modified characteristics. Therefore, the study has moved into the next level to replace the non-renewable petroleum resources based TO with renewable and naturally occurring vegetable oil (VO) as a liquid dielectric for transformer application. The VO based TO, being a potential liquid dielectric, the researchers are keenly focusing on its application for the transformer. Moreover, the transformer industries like ABB (Hitachi Energy) and Siemens have already implemented the VO based liquid dielectric for transformer application [8, 9]. The VO such as BIOTEMP from sunflower and ENVIROTEMP from soybean are extensively used as TO [10]. The AC breakdown voltage (ACBDV) and fire resistance properties are the main thrust of their study. However, all the physicochemical properties and

TH-2868_156302003

thermal conductivity of the VO are not investigated [11-15]. Therefore, the physicochemical and heat transfer performance of the VO requires special attention. The main component of VOs is triacylglycerol which constitutes 98% of the total and the rest are fatty acid molecules linked to a single glycerol arrangement. The remaining constituents of VOs consist of free fatty acids, diglycerols, tocopherols and sterols, which are lesser in quantity. The triglyceride configuration is formed by condensation of three hydroxyl groups with carboxyl groups of three fatty acids, as shown in Figure 1.2.

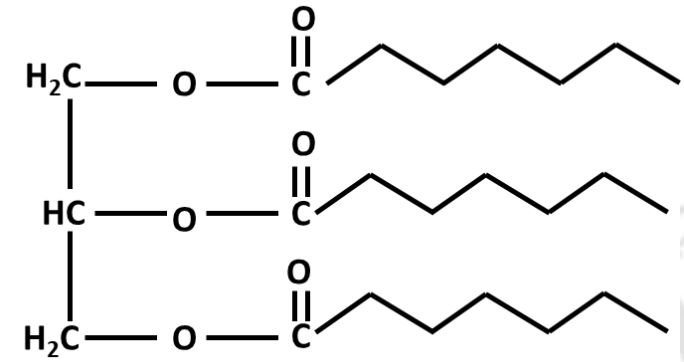

Figure 1.2: Triglyceride structure.

The structure of triglyceride makes the VO highly viscous because of its high molecular weight. The typical fatty acid contents of some VOs are given in Table 1.1. There are three types of fatty acids-saturated, mono-unsaturated and poly-unsaturated. In a fatty acid chain, if there are only single bonds between neighboring carbons in the hydrocarbon chain, the fatty acid is said to be saturated. The difference between saturated and unsaturated fatty acid is the content of C=C double bonds. Saturated fatty acids does not contain C=C double bonds. But the unsaturated fatty acids have either one or more C=C double bonds. Oxidation is a process between molecules of unsaturated fatty acids and oxygen. The weak spot is the C=C double bond in unsaturated fatty acids. The oxidation is a slow process but can be accelerated by the presence of contaminants and temperature. Generally, the percentage of unsaturated fatty acid is higher in case of NEO which makes it more prone to oxidation. Thus, having lower percentage of unsaturated acids makes oil more oxidation stable. The viscous character of the NEOs is also because of the unsaturated fatty acids [16].

There are many sources available for the production of VO e.g. rapeseed, palm kernel, colona, sunflower, soybean etc. The careful processing of the crude VO yields the suitable NEO and it is the potential candidate for TO. Since the oil requirement for the transformers is huge, to meet the requirement of ester oil, edible food crops are being used to extract the oil for the transformer which is likely to cause food crises in the future [17]. Therefore, an

TH-2868_156302003

investigation is needed to be carried out to evaluate the possible implementation of non-food crop oil as a dielectric fluid for the transformer. Hence, it is required to study the option left with the nonedible VO and its application as TO in the context of thermophysical and electrical characteristics.

Table 1.1: Typical fatty acid composition of some vegetable oils [2, 18-20].

Vegetable Oil	Saturated Fatty Acids %	Unsaturated Fatty Acids %		
		Mono-	Di-	Tri-
Rapeseed/Canola oil	7.9	55.9	22.1	11.1
Corn oil	12.7	24.2	58	0.7
Cottonseed oil	25.8	17.8	51.8	0.2
Peanut oil	13.6	17.8	51.8	0.2
Olive oil	13.2	73.3	7.9	0.6
Safflower oil	8.5	12.1	74.1	0.4
Safflower oil, high oleic	6.1	75.3	14.2	-
Soybean oil	14.2	22.5	51	6.8
Sunflower oil	10.5	19.6	65.7	-
Jatropha curcas oil	19.1	46	34.9	
Rice oil	12.4	15.9	71.7	
Pongamia oil	13.76	60	23	
Neem oil	40	20.9	39.1	
Mustard oil	12.9	64.5	22.6	
Punna oil	39	58.9	2.1	
Castor oil	1.1	97.8	1.1	

Researchers have compared NEO and MO and observed that natural ester proves as fire safe with high fire point ("K" class liquid). Water saturation limits of the natural ester being very high can hold more water. Also, due to its the hygroscopic nature, water remains in liquid instead of migrating to solid insulation which extends the life of the solid insulation. They also observed that the breakdown strength of natural ester is better than MO for a smaller gap. However, for a larger gap, breakdown voltage decreases for natural ester [21]. Breakdown strength analysis was conducted by considering three different MOs (MO3, MO4 and MO5), one synthetic ester (SE1) and three different natural esters (VO2, VO3 and VO4).

TH-2868_156302003

They observed that the measured BDV data follow better normal than Weibull distribution. Basing on the BDV at the levels of risk 1, 10 and 50% probability, the dielectric withstand capacity of ester oils, under AC, homogeneous field and a small gap is slightly better compared to MOs [22]. Experiments have been conducted with BN nanoparticles (NPs) in VO and it was observed that thermal conductivity improves when nanofluids (NF) is compared with VO. Also, the dissipation factor and electrical conductivity are lower, which are essential for better performance of the insulating medium. The breakdown property is also enhanced with BN NPs [23]. The non-edible jatropha extracted from the fruit seeds of jatropha curcas plants was studied and it is found as a potential substitute for MO. They observed that the streamer characteristics namely the shape of the streamers, their stopping length, the associated current and electrical charge in jatropha curcas methyl ester oil and MO are similar. Basing on these results, one can conclude that jatropha curcas methyl ester oil could constitute a potential substitute for MO for electrical insulation and especially in high voltage power transformers [24]. MO, synthetic ester oil and NEO were compared and it was observed that the stopping lengths are longer and the conductivity higher when the point is positive than when it is negative. The stopping length is generally longer in ester oils (natural and synthetic) than in some MOs. When the point is negative, stopping length can be ten times higher in ester oils than in mineral ones [25]. A very few researches have also been carried out in the field of thermophysical and electrical properties of the VO based TO for the replacement of MO [26-29]. But enough attention is not given to the applicability of nonedible VO as an insulant and coolant. Very few non-food seeds such as jatropha curcas, neem, mahua, pongamia etc. are available for the extraction of nonedible VO. However, a limited study on AC, DC and impulse BDV is carried out on the jatropha curcas oil. The streamer propagation is studied for the jatropha curcas methyl ester [17, 24]. But the research did not reveal the response of heat transfer and other allied physicochemical and electrical properties of the nonedible VO.

1.2.2 Dissolved gas analysis (DGA) of oils

Faults in the power system network are inevitable, but monitoring them can prevent any catastrophic occurrence. Thermal and electrical faults are the two main types of faults occurring in the transformers, so it is very much crucial to gauge the state of the transformer at regular intervals of time [30, 31]. Dissolved gas analysis (DGA) is a very important tool in condition monitoring of a transformer in case of incipient faults. The faults occurring in a transformer may cause the insulation to breakdown, thereby releasing some gases which

TH-2868_156302003

dissolve in the fluid. Many types of faults occur in the transformer, such as thermal faults, corona or partial discharge (PD) and arcing. Arcing causes the utmost damage to the insulation. The major gases evolving in the transformer as a result of fault and ageing are: (i) hydrogen and hydrocarbons- Hydrogen (H_2), Methane (CH_4), Ethane (C_2H_6), Ethylene (C_2H_4), Acetylene (C_2H_2) (ii) Carbon oxides- Carbon monoxide (CO) and Carbon dioxide (CO_2) and (iii) Propane (C_3H_8) and Propylene (C_3H_6) [32, 33]. All of these gases are produced when the temperature rises and also the concentration levels change with temperature and duration of stress. Detecting the individual concentration and applying the various standard methods can help to identify the incipient faults that might occur inside the transformer.

The DGA process is divided into 4 steps in general,

i. collect oil sample,
ii. extract dissolved gas,
iii. gas chromatograph measurement
iv. data interpretation.

The oil samples are collected based on the IEC 60567 which recommends the procedure for taking out oil from the transformer [143]. The extraction of the dissolved gas from the oil sample is carried out by the traditional vacuum method or the alternative vacuum pump method such as headspace and stripper methods which are available in IEC 60567. For the detection of gases, the gas chromatograph (GC) is used which separates and analyses the different gas components. The last step is to interpret the transformer insulation conditions using the data generated from the GC. The international standards IEC 60599 [144] and IEEE C57.104 [145] provide many diagnostic tools for DGA results. The interpretation methods are all developed based on the known transformer fault data, thus they may not give suitable results for some cases, like the application of new ester liquids. IEEE C57.104 is mainly dedicated to MO whereas the standard IEEE C57.155 [146], which is newly introduced in 2014, is dedicated to ester oils.

The interpretation schemes are generally based on defined principles such as gas concentrations, key gases, key gas ratios, and graphical representations. The DGA method distinguishes faults such as partial discharge (corona), overheating and arcing in many different power transformers. DGA can provide the early diagnosis needed to increase the chance of finding an appropriate cure. The different methods mentioned in IEEE Standard

TH-2868_156302003

C57.104-2008 available for analyzing dissolved gas data to diagnosis fault type are given below:

i. Key gas method
ii. Dornenburg ratio method
iii. Rogers ratio method
iv. Nomograph method
v. IEC ratio method
vi. Duval triangle method
vii. Duval pentagon method
viii. CIGRE method.

Transformers generally use the MO as the insulating fluid along with solid insulation like kraft papers and pressboards. The introduction of NEOs in this area leads to a complete ecological solution. MO has some disadvantages as it is extracted from fossil fuels which are going to exhaust in the remote future. Moreover, MO is very poorly biodegradable, so if the oil spills accidentally, there is a concern for environmental hazard. Alternatively, NEOs considered to be used as insulating agents in transformers, are gaining importance because of the better biodegradability, environment-friendly nature, higher flash and fire points [34]. This is very much necessary from a fire safety viewpoint [35]. NEOs also have higher water retention capacity than MO as the oxygen atoms present in the ester group (COOR) bonds with the hydrogen atoms of water molecules. Thus the dielectric integrity of esters is not affected much by the presence of moisture. When NEOs are used with cellulosic solid insulation, the cellulose remains dry and the degradation rate of cellulose is lesser than in MO [36]. DGA has been used for many years as an effective and reliable tool to detect incipient faults in MO-filled transformers. Therefore, it is important to confirm that traditional DGA techniques can be used if alternative oils are used in transformers.

The two main types of faults occurring in a transformer are electrical and thermal faults. As per IEC 60599, the thermal faults are defined in three different temperature ranges, T1 indicates temperatures <300ºC, T2 indicates temperatures >300ºC (T2) and T3 indicates temperatures >700ºC. The electrical faults are identified as partial discharges (PD), low energy discharges (D1), and high energy discharges (D2). The triangular graphical method known as Duval triangle uses the concentrations of CH_4, C_2H_4, and C_2H_2 as percentages of the total concentration of the three gases and plotted as a point in a triangular chart which has been subdivided into fault zones to identify the likely fault type. The IEEE key gas method

TH-2868_156302003

identifies the key gas for each fault type by considering the highest percentage of this gas to the other gases. The low-intensity PD or corona generates primarily H_2, arcing produces C_2H_2, overheating of the oil leads to the formation of C_2H_4 and overheated cellulose produces CO [37]. The major fault indicator gases are presented in Table 1.2.

Table 1.2: Fault indicator gases [37].

Fault gases	Primary indicator	Secondary indicator
CH_4		Corona, arcing, and overheating
H_2	Corona	Arcing and overheating
C_2H_2	Arcing	Severely overheated oil
C_2H_6		Corona and overheating
C_2H_4	Overheating in oil	Corona, arcing
CO	Overheated cellulose	Arcing if the fault involves cellulose
CO_2		Overheated cellulose, arcing if the fault involves cellulose
O_2		Indicator of system leaks, over-pressurization, or changes in pressure or temperature.
N_2		Indicator of system leaks, over-pressurization, or changes in pressure or temperature.

TDCG: The total concentration of the six combustible gases (H_2, CH_4, C_2H_2, C_2H_4, C_2H_6, CO) in ppm.

Studies have shown that while comparing the three diagnostic methods key gas, IEC and Duval triangle on three different types of oil: MO, synthetic ester and natural ester, under electrical and thermal tests, it is observed that IEC methods and Duval triangle are more applicable than the IEEE key gas method. Esters have the same fault gases like in MO but to produce the precise fault diagnosis of the NEOs, the conditions of fault gas ratio or percentage needs to be modified [37].

Perrier et.al studied and observed that for electrical faults and especially for low energy discharges, the same gases H_2 and C_2H_2 are generated in esters and MO in relatively the same amounts. They also confirmed that Duval's triangle 1 is well applicable for this type of fault confirming thus the results reported in the literature. For thermal faults and especially for stray gassing issue (low thermal faults), C_2H_6 (associated with H_2) constitutes the key gas

TH-2868_156302003

of NEOs. The new Duval's triangles 4 and 6 match the faults better in this case and can be applied for MO and NEOs respectively [38].

The oil-paper interaction shows enhanced characteristics when VO replaces MO. VO has superior performance as an insulating fluid with enhanced heat transfer characteristics [9, 18]. Many DGA studies have been conducted considering MO and other types of natural and synthetic esters. The molecular structure of NEOs is dissimilar to the MO however; the gases produced under electrical and thermal faults are similar for both oils. The gas generation rate in esters is lesser when compared to MO. However, FR3 has produced a substantial amount of C_2H_6 in case of thermal faults, signifying that this should be used as a key indicator of thermal faults. The thermal tests also confirm that CO and CO_2 are the key indicators of cellulose degradation in both MO and esters [37]. For the electrical faults, C_2H_2 is the key fault gas observed for low energy discharges, and H_2 is the key fault indicating gas for partial discharges. There is also less gas generation in esters when compared to that evolved by MO [37]. Many types of researches have been conducted with varied types of vegetable seed-based oils to be used as insulating fluid [38-41]. A few works suggest jatropha curcas oil (JAT) as a potential insulating fluid [17, 24, 42]. However, the ageing behaviour and long term performance of the oil is not reported which is the main area of focus in this work.

1.2.3 Frequency domain spectroscopy (FDS)

The power transformers form an integral component of any efficient power system network. The insulation system in a transformer is highly stressed during its lifetime because of the thermal, electrical and chemical factors. The dielectric liquid, which forms the backbone of the transformer, performs a dual task of insulation as well as heat dissipation. And this is the part that undergoes maximum stress with increasing moisture and elevated temperatures. The ageing of the transformer occurs majorly due to the degradation of the insulation. The byproducts, which are generated in the oil, are water and substances which are partly polarizable and ionizable. The life of cellulosic insulation is calculated to be 10 years when the operating temperature is 110^{o}C [44]. However, at lower operating temperatures, the life span increases. The ageing process is significantly influenced by the moisture content, thermal stress, and type of cellulose and the acidity level of the insulating liquid. In addition to ageing, failures also occur when electrical discharges arise in the insulation. Various dipole groups present in the oil-paper insulation behave differently under the influence of an external electric field [45]. The dependence of moisture solubility of TO on temperature and the

TH-2868_156302003

existence of a large number of equilibrium curves make it difficult to analyze the condition of transformer insulation using oil-moisture content alone. As a result, assessment of insulation condition based on oil-moisture may lead to erroneous results. It is not possible to perform any invasive test on a working power transformer and hence non-invasive techniques are important. Further, it is reported that in recent years most of the researchers and utilities are interested in developing various non-invasive methods, which are capable of providing reliable results related to the condition of the insulation [26]. Recent researchers have used dielectric response measurements extensively because of their simplicity and ability to provide a large amount of information regarding the condition of the insulation [45, 46]. As per available literatures, the time domain spectroscopy (TDS) and the frequency domain spectroscopy (FDS) data analysis are among the preferred techniques for researchers and utilities. These dielectric spectroscopy techniques are dependent on how the relaxation characteristics of dipole groups change with time. The dielectric response analysis is a significant basis for the health assessment of the insulation of the transformer. The time-domain analysis consists of the polarization and depolarization current (PDC) and recovery voltage measurement (RVM). The frequency domain analysis consists of the tanδ measurement or FDS. For condition monitoring of the insulating liquids, many researchers have studied the partial discharge (PD) measurements and some non-invasive measurements. However, the PD measurements are not very accurate as they are affected by high frequency noises, so non-invasive methods like PDC and FDS techniques are preferred by the utilities. The PDC measurements are influenced by noise and interference and thus the estimation of parameters may not be accurate. Also, the time required for measuring both polarization and depolarization currents is high. Thus, the FDS is considered in this work, which is a non-invasive offline measurement technique as it provides an insight into the variation of the dielectric properties over a wide range of frequencies. The alignment of the dipoles as well as the movement of the electrons in a dielectric under electric field is a very slow process and active in lower frequency range. Therefore, to get a clear picture, the FDS is performed at very low frequencies.

Depending on the nature of the material, the polarization will vary and so will the polarizability. The permanent dipole is formed because of the interactions between dissimilar atoms in a molecule. The dipoles are randomly oriented within the dielectric, when there is no external field. The dielectric polarization results because of the orientation of both types of charges in the material, on the application of an electric field. The charges are confined

TH-2868_156302003

within the material, so there is no probability of inherent conduction. The dielectric response methods are used to study the interactions between the fundamental electric quantities [46].

The S-shaped curve typically defines the characteristic of the insulation system. The low value of tan δ indicates the proper health of the insulation system. The effects of rise in moisture content or weakening of the insulation due to ageing are observed significantly at very low frequencies typically in the range of 10^{-4} to 10^{-3} Hz in terms of increase in tan δ. These effects of ageing and moisture content in paper are also seen around 10^{2} to 10^{3} Hz at higher frequency regions. The insulation geometry effects are seen in the frequency range between 10^{-3} Hz to 10^{-1} Hz. The middle part of the curve in the range between 10^{-1} Hz to 10^{2} Hz signifies the oil characteristics. This region is affected by the changes in conductivity of the oil.

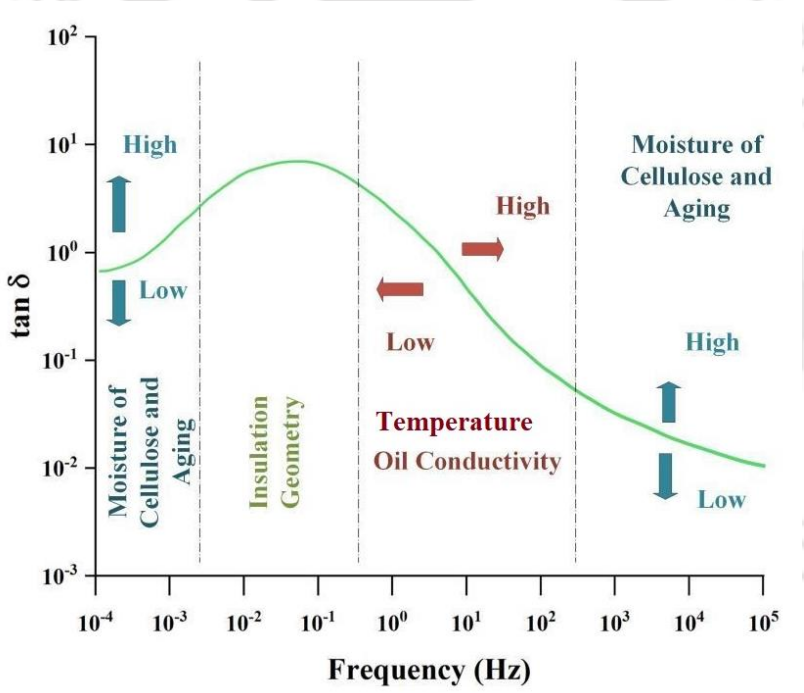

Figure 1.3: S-shaped curve for FDS.

Studies have been conducted on the complex permittivity, ac conductivity and dc conductivity in the broad frequency range (0.01 Hz–10 MHz) and temperatures from 273.15 to 333.15 K for ethylene glycol with titanium oxide (TiO_2) and it has been reported that frequency has a strong influence in the range below 10 kHz. Also, the imaginary part of permittivity is strongly linked with the frequency in the whole range [47]. AC breakdown performance of the TO-based NFs (TNFs) has been improved with the addition of NPs. But when the NPs concentration reaches a limit, the breakdown voltage starts to decrease which can be explained by the electric double-layer (EDL) model. The FDS measurement of the TO

TH-2868_156302003

modified by silica (SiO_2) NPs was performed to make a better understanding of the relationship between the dielectric properties and the EDL structure of the TNFs in a wide frequency range from 10^{-2} to 10^{6} Hz. Two different relaxation processes and a conductivity contribution were observed by FDS measurement which can verify the assumption. The introduction of the EDL structure provides an idea to account for the insulating strength improvement of TNFs for the first time [48]. For both pure oil and TNFs, dielectric spectroscopy measurements show that the curve is composed of different loss contribution, i.e., in the low-frequency range, the loss curve defined conductivity loss, while in the high-frequency region the curve defined relaxation loss. With the NPs concentration increasing, more EDL structures will form under an external electrical field which accounts for the low frequency polarization peak tending to move to the high frequency [49]. Electrochemical impedance spectroscopy has also been used to accurately estimate olive oil acidity by measuring the electrical conductance of an emulsion between the oil and a hydro-alcoholic solution (60% ethanol 40% distilled water) [50]. FDS has been carried out on oil-immersed bushing at different temperatures, and a method to estimate the moisture content was proposed and suggested that such studies may be extended to oil-paper insulation system in transformers [51]. Studies have been carried out for correcting the temperature effect on the FDS measurements and suggested that the variation of the tan δ curve at any temperature depends on conductive behaviour, polarization behaviour and the migration of moisture between oil and cellulose. Fitting models are proposed to ensure that the master curve technique is universal [52]. It has also been observed by many researchers that real dielectrics do not follow the standard Debye model which gives a semicircular arc with its centre on the x-axis. K. S. Cole and R. H. Cole in [53, 54] developed a method to correlate the dielectric response of real materials with idealized Debye behaviour. Such deviation in the Cole–Cole plot from the Debye model was attributed to the distributed nature of relaxation process taking place in the complex dielectric material. These plots have been used by researchers for characterizing different materials and composites [55-58]. However, not much study has been performed to assess the ageing of insulating liquids over a long duration of time. Also, the temperature effects on the insulating liquids and their NFs are not discussed much in the reported works.

1.2.4 Mineral oil and natural ester-based nanofluids

In recent times, NFs have been developed by dispersing NPs in the TO and they displayed higher insulating and cooling properties. Using various NFs, the thermal properties

TH-2868_156302003

of base fluids could be improved by choosing suitable volume fractions of desired NPs. To improve the performance in the existing TO, in 1994 T. J. Lewis introduced the concept of NF with enhanced thermal and dielectric properties. Since then various researches have been carried out for the application of NF in thermal management and superior thermal performances for transformer application [59]. However, very little researches have been carried out on the dielectric and electrical performance enhancement of the NFs [60].

It is observed that the use of NPs in fluids such as ethylene glycol, ester oil and MO increase the heat transfer properties. This motivates the researchers to explore the possibilities to develop the NFs to increase the cooling and other effects which will enhance the life of the transformer. The studies are aimed to investigate the cooling effect of the transformer using various MO-NF based TO. Though different types of NPs have been used to prepare the MO-NFs for thermal management, very few of them have the ability to provide electrical insulation [61, 62]. To enhance the life of a transformer at the higher loading condition, the requirement of providing sufficient cooling effect and dielectric strength of the TO are the major challenges. Researchers have focused on the development of a new liquid dielectric alternative to MO with enhanced thermophysical and electrical performances [63]. Therefore, researchers have found out that the thermal performances of the fluid can be enhanced with the implementation of nanotechnology [64]. New nanotechnology-based materials with superior properties have been developed and are already used in many everyday products and processes. Development, characterization and implementation of the nanodielectrics in the field of electrical insulation are the major areas of dielectric material research.

There are three different kinds of NPs such as conductive, semi-conductive and insulating, which are used to prepare the NF. The example of conductive NPs are iron oxide (Fe_3O_4), semi-conductive are TiO_2, copper oxide (CuO), and insulating are aluminium oxide (Al_2O_3), SiO_2, hexagonal boron nitride (h-BN). The diameter of the aforementioned NPs diameter is in the range of 10-70 nm [65-67]. Most of the reported research works presented in the context of NF based TO are developed by taking MO as the base fluid. Moreover, very few pieces of literature have reported taking natural ester-based VO and synthetic ester-based oil as the base fluid for the preparation of NF in transformer application [68-73]. Choi et al. prepared TO-NF by considering 0.5% by volume of Al_2O_3 NPs with an average diameter of 13 nm and aluminium nitride (AlN) NPs with a diameter of 50 nm. Oleic acid was used as a surfactant for better dispersion of NPs in TO and they observed up to 8% enhanced thermal conductivity of NFs with regards to conventional oil for different volume % of NPs. They

TH-2868_156302003

also reported on the stability of NPs which was found to be about 1 hour [74]. Jin et al. prepared MO-NF with SiO_2 NP and studied the breakdown voltage at different ppm humidity levels. They found that at 25 ppm humidity, enhancement in breakdown voltage was 71% and with 15 ppm humidity, breakdown voltage was less affected and it was about 57% enhancement [75]. Mansour et al. used TiO_2 NP and dispersed in TO to prepare NF for their study. They conducted a study on two groups, the first one focused on the surfactant concentration on dispersion behaviour and agglomerate size and the second one concentrated on the breakdown strength of the NF. The enhancement in breakdown strength was nearly 27% of base oil [76]. Liu et al. observed for CuO-ethylene glycol suspensions at 5 vol.% and Cu-water at 0.1 vol.%, thermal conductivity is enhanced by 22.4 and 23.8% respectively [77]. Lee et al. suggested that the measured thermal conductivities of the dilute Al_2O_3-water NFs increase nearly linearly with the concentration [78]. Eastman et al. reported the enhancement of thermal conductivity by adding the CuO NPs to water and found the thermal conductivity is enhanced by 60% compared to water without NPs [79].

Addressing the electrical properties of the NFs, researchers have focused on the development of NF by the dispersion of magnetic NPs into the MO. The AC and impulse breakdown voltage (BDV) is measured in which, the NF shows significant improvement in the properties compared to the base fluid. The partial discharge inception voltage (PDIV) of the NF is observed to be superior to the MO [80]. The improvement in ACBDV of the magnetic NF is explained through streamer analysis using needle sphere electrode. The charge dynamics of the NP during the applied voltage to the NF are studied to understand the enhancement in the ACBDV [81, 82]. Many researchers investigated that the dispersion of semi-conductive NP such as TiO_2 into the MO improves the thermal and electrical performances of the NF. The ACBDV and the thermal conductivity of TiO_2/MO-NF have enhanced at a certain vol. % of NP dispersion. The PD analysis of this batch of NF results in the delay of PD propagation and affirming the superior liquid dielectric fluid [83-85]. Though surfactant addition has improved the stability of the semi-conductive NF, long-term stability in real time application is a challenge.

The NFs prepared by the dispersion of the conducting and semiconducting nanofillers upon exposure to the electric field, likely to align in the direction of the electric field to form the conducting channels in NFs. Hence, an early breakdown may take place for the NF based TO. Since the transformer is a long run device, the reliability of high dielectric strength is essential. Therefore, the research is focused on alternative nanofillers to enhance the electric breakdown strength and thermal performance in the NF. An investigation is carried out on the

TH-2868_156302003

insulating NP-based dielectric fluid in which various insulating NPs such as Al_2O_3, ZnO, SiO_2, and BN etc. are dispersed as the potential nanofillers in the MO. The study shows that the dielectric strength of the insulating BN NF enhances compare to the base fluid at the same time the thermal performance either enhances or unaffected. The mean ACBDV of the insulating NF is superior to that of the MO. Therefore, the failure analysis using Weibull statistical analysis is carried out to evaluate the percentage of probability failure in ACBDV [86-89]. Tijerina et al. and Coleman et al. performed experiments with exfoliated layers of h-BN in oil and have found high thermal conductivity compared to the base oil. The exfoliation process is performed, which converts h-BN of 1-micrometre size nanopowder to 2D nanosheets of 150-300 nanometres which is named as exfoliated h-BN (Eh-BN) [90]. It is observed that Eh-BN is evolving as a new class of insulating NP for the enhancement of the thermal conductivity of NF [91]. Eh-BN is found to be thermally conducting and electrically insulating. It is a very unique material for application in heat transfer of fluid because of its very high thermal conductivity and well-suited particle surface for exfoliation [92-94].

From the aforementioned literature of NFs and their application in liquid dielectric for transformer, it is observed that the thermophysical and electrical performance of the insulating NF is improved compared to the base fluid. However, its usage in VO is not much explored. Moreover, because of the poor biodegradability and lower fire resistance capability of MO and MO-based NF, VO-based NF is explored in this work. Hence, in this research work, the development of a new nonedible VO, named Pongamia oil methyl ester (POME), as a novel TO is presented. Pongamia pinnata belongs to a species of family Leguminosae and genus Pongamia. Commonly known as karanji, this plant is resistant to drought and has the property of nitrogen-fixing. An investigation report shows that a single tree can produce 9-90 kg Pongamia pinnata seeds per year. In recent times, Pongamia pinnata has been accepted as a practical source of non-edible oil for biofuel production [95-97]. The Pongamia seeds are processed into suitable biodiesel, which acts as a less polluting fuel compared to petroleum-based oil [96]. The POME is derived by the process of two-step transesterification from the crude oil [98]. The thermophysical, chemical and electrical properties of POME are studied and compared with MO and other two natural esters FR3 and jatropha (JAT).

1.3 Motivation

Liquid insulation has the many benefits of gaseous insulation like self-healing and comparable dielectric strength, but in addition to all these liquid insulation is very effective as a coolant in HV apparatus as they are thermally conducting because of the convection

TH-2868_156302003

phenomenon. But all insulating agents are limited by their dielectric strength, which is the maximum electric field beyond which they become conductive. In the available literature, the importance of an alternative and environment-friendly liquid dielectric for the power and distribution transformer is studied. In addition, considering the application of nonedible VO in the transformer as a dielectric liquid, very few works have been reported. For this reason, the nonedible NEO based liquid dielectric is considered for our studies. Also, many researchers have put their effort to study the thermal performances of the NFs but very little researches have been reported on the dielectric characteristic of the NFs with NEOs. From the above survey, there is no clear summary of the nonedible VO properties and their application for power and distribution transformer. The technical gaps which are big hurdles for using NF and nonedible VO based liquid dielectric with improved insulation and heat transfer applications are as follows:

- The generation of gases in the TO is a major area to be looked into and more so when NEOs are used, as not much literature is available regarding the formation of gases in a simulated transformer environment, as it is difficult to get real time data from transformers filled with NEOs. However, its study is important as recently NEOs are being advocated for usage in power transformers. So, the aspect of dissolved gases needed to be emphasized.
- As low frequency dispersion is an important characteristic of any dielectric, the FDS of fresh and aged oils will be studied. An ageing model needs to be developed to understand how the properties vary over a period of time. Also, the study of temperature dependence on the dielectric parameters over a wide range of frequencies is required to be studied.
- The application of NPs to VOs for further enhancement of properties needs to be analyzed for real time usage of such fluids in transformers. The studies have been conducted extensively on the enhancement of thermal conductivity of NF, but other important characteristics of NF for transformer application like flash point, ACBDV, etc. needs to be looked into.
- The charging dynamics of a dielectric NP in VO has not been discussed much in previous literature, which is the underlying cause of the increase of breakdown strength in NFs.

TH-2868_156302003

1.4 Objective of the thesis

The study has been performed to introduce alternative liquid dielectric for power and distribution transformer and its condition assessment. The objectives of the thesis are described as follows:

- To consider the available NEOs and study the dissolved gases generation in aged oil samples by using the DGA technique and analyze the incipient faults using the various gas ratios and Duval triangle method.
- To analysis the FDS of fresh and aged NEO under different ageing environment and develop an ageing model to assess the integrity of the dielectric.
- To study the temperature dependence of the dielectric parameters of MO and NEO and their NFs over a wide range of frequencies using FDS and develop a predictive model to assess the parameters at different temperatures.
- To study the dielectric breakdown probability of the fresh and aged NEO and carry out a statistical analysis using normal and Weibull distribution for ascertaining its conformity to a specific distribution and check which distribution fits the data well.
- To develop a new non-edible NEO and examine the electrical and thermophysical properties of the oil and compare with the existing MO and study the charging dynamics of the NP when dispersed in the base fluid.

1.5 Contribution of the thesis

The major contributions of the thesis for the condition assessment of alternative dielectric fluid for power and distribution transformer are given as follows:

- The condition assessment using DGA of two different NEOs like FR3 and JAT is carried out under different ageing durations using a sealed beaker test setup, as NEOs are a potential substitute for the conventional MO, used in the power and distribution transformers. The FTIR and NMR studies are performed to understand the variation in the structure of the oil and a regression model is developed for total dissolved combustible gas (TDCG) prediction.
- The FDS analysis of the fresh and accelerated aged NEO under different ageing durations is done to observe the variation on the dielectric properties at low frequency ranges and a statistical ageing model is developed to establish a relation between the dielectric parameters, frequency and ageing time.

TH-2868_156302003

- The FDS of the MO and VO along with their NFs is studied at different temperatures and a predictive machine learning (ML) model is developed to estimate the dielectric properties at different temperature and frequencies.
- An open beaker oxidative ageing study is performed for VO and a statistical investigation is carried out to understand the failure probabilities at different ageing durations for normal and Weibull distributions.
- A thermally conducting, electrically insulating h-BN is dispersed in MO and VO to prepare the NFs. The thermophysical and electrical characteristics of the NFs are analyzed in the context of efficient cooling and insulation in the transformer. A nonedible VO based liquid dielectric POME is studied for transformer application.

1.6 Organization of the thesis

This thesis is organized into seven chapters as follows:

Chapter 2 presents the DGA and long term performance of two NEOs: Environtemp FR3 and jatropha curcas oil (JAT). The DGA helps in monitoring the emission pattern of gases when the oil is subjected to stress for a longer duration. Thermal stress is applied on both oils in a sealed beaker setup at 150^{o}C for up to 2000 hours, and samples are taken out at intervals of 500 hours. The dissolved gases generated during thermal stress are analyzed, and compared for both types of oils. It is observed that FR3 is more prone to stray gassing when compared to JAT. The alterations in the structure of the oils are studied by the FTIR and 600 MHz NMR spectroscopy analyses. The DGA interpretation is done by classic Duval triangle, Dornenburg ratio, Rogers ratio and IEC method. In the proposed study, a regression model for the two types of oils is developed to predict the TDCG over a period of time. The findings show that JAT holds considerable properties of insulating fluid and is a decent substitute for other insulating oils because of its non-edible nature and better biodegradability.

Chapter 3 uses the non-invasive technique of the FDS analysis to see the variation in the relative permittivity and dielectric dissipation factor (tan δ) of the aged oil samples of JAT, over a wide range of frequency. The oil is subjected to thermal stress in an open beaker ageing test setup at 115^{o}C for up to 500 hours, and samples are taken out at intervals of 100 hours for testing. This technique is applied to understand the dielectric response of the oil at different ageing durations. FTIR spectroscopy and ultraviolet-visible (UV-Vis) spectroscopy analyses are implemented before and after ageing to observe the alterations in the structure of the two oil samples. The statistical technique of regression modelling is used to develop an

TH-2868_156302003

ageing model that gives the values of the relative permittivity and dielectric dissipation factor (DDF) with respect to frequency of excitation and ageing time. The quantitative analysis with fitting models helps in ascertaining by what range the values are changing when the transformer insulation ages, by considering aged samples up to 500 hours. This model may be further extended for different oils and ageing hours.

Chapter 4 further explains the effect of temperature on the addition of NPs to the oil samples with the help of FDS analysis. In this study, TiO_2 and Eh-BN NPs are used to prepare the NFs in MO and FR3. The FDS response is calculated in the frequency range of 10^{-3} to 10^{4} Hz and the temperature range varies from 30 to 90^{o}C with an interval of 15^{o}C between two successive temperatures. The permittivity and the DDF obtained from the FDS are compared for all the oil samples-MO, FR3, MO-NF and FR3-NF. Based on the experimental results, low frequency dispersion of the oils is investigated to obtain an insight into the integrity of the oil samples. A predictive analysis model is proposed using ML algorithms to predict the dielectric properties like permittivity and dielectric losses of all the oil samples considering its dielectric response using the FDS. For the predictive study, two supervised ML models, the decision tree regression (DTR) and the K-nearest neighbour (KNN) are used. The prediction accuracy is determined and a comparative analysis of these model errors is done. The model is developed using a dataset of 355 experimentally measured values of the dielectric properties.

Chapter 5 explains the performance of NEO using NPs and statistical analysis is carried out to understand the breakdown probability of the fresh and aged FR3 and FR3-NFs. The semi-conductive TiO_2 NPs are used for this study. An open beaker oxidative ageing setup is considered to comprehend the process of ageing. To understand the statistical behaviour of the ACBDV of the oil samples, normal, 2-parameter Weibull and 3-parameter Weibull distributions are considered. To confirm whether these distributions belong to that specified distribution, hypothesis testing with Anderson-Darling test is used, which is a powerful technique to ascertain if the distribution of experimental data follows a theoretical distribution. The goodness of fit is used to measure how well the data fits a specified distribution.

Chapter 6 presents the development of a new non-edible NEO, Pongamia pinnata oil (PPO) including the performance of its NFs with suitable NPs. The molecular structure of PPO is changed by the transesterification process and converted to POME as the crude oil is

TH-2868_156302003

not suitable for direct use because of its high viscosity, high pour point and acid number. For preparing the NF, 0.01wt.% of Eh-BN is dispersed in MO and POME to prepare MO-based NF (MO-NF) and POME based NF (POME-NF) respectively. The exfoliation process for the surface modification of the insulating h-BN NP of 3D structure to 2-D nanosheets is carried out. In this work, the various thermophysical and electrical properties of four types of oils - MO, MO-NF, POME and POME-NF are explored. The thermophysical properties like thermal conductivity, interfacial tension, flash point, pour point and the electrical properties such as dielectric constant, tan δ, and dielectric strength are measured and a comparative analysis is carried out among all four types of oil. The influence of the polarization on the NP on the dielectric constant is further analysed by using the Clausius-Mossotti equation. The charging dynamics study has also been investigated to understand the phenomenon underlying the enhanced breakdown voltages of VO based NFs.

In Chapter 7, the conclusion of the thesis and the suggestions for the extension of this research work are presented.

TH-2868_156302003

TH-2868_156302003

2

Dissolved gas analysis of non-edible natural esters

Contents

TH-2868_156302003

2.1 Introduction

Transformers generally, use the MO as the insulating fluid along with solid insulation like the kraft papers and pressboards. The introduction of VOs in this area leads to a complete eco-friendly solution. MO has some shortcomings as it is mined from fossil fuels. Also, MO is poorly biodegradable, so if the oil spills accidentally, there is a concern for environmental hazard. Alternatively, VOs as insulating agents in transformers, are gaining importance because of the better biodegradability, environment-friendly nature, higher flash and fire points. The oil-paper combination shows enhanced properties when VO replaces MO. VO has superior performance as a dielectric fluid with enhanced thermal conductivity and specific heat capacity [2, 3]. The breakdown voltages and thermal conductivity of natural esters are higher, when compared with MO [21]. The streamer characteristics like streamers shape, their stopping length, the associated current and electrical charge of NEO are quite similar to MO [24].

In consideration of the aforesaid properties, NEO is taken for the study. As many studies have been conducted considering MO and other types of natural and synthetic esters, so in this study, MO is not taken into account [38, 39, 99]. Two kinds of NEO are considered here, one is the FR3 obtained from Cargill India, and the other is the JAT procured from a govt. agency which is a non-edible NEO. Using the JAT for transformer application will not only take care of the environmental impact but also not affect the food industry dealing with edible oils. Many research works have been conducted with varied types of vegetable seed-based oils to be used as insulating fluid [40]. A few works suggest JAT as a potential insulating fluid [17, 24]. The ageing study is essential to understand the behaviour of insulating oil under thermal stress. The DGA helps in monitoring the emission pattern of gases when the oil is subjected to stress for a longer duration. However, the ageing behaviour of JAT is not reported, and further analysis of its dissolved gases is not conducted, which is the main area of focus in this work. Faults in the power apparatus are inevitable, but monitoring them can prevent any catastrophic occurrence. Thermal and electrical faults are the two main types of faults occurring in the transformers, so it is very much crucial to gauge the state of the transformer at regular intervals of time [30, 31]. The faults occurring in a transformer cause the insulation to breakdown, thereby releasing some gases which dissolve in the fluid [30]. DGA is an essential technique in condition monitoring of a transformer in case of incipient faults. In this study, the oils are considered along with an equivalent amount of solid insulation in the ratio of 20:1:1 for oil/paper/pressboard, and they are subjected to

TH-2868_156302003

temperatures of 150^{o}C for duration of 2000 hours in a sealed beaker. The oil samples are taken out from the vessel at intervals of 500, 1000, 1500 and 2000 hours for the purpose of DGA. A comparative analysis is done between the two oils to understand the behaviour of the oils at accelerated thermal ageing for longer durations. Thus, the investigation of the dissolved gases in the NEOs will establish a good indicator of the types of faults the oils can sustain. To estimate the pattern of generation of gases in the insulating fluids, laboratory ageing tests are performed replicating the atmosphere inside the transformer.

In this research work, section 2.2 addresses the materials and methods used, 2.3 describes the test methods, section 2.4 addresses the standard gas ratios, section 2.5 focuses on the results and discussions and the conclusions are incorporated in section 2.6.

2.2 Materials and methods

2.2.1 Environtemp FR3

(a) (b)

Figure 2.1: Oil samples (a) Fresh FR3 and (b) Fresh JAT.

FR3 is based on renewable resources and produced from refined soybean oil after mixing some additives. The main component of any vegetable-based oil is triacylglycerol and rests are fatty acid molecules connected to a single glycerol structure. A sample of FR3 oil is seen in Figure 2.1(a).

2.2.2 Jatropha curcas oil (JAT)

The other NEO is the JAT which is derived from the jatropha curcas seeds. The JAT is potentially used as biodiesel to fight the ever-increasing energy crisis. It is derived from plant seeds, and hence it is environment-friendly, helps in reducing greenhouse gas emissions. The most important advantage of using JAT for the benefit of mankind without

TH-2868_156302003

affecting the food economy is its non-edible nature. The finished product of the Jatropha oil, as seen in Figure 2.1(b), is procured from a govt. agency to carry out the experiments. The liquids are dried in vacuum oven at 60^{o}C for 72 hours.

Table 2.1: Specifications of MO, FR3 and JAT.

Characteristic	Specification		
	MO	FR3	JAT
Density (kg/m^3)	0.828	0.91	0.879
Kinematic viscosity at 27^{o}C (cSt)	13.67	59	22
Interfacial tension at 27^{o}C (mN/m)	47	20.6	10.7
Flash point (^{o}C)	146	268	190
Pour point (^{o}C)	-40	-18	0
ACBDV (kV) at 2kV/sec and 50Hz	35	82	79
Thermal conductivity (W/m-K)	0.128	0.163	0.162
Dielectric dissipation factor at 90^{o}C and 50Hz	0.0085	0.00863	0.0088

It is fully natural and is in form of fatty acid methyl ester. The characterization of the JAT was done by the gas chromatography mass spectroscopy (GCMS) to ascertain the formation of methyl esters. The GCMS is carried out using PerkinElmer Clarus GC/MS to determine the percentage of methyl esters present in the JAT oil. In the gas chromatograph, the sample is vaporized, and the various components present are segregated and extracted from the column at different times, called as their retention times. The specifications of MO, FR3 and JAT measured are shown in Table 2.1. The major components of JAT are shown in Table 2.2.

Table 2.2: Composition of JAT.

FAME	Retention time (min)	Molecular formula	Molar mass, kg/k mol
9-Hexadecanoic acid	36.31	$C_{17}H_{34}O_2$	268
Hexadecanoic acid	36.525	$C_{17}H_{34}O_2$	270
Pentadecanoic acid	36.55	$C_{16}H_{32}O_2$	256
9-Octadecenoic acid	38.52	$C_{19}H_{36}O_2$	296
Heptadecanoic acid	38.741	$C_{19}H_{38}O_2$	298

TH-2868_156302003

2.2.3 Thermal ageing experimental setup

For carrying out the ageing experiment, the single temperature technique is used, whereby the oil and the equivalent amount of solid insulation are subjected to thermal stress at a single temperature. The duration of thermal stress is varied, and samples are taken out after the prescribed intervals for testing. In this test, a sealed steel tube is used for the ageing of the oil samples, which allows the possibility to simulate the temperature conditions inside a transformer as shown in Figure 2.2. The vessel also contains the equivalent amount of pressboards and kraft paper which is vacuum-dried for 24 hours before immersing in the oil. Around 1.5 litres of insulating liquid is used for the ageing process. All the solid insulations are dried as much as possible completely to make them free from any moisture. The thermal ageing is carried out by heating the vessel to a temperature of 150ºC continuously and a thermocouple attached to the vessel measures this constant temperature of 150^{o}C. As per IEEE C57.147 [147], to avoid fluid scorching, the thermal ageing temperature of natural esters is kept below 180^{o}C. The oil samples are taken out after 500, 1000, 1500 and 2000 hours from different vessels to analyze the various characteristics.

(a) (b)

Figure 2.2: (a) Experimental set-up and (b) ageing vessels.

2.3 Test methods

2.3.1 Fourier transform infrared (FTIR) spectroscopy

The FTIR study is executed to recognize the presence of the different functional groups in the new and aged oil samples. This method helps to analyze the consistency of the oil before and after ageing. Every functional group requires different frequency for absorption, and thus a molecular fingerprint of the sample is created representing the molecular absorption and transmission in the spectrum. A molecular vibration takes place as a result of this absorption, and it results in either stretching or bending of the bonds. The schematic of FTIR spectroscopy is shown in Figure 2.3. In FTIR spectroscopy technique,

TH-2868_156302003

infrared (IR) light from the light source is passed through an interferometer along the optical path. The interferometer consists of a beam splitter, a scanning mirror and a fixed mirror. The beam splitter splits the light beam into two parts, one part is reflected from the moving mirror and the other part is reflected by the fixed mirror. Then, the two reflected beams are recombined by the beam splitter. As the scanning mirror makes movements, the optical path difference to the fixed mirror changes, such that the phase difference changes with time. The recombined light is used to produce the interference light which is passed through the sample. The molecules in the sample absorb some amount of the light and shows vibrations. The rest of the light is transmitted and is detected by the detector. The spectrum formed by the detector is called the interferogram. The fourier transform of the transmitted signal (interferogram) is obtained which is known as the FTIR spectrum. This is done for easy analysis of the specific sample and obtains its structure. The functional groups in the FR3 and JAT with ageing at 1000 and 2000 hours are identified by considering wave number in the range of 450-3500 cm^{-1} using a Perkin-Elmer Spectrum Analyzer.

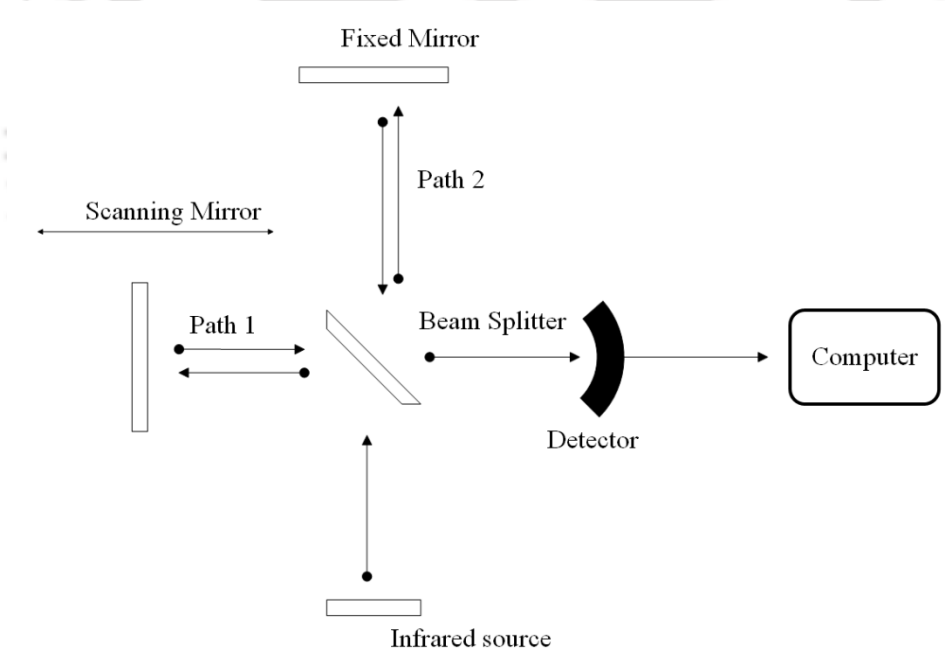

Figure 2.3: Mechanism of FTIR spectroscopy.

2.3.2 Nuclear magnetic resonance (NMR) study

The modification of the chemical structure of the two oil samples before and after ageing is studied using the 600 MHz nuclear magnetic resonance (NMR) spectroscopy. The schematic diagram of NMR is shown in Figure 2.4. The ^{1}H-NMR study is performed by

TH-2868_156302003

using deuterated chloroform ($CDCl_3$) as a solvent for both FR3 and JAT at 0 and 2000 hours of thermal ageing.

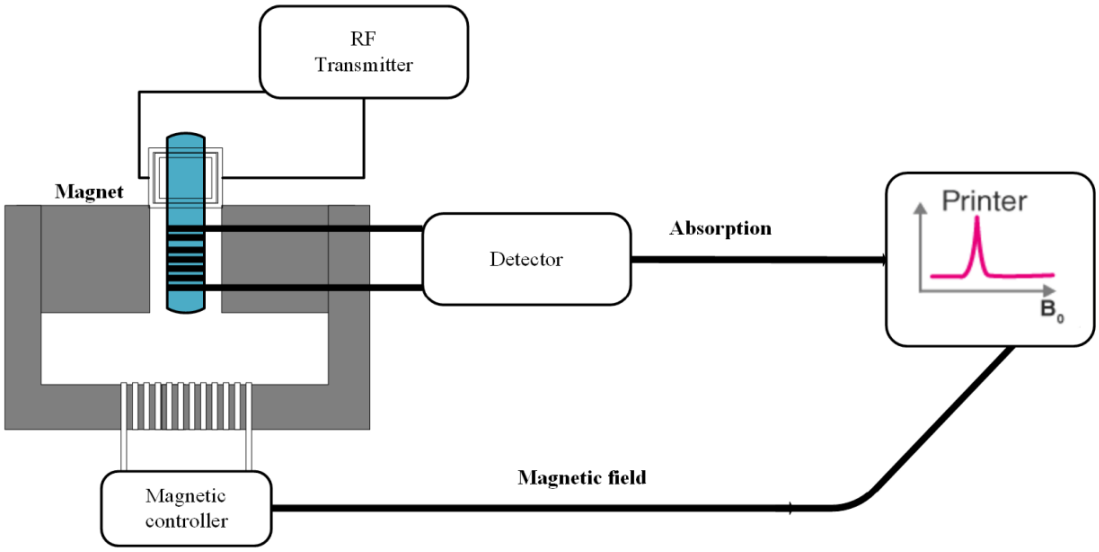

Figure 2.4: Mechanism of NMR spectroscopy.

2.3.3 Dissolved gas analysis (DGA)

The number of cases with transformers filled with NE oils is very less, so to evaluate the gas formation patterns in these insulating liquids, simulating the temperature profile in the laboratory similar to the actual transformer provides valuable results. In this DGA, the focus is on the gases present in the oil, which aids in the degradation of the oil. The insulating oil is a mixture of hydrocarbons, which decomposes on application of thermal stress into lower molecular weight compounds which are gases like C_2H_6, CH_4, C_2H_2, C_2H_4, CO, CO_2, H_2, etc. The different combinations of gases evolve depending on the temperatures created by the faults. The formation of H_2 and CH_4 at low temperatures indicates partial discharge. The formation of C_2H_2 at higher temperatures indicates arcing faults. CO and CO_2 are formed when the degradation of solid insulation starts and reacts with the oil [37].

2.4 Standard gas ratios

There are numerous methods to interpret the DGA results of the insulating oil in a transformer. The major five hydrocarbon gases namely CH_4, C_2H_6, H_2, C_2H_4 and C_2H_2 are considered either as 2-gas ratios (in IEC, Rogers, Dornenburg) or 3-gas ratios (in Duval's triangle). In this study, all these gas ratio methods are used to interpret the concentration of gases into types of faults likely to occur in a transformer after subjecting the two NEO to thermal stress. The five gas ratios as per standard are: Ratio 1 (R1) = CH_4/H_2, Ratio 2 (R2) =

TH-2868_156302003

C_2H_2/C_2H_4, Ratio 3 (R3) = C_2H_2/CH_4, Ratio 4 (R4) = C_2H_6/C_2H_2, and Ratio 5 (R5) = C_2H_4/C_2H_6.

2.4.1 IEC gas ratios

The IEC 60599 standard [144] is one of the widespread methods for an explanation of the faults in a transformer, which is based on ratios of five key gases: CH_4, H_2, C_2H_4, C_2H_6 and C_2H_2. In this approach, the ratios R1, R2 and R5 are considered to make the interpretation of the faults as per Table 1 and 2 of [100]. A grouping of the individual codes of R1, R2 and R3 indicates the type of incipient fault. However, this ratio is not very accurate to measure all fault types.

2.4.2 Dornenburg ratio Method

This method uses the ratios R1, R2, R3 and R4 to diagnose faults in the transformer. In this approach, it is initially determined whether a fault is present in the transformer by investigating the amount of each gas compared to a minimum concentration limit L1 as given in Table 4 of IEEE C57.104, 2008 [145]. The transformer has a fault condition if any one of the one gas from H_2, CH_4, C_2H_2, and C_2H_4 doubles the limit prescribed limit and the concentration of any one of the other two gases surpasses this limit. This technique is credible only if the amount of minimum one of the gases in each ratio surpasses the boundary value. If the ratio analysis is valid, then each successive ratio is compared in the order of R1, R2, R3, R4 and the fault type is determined as given in Table 5 of IEEE C57.104, 2008.

2.4.3 Rogers ratio method

In this method, three gas ratios R1, R2 and R5 are used for the interpretation of the incipient faults in a transformer. The bounds of each gas ratio signifying a specific fault type is given in Table 6 of IEEE C57.104, 2008. Rogers method is not dependent on specific gas concentrations for the diagnosis to be valid. This method may not always give the proper analysis of faults, and so other methods are required.

2.4.4 Duval's triangle

The Duval Triangle uses three hydrocarbon gases only, namely CH_4, C_2H_4 and C_2H_2 to detect the fault types as seen in Figure 2.5. The coordinates are plotted in a triangular coordinate system by considering the gas levels (in ppm) of the aforementioned gases. These three gases relate to the increasing levels of energy necessary to yield gases in transformers in service. There are six individual fault zones in this method as mentioned in Table 2.3 (PD, D1, D2, T1, T2 or T3) and an intermediate zone DT which denotes a mixture of electrical and thermal faults. The coordinates of the fault are denoted by the points A1 = $\%m_1$, A2 = $\%m_2$,

TH-2868_156302003

A3 = $\%m_3$ respectively for the percentage concentration of CH_4, C_2H_4 and C_2H_2 gases. The concentration of gases in ppm are considered for $CH_4 = m_1$, $C_2H_4 = m_2$ and $C_2H_2 = m_3$ and are converted to triangular coordinates. The relative proportion of the three gases, are calculated as below [101]:

$$Ak = \%m_k = \frac{m_k}{\sum_{i=1}^{3} m_i} \times 100 \tag{2.1}$$

where k = 1, 2, 3 as per the three gases mentioned above.

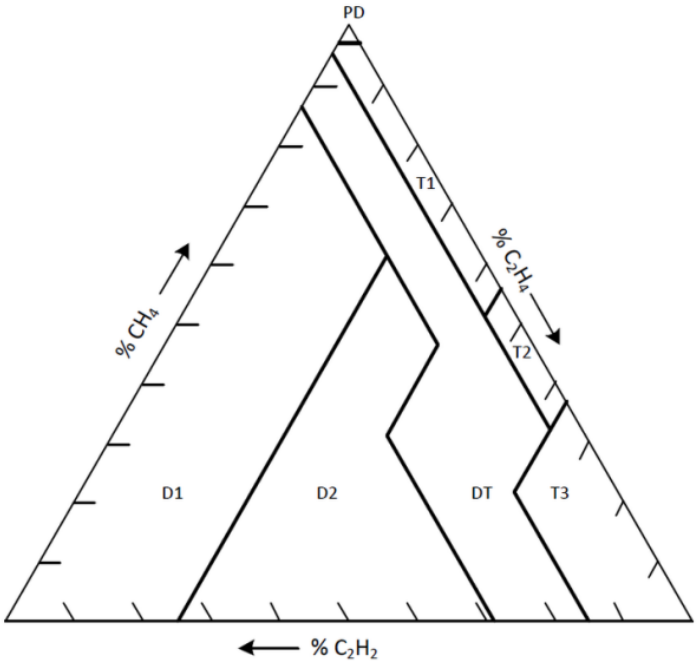

Figure 2.5: Duval Triangle.

Table 2.3: Types of faults.

No.	Type of fault	Symbol
1	Partial discharge with low energy density	PD
2	Discharge (arc) with low energy	D1
3	Discharge (arc) with high energy	D2
4	Mixture of electrical and thermal faults	DT
5	Thermal faults of temperatures < 300°C	T1
6	Thermal faults of temperatures between 300°C and 700°C	T2
7	Thermal faults of temperatures >700°C	T3

TH-2868_156302003

2.5 Results and discussion

2.5.1 FTIR spectroscopy

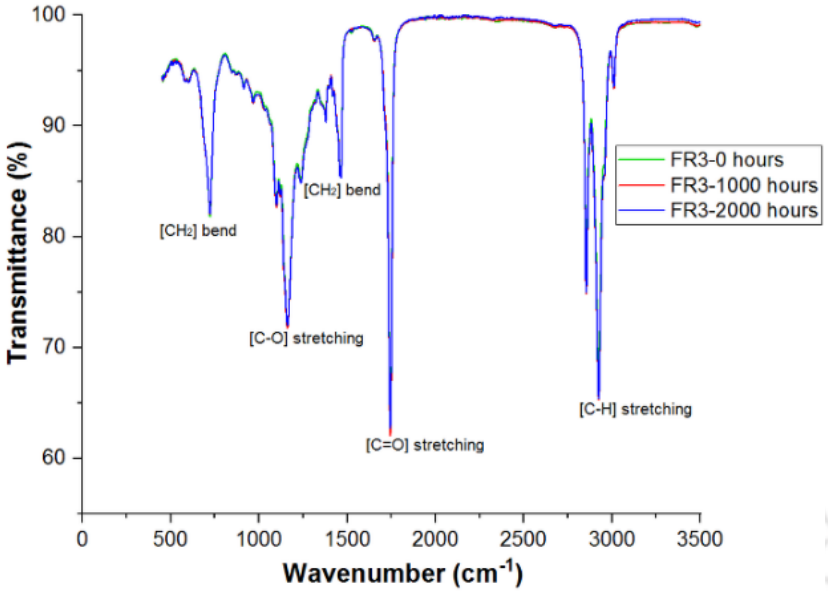

(a)

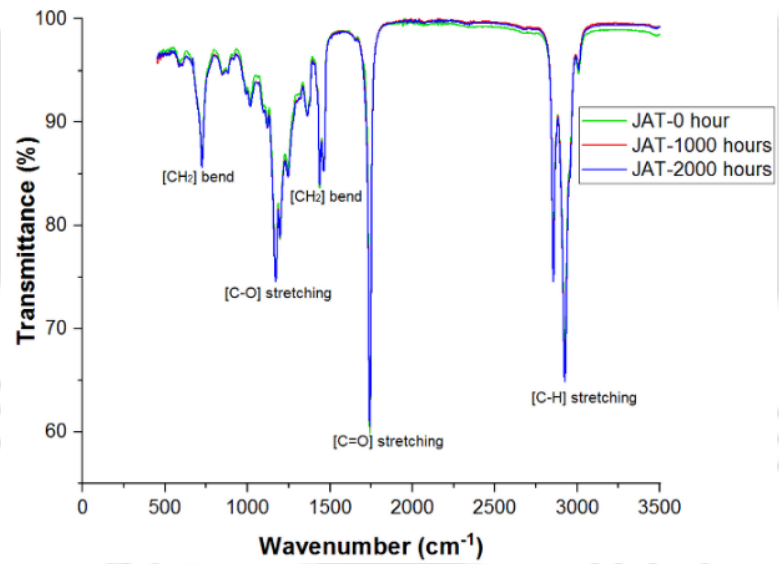

(b)

Figure 2.6: FTIR spectrum of (a) fresh FR3, aged FR3 for 1000 hours and aged FR3 for 2000 hours and (b) fresh JAT, aged JAT for 1000 hours and aged JAT for 2000 hours.

In the present study, with ageing, the transmittance of the FR3 and JAT is nearly unaffected. As seen in Figure 2.6, at wavenumbers of 2924 cm^{-1} and 2854 cm^{-1} for both FR3 and JAT oil samples respectively, two peaks are observed indicating C-H stretching for the presence of alkanes. For FR3, at the wavenumber 1744 cm^{-1} there is a sharp peak for all the fresh and aged samples indicating C=O stretching for the esters present in the oil. The similar stretching is observed for all the JAT oil samples at the wavenumber of 1742 cm^{-1}. Some amount of CH_2 bending is observed at wavenumbers 1464 cm^{-1} and 1460 cm^{-1} for FR3 and

TH-2868_156302003

JAT oil samples, respectively. At wavenumbers of 1000-1260 cm^{-1} for both FR3 and JAT oil samples, there is C-O stretching indicating alcohol. With ageing, the development of the carbonaceous particles is likely to form in oils. However, the consistency of the oil is intact as all the functional groups exist even after 2000 hours of thermal ageing for FR3 and JAT.

The FTIR spectroscopy is carried out to observe any changes in the functional groups of the oil samples over a period of time. However, no significant difference is observed for particular oil in various ageing times considered. The FTIR might provide information if the accelerated ageing is carried out for a longer period of time. Thus, for this particular duration of up to 2000 hours, the FTIR spectroscopy does not show any difference of the oil spectra relative to ageing time.

2.5.2 NMR study

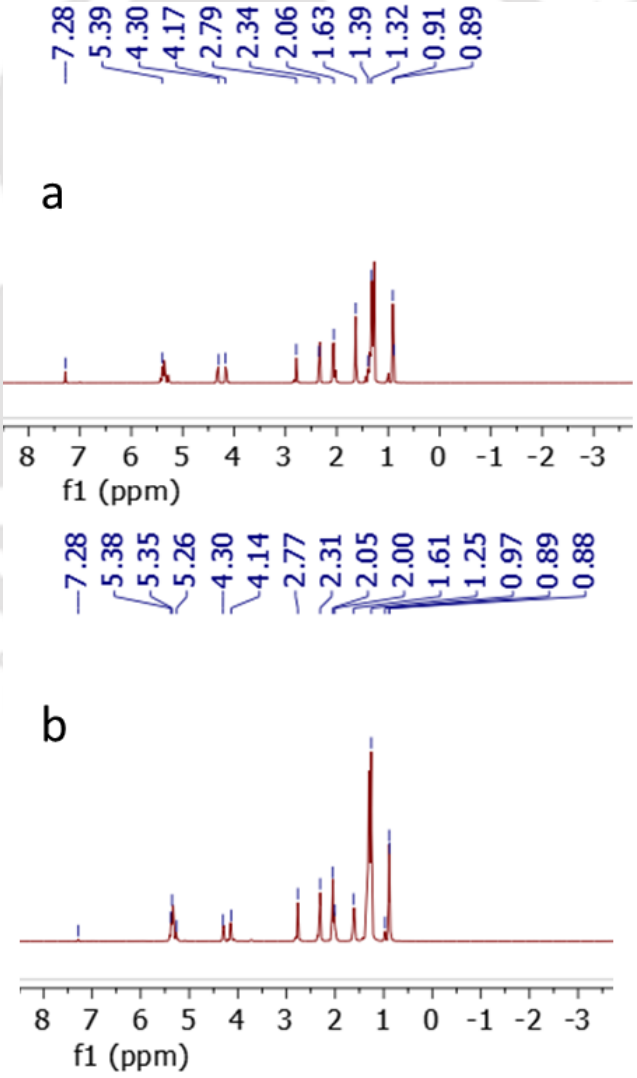

Figure 2.7: NMR analysis of (a) fresh FR3 and (b) 2000 hours aged FR3.

TH-2868_156302003

In the NMR spectrum, for both FR3 and JAT, as seen in Figure 2.7 and 2.8 respectively, multiplets are observed for CH_3, CH_2 and allylic protons of the fatty acid fragments in the section of 0.87-2.78 ppm. Two multiplets are detected for the CH_2 and CH protons of the glycerol moiety in the range of 4.12-5.35 ppm. At 2.3 ppm, the presence of methyl ester is confirmed as this peak signifies α-carbonyl methylenes. The peaks at 7.28 ppm, represent the chloroform solvent for both FR3 and JAT, which is considered the reference peak [102]. The chemical structure of both oil samples before and after ageing shows a marginal variation in the peak intensity.

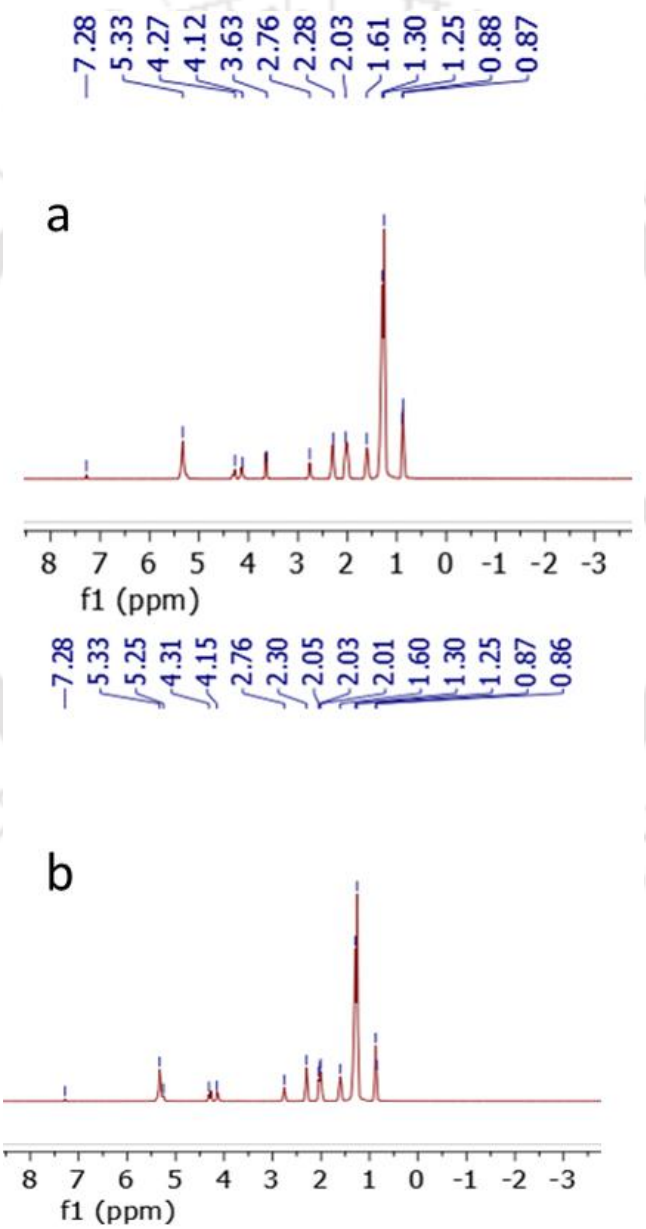

Figure 2.8: NMR analysis of (a) fresh JAT and (b) 2000 hours aged JAT.

TH-2868_156302003

The NMR spectroscopy is carried out to observe any changes in the chemical structure of the oil samples over a period of time. However, no significant difference is observed for the oil spectra in various ageing times. The NMR spectra might provide information if the accelerated ageing is carried out for a longer period of time. Thus, for this particular duration of up to 2000 hours, the NMR spectroscopy does not show any difference of the oil spectra relative to ageing time.

2.5.3 DGA study

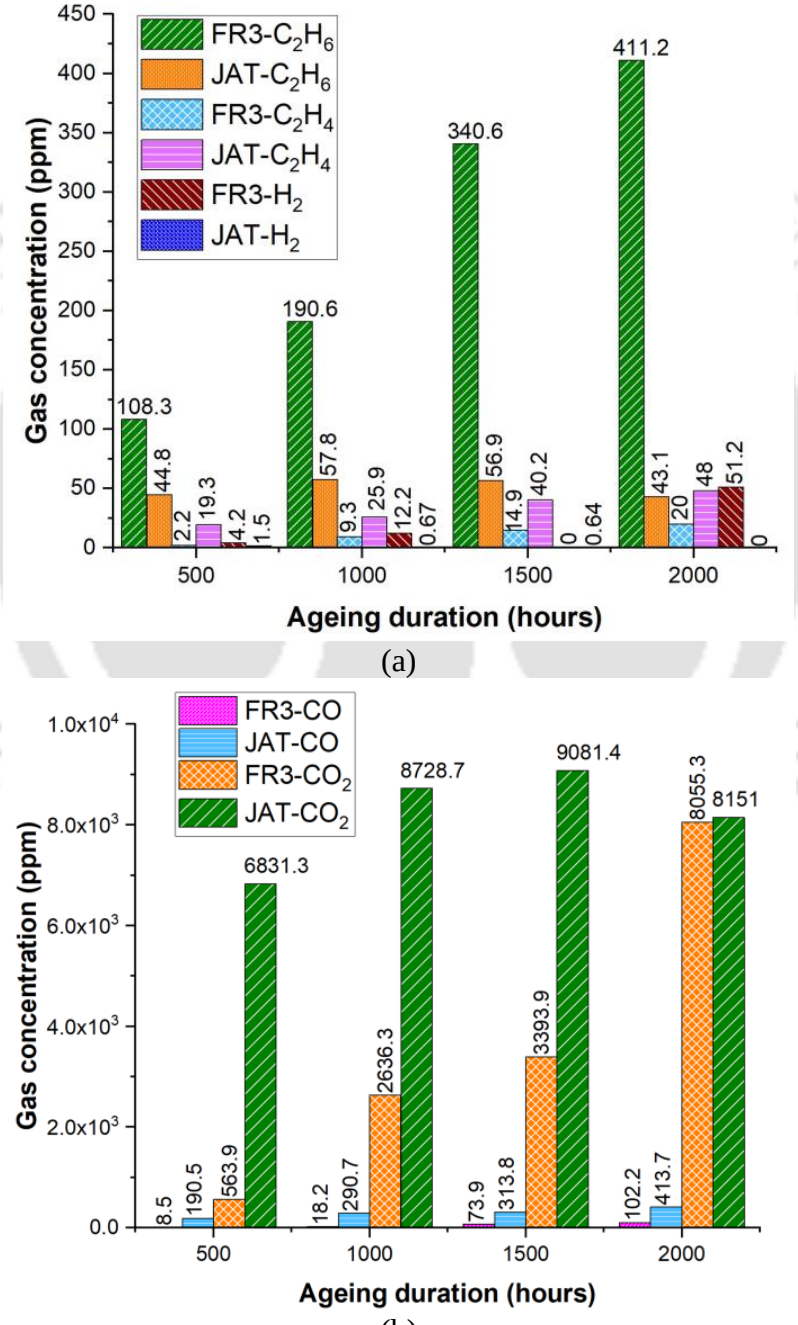

Figure 2.9: DGA analysis of aged FR3 and JAT (a) C_2H_6, C_2H_4, H_2 and (b) CO, CO_2.

TH-2868_156302003

In this process, the dissolved gases are extracted and measured in a gas chromatograph (GC) and only seven of the gases (CH_4, C_2H_6, C_2H_4, C_2H_2, H_2, CO and CO_2), which are more prone to cause deterioration are considered for the diagnosis. The results of DGA with oil samples at different ageing duration are shown in Figures 2.9(a) and 2.9(b). The analysis is done by using GC from Agilent Technologies, as per ASTM D3612 [148] and the gas extraction process followed is the headspace method. The total gas content (TGC) is calculated using the formula below:

$$\text{Total Gas Content (TGC)} = \frac{\text{Vol. of gas extracted (ml)} \times \text{atm.pressure (cm)} \times 293 \times 10^6}{76\ \text{cm} \times (\text{temp.of gas extracted} + 273) \times \text{quantity of oil (ml)}}\ \mu l/l \quad (2.2)$$

The H_2 generation is not very significant, but it is higher in the case of FR3 for all aged samples when compared with JAT. The detection of H_2 is observed more significantly after 1000 hours of ageing for the oil samples, so the flammable gases at 1000 hours of ageing are expected. In case of natural esters, there is stray gas formation under the effect of thermal stress as per IEEE C57.155, 2014 [146]. The negligible concentration of H_2 gas even after 2000 hours of ageing makes the JAT better in terms of stray gassing compared to FR3. Compared to JAT, FR3 generated significant amounts of C_2H_6 during thermal degradation. This shows that this gas has a greater association with triacylglycerol molecules present in FR3. A few works show that the higher concentration of C_2H_6 may be due to faults at low temperatures below 150^{o}C. C_2H_4 which is the primary pointer for high energy thermal faults is similar for both oil types. The presence of kraft paper and pressboard leads to the generation of CO and CO_2 in significant amounts in the oil samples because paper starts degrading at temperatures above 105°C. These gases are primary indicators for degradation of cellulose. The formation of CO_2 in the oil may be from the ageing atmosphere or deterioration of oil in the presence of heat [103]. CO is the degraded byproduct of aged oil-impregnated cellulosic material, and its concentration is highest at 2000 hours of ageing. The concentrations are quite significant in the case of JAT, as compared to FR3. This might indicate that paper insulation is protected by FR3 in a better way. By comparing the two NE oils, it is seen that FR3 produced more C_2H_6 and H_2 gas. Also, in general, the concentrations of all the gases in this oil increased with the ageing duration. However, the concentration of CO is higher in case of JAT.

The two oils used in this work are made from different plant seeds, so small variations in gas concentrations can be ascribed to the different origination of these oils. Using the

TH-2868_156302003

various gas ratio techniques in Table 2.4, the incipient faults are detected under the condition of thermal stress on the insulation. The IEC method detects PD with low energy for FR3 oils at 500 and 1500 hours' duration, whereas no fault detection occurred at 1000 and 2000 hours. For the JAT oil, IEC method predicts thermal faults for all the ageing durations, which is correctly diagnosed, although there is a slight mismatch with the temperature boundaries. The Rogers method is unable to predict any fault type for the JAT oil samples, and only for FR3 oil samples, PD with low energy is predicted as in case of the IEC method. The Dornenburg method is unable to predict any fault type for both FR3 and JAT oil samples for all four durations. Some of the DGA methods may fail to identify the faults accurately, as the fault zone boundaries and gas concentrations vary for different oils.

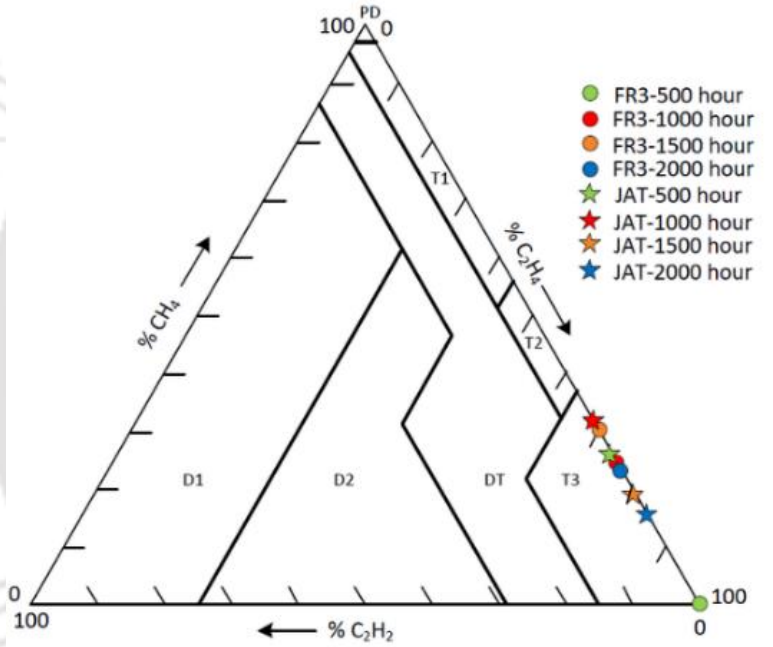

Figure 2.10: Duval triangle 3 for the aged FR3 and JAT oil samples.

In this study, the Duval Triangle 3 (recommended for non-mineral oils) is used for aged FR3 and JAT oil, as formulated by Michael Duval. The two NE oils studied in this paper are based on the compositions of saturated and unsaturated oleic and fatty acids. The non-mineral oils have diverse chemical compositions, which result in different patterns of gas generation. Accordingly, CH_4, C_2H_4 and C_2H_2 are chosen as three sides of the Duval Triangle 3, which represents low-, high-, and very high-energy or temperature faults respectively. The fault gas data are replaced into it, and it is observed from Figure 2.10, that all of the data points for both oil types fall in corresponding thermal faults region T3, which indicates faults at temperatures above 700^{o}C, which is not correctly placed. This may be due to the longer

TH-2868_156302003

duration of ageing carried out and for this separate triangle needs to be formulated. In some cases, when the data points lie in the boundary regions, it is difficult to identify the faults.

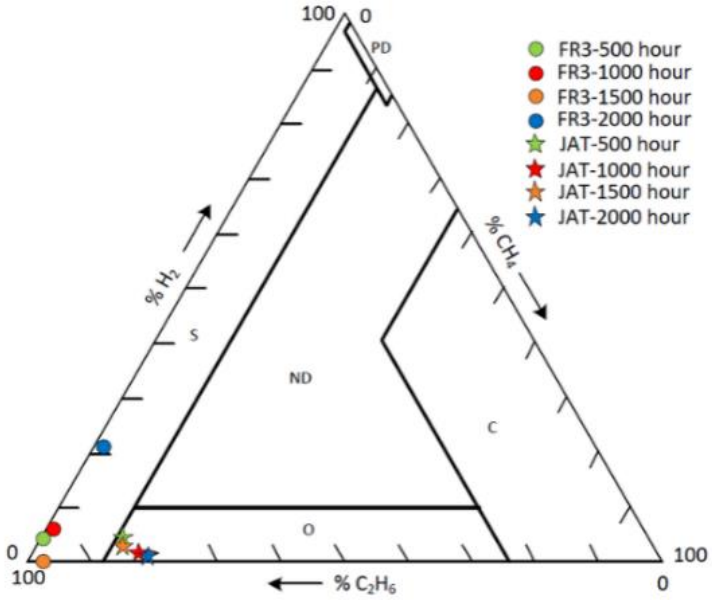

Figure 2.11: Duval triangle 6 for the aged FR3 and JAT oil samples.

Table 2.4: Gas ratios for all aged oil samples.

Ratios	FR3 500 h	JAT 500 h	FR3 1000 h	JAT 1000 h	FR3 1500 h	JAT 1500 h	FR3 2000 h	JAT 2000 h
IEC gas ratio method								
R2= C_2H_2/C_2H_4	0	0	0	0	0	0	0	0
R1= CH_4/H_2	0	4.467	0.246	17.612	ND	14.375	0.117	ND
R5= C_2H_4/C_2H_6	0.020	0.431	0.049	0.448	0.044	0.707	0.049	1.114
Fault indication	PD with low energy	Thermal faults (^oC) 150< T<300	No faults	Thermal faults (^oC) 150< T <300	PD with low energy	Thermal faults (^oC) 150< T< 300	No faults	Thermal faults (^oC) T<150
Rogers ratio method								
R1= CH_4/H_2	0.000	4.467	0.246	17.612	ND	14.375	0.117	ND
R5= C_2H_4/C_2H_6	0.020	0.431	0.049	0.448	0.044	0.707	0.049	1.114
R2= C_2H_2/C_2H_4	0.000	0.000	0.000	0.000	0.000	0.000	0.000	0.000
Faults indication	PD with low energy	ND	No faults	ND	PD with low energy	ND	No faults	ND
Dornenburg ratio method								
R1= CH_4/H_2	0.000	4.467	0.246	17.612	ND	14.375	0.117	ND
R2= C_2H_2/C_2H_4	0.000	0.000	0.000	0.000	0.000	0.000	0.000	0.000
R3= C_2H_2/CH_4	ND	0.000	0.000	0.000	0.000	0.000	0.000	0.000
R4= C_2H_6/C_2H_2	ND	ND	ND	ND	ND	ND	ND	ND
Faults indicated	ND	ND	ND	ND	ND	ND	ND	ND

*ND-Not determined.

TH-2868_156302003

Table 2.5: Duval triangle method for all aged oil samples.

	FR3 500 h	JAT 500 h	FR3 1000 h	JAT 1000 h	FR3 1500 h	JAT 1500 h	FR3 2000 h	JAT 2000 h
Duval triangle 3								
Faults indication	Thermal faults (T>700°C)							
Duval triangle 6								
Faults indication	SGO	Overheating (T< 250°C)	SGO	Overheating (T< 250°C)	SGO	Overheating (T< 250°C)	SGO	Overheating (T< 250°C)

*SGO-Stray gassing of oil

Also, sometimes stray gases are generated at low temperatures below 200°C in the PD, T1, or T2 zones, and consequently may affect the correct detection of these faults [99]. Although the main Duval triangle 3 shows faults in T3 region for both oil types, for analysis purpose Duval triangle 6 for low-temperature faults (LTF) is considered for further study. Duval triangle 6 is presented in Figure 2.11 and it uses the low-energy gases (H_2, CH_4, and C_2H_6) for the analysis. It is seen that for FR3, fault detection for all ageing durations is in the stray gassing zone S, however, for JAT, the fault detection zone is the overheating zone O. All these cases are depicted in Table 2.5.

2.5.4 Total dissolved combustible gases (TDCG)

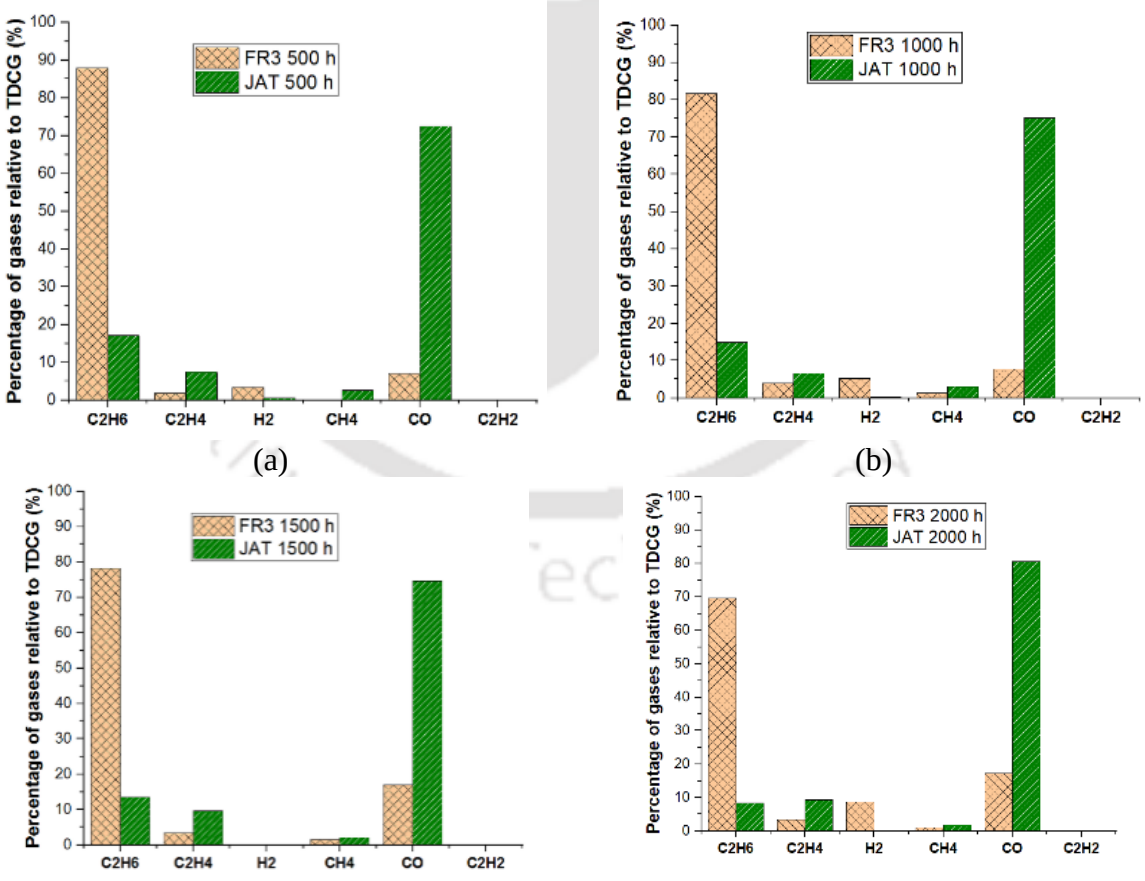

Figure 2.12: Relative percentages of dissolved combustible gases for both FR3 and JAT samples at different hours of ageing (a) 500 hours (b) 1000 hours (c) 1500 hours, and (d) 2000 hours.

TH-2868_156302003

The severity of faults is majorly attributed to the 7 major gases. However, it is desirable to identify a single gas which contributes majorly to the incipient fault in the transformer. Considering the total dissolved combustible gas (TDCG), an assessment may be done as to which gas comprises the major portion of the total concentration of gases. Figure 2.12 compares the gas concentrations of FR3 and JAT oils at different ageing durations in the presence of solid insulation at 150^{o}C. The concentration of CO has increased with ageing duration due to the inclusion of cellulosic paper. The generation of CO is less in FR3 than in JAT, suggesting that they may be shielding the paper insulation. However, the concentration of C_2H_6 is higher in FR3, and this gas also constitutes the major portion of TDCG. This also indicates that C_2H_6 must be taken into account when analyzing thermal faults for all types of insulating liquids, as it is present in considerable amount. Also, it is observed that H_2 concentration is more in FR3, which may due to stray gassing in the oil. For JAT, the concentration of H_2 is negligible, and thus it is less prone to stray gassing than FR3.

2.5.5 Regression models for TDCG

Regression analysis is a statistical modelling technique to forecast the behaviour of a set of data with one independent and one dependent variable. There may also be more numbers of independent variables. In this work, the ageing time is considered as the independent variable, and the TDCG is considered as the dependent variable, as the concentrations of gas generations vary with the ageing time. A 2-degree polynomial regression is considered for the data, as it gives the best result relating to the data. The polynomial regression equation of 2 degrees is as follows [104]:

$$y = b_0 + b_1 x + b_2 x^2 \tag{2.3}$$

where b_0 is the intercept, b_1 and b_2 are constants, and x is the independent variable (predictor variable), and y is the dependent variable (criterion variable). Here, y denotes the concentration of TDCG in ppm and x denotes ageing time in hours. The regression models for FR3 and JAT are observed in Figure 2.13.

Considering the matrix form,

$$X = \begin{bmatrix} 1 & x_1 & x_1^2 \\ 1 & x_2 & x_2^2 \\ . & . & . \\ . & . & . \\ . & . & . \\ 1 & x_n & x_n^2 \end{bmatrix}, \quad y = \begin{bmatrix} y_1 \\ y_2 \\ . \\ . \\ . \\ y_n \end{bmatrix}, \quad b = \begin{bmatrix} b_0 \\ b_1 \\ b_2 \end{bmatrix} \tag{2.4}$$

TH-2868_156302003

$$y = Xb \tag{2.5}$$

The coefficients are calculated as follows,

$$X^T y = X^T Xb \tag{2.6}$$

$$(X^T X)^{-1} X^T y = b \tag{2.7}$$

Plotting the graphs, the following values of the regression model are achieved as given in Table 2.6. The residual sum of squares (RSS) is the sum of the square of the perpendicular deviations from individual recorded point to the fitted line. The R^2 or coefficient of determination (COD) defines how well the variation in '*y*' is explained by the variation in '*x*'. R^2 is always between 0 and 1, and the model gives the best fit when the value of R^2 is larger. By analyzing the models and implementing the equations, an estimate of the total dissolved gases over a period of time is achieved. It is observed that the TDCG increases over a period of time; however, for JAT, the TDCG is relatively lower than FR3 as time progresses, as seen in Figure 2.13. This establishes that JAT performs considerably well and holds considerable properties to be considered as a prospective alternative insulating liquid for the transformer. From Table 2.7 it is observed, that JAT has comparable properties and stable integrity to be used as an insulating liquid.

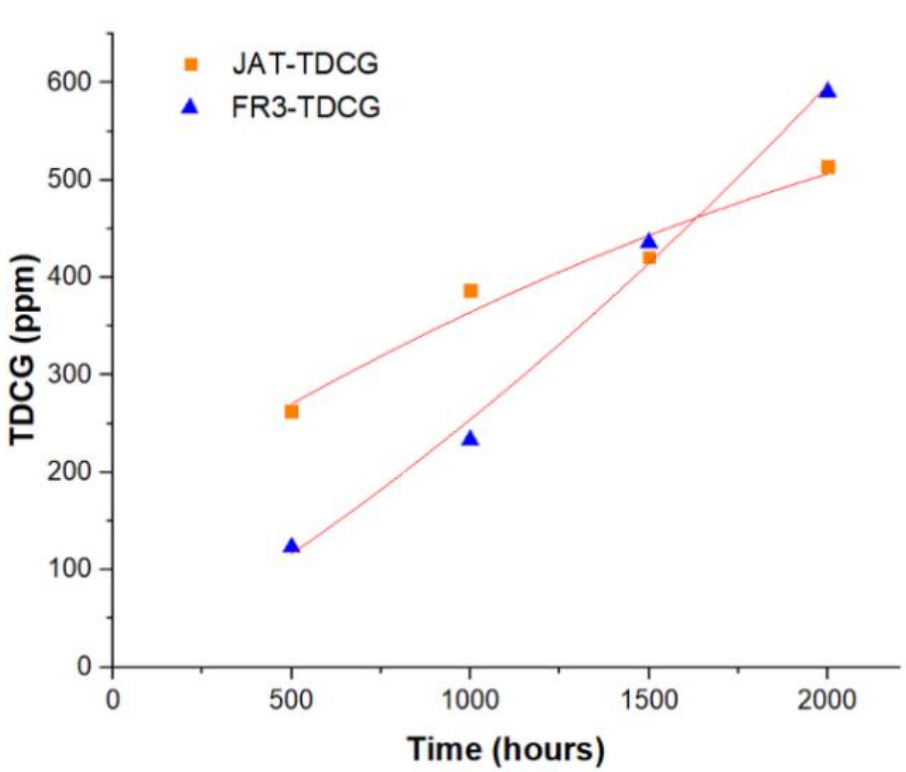

Figure 2.13: Regression model for TDCG of FR3 and JAT.

TH-2868_156302003

Table 2.6: Regression model parameters.

Parameters	FR3	JAT
b_0	0.55 ± 87.02	160.67 ± 92.93
b_1	0.21 ± 0.16	0.23 ± 0.17
b_2	(4.48 ± 6.25) x 10^{-5}	(-3.09 ± 6.676) x 10^{-5}
RSS	977.2	1114.5
R^2 (COD)	0.9925	0.9655
Adjusted R^2	0.9775	0.896

Table 2.7: Performance parameters.

Parameters	FR3	JAT
Edible/ Non-Edible	Edible	Non-Edible
Biodegradability	Biodegradable	Biodegradable
C_2H_6 generation	Higher	Lower
H_2 generation	Higher	Lower
CO and CO_2 generation	Lower	Higher
Stray gassing	More prone to stray gassing	Less prone to stray gassing

2.6 Summary of the chapter

The molecular structures of both NEOs are slightly different owing to the chemical structure. However, the types of gases generated by thermal faults in both NE oils are marginally similar. The main outcome of this work are as below:

- The oil consistency remains unaltered for 2000 hours ageing for both FR3 and JAT, as confirmed by the FTIR and NMR studies.
- FR3 generates a significant amount of C_2H_6 when thermal stress is applied. Also, the generation of H_2 in case of FR3 is higher compared to JAT, indicating FR3 is more prone to stray gassing at 150°C.
- The JAT shows a higher generation of CO and CO_2, indicating FR3 keeps the paper insulation more intact.
- The gas ratio methods are used to predict the fault types, but only the IEC method predicts the thermal faults for JAT correctly. Using the LTF Duval triangle 6, stray gassing is obtained in case of FR3 and overheating fault in case of JAT.
- It is observed that the TDCG generation for FR3 increases sharply with ageing time, which makes JAT fair better in terms of TDCG.

TH-2868_156302003

The analysis of dissolved gases for JAT under thermal ageing is not performed till now, so this study will help to investigate more into using this NEO as a substitute for the other oils, as it has the advantage of being non-edible in nature added to its higher biodegradability.

To further study the effects of ageing on the dielectric parameters, the non-invasive technique of FDS is used on the aged JAT samples and the properties of relative permittivity and the dielectric dissipation factor are studied.

भारतीय प्रौद्योगिकी संस्थान गुवाहाटी • Indian Institute of Technology Guwahati •

Note: This work, "Evaluation of dissolved gas analysis and long-term performance of non-edible natural ester," has been published in IEEE Transactions on Dielectrics and Electrical Insulation, 2020, Vol. 27, Iss. 5, pp. 1561-1569.

TH-2868_156302003

TH-2868_156302003

3

Quantitative effect of ageing on dielectric parameters

Contents

TH-2868_156302003

3.1 Introduction

The ageing of the transformer occurs majorly due to the degradation of the insulation. The byproducts, which are generated in the oil, are water and substances which are partly polarizable and ionizable in nature. The life of cellulosic insulation is calculated to be 10 years when the operating temperature is 110^{o}C [44]. However, at lower operating temperatures, the life span increases. The ageing process is significantly influenced by the moisture content, thermal stress, and type of cellulose and the acidity level of the insulating liquid. In addition to ageing, failures also occur when electrical discharges arise in the insulation. To ascertain the state of a transformer, it is important to monitor the health of the insulation system, which consists of both solid and liquid part. Many researchers have studied the PD measurements and the non-invasive measurements. However, the PD measurements are not very accurate as they are affected by high frequency noises, so the non-invasive methods like PDC and FDS techniques are preferred by the utilities [105, 106]. The PDC measurements are influenced by noise and interference and thus the estimation of parameters may not be accurate. Also, time required for measuring both polarization and depolarization currents is high [112]. The FDS technique is considered in this work for analysis, which basically processes the complex permittivity of the dielectric in a varied frequency range and helps in predictive modelling of the insulation system.

In this work, JAT is studied as it is reported to possess superior dielectric properties. However, the ageing behaviour of this oil with open beaker under thermal stress is not reported. This work aims to investigate the change in the dielectric properties of JAT by considering ageing for 500 hours in an open beaker oxidative ageing test set up. The samples are taken out at intervals of 100 hours up to 500 hours of ageing duration. The frequency domain spectroscopy analysis is carried out to see the variation in the relative permittivity and dielectric dissipation factor (tan δ) over a wide range of frequency. Also, the characterization of the oil is done by FTIR and UV-Vis spectroscopy at various ageing duration.

The statistical technique of regression modeling is used to determine the variation of the dielectric parameters with respect to ageing duration at different decades of the frequency range. An expression is developed which gives the values of the relative permittivity and tanδ with respect to frequency of excitation and ageing time. The quantitative analysis with fitting models help in ascertaining by what range the values are changing when the transformer insulation ages during its operation lifetime, by considering aged samples up to 500 hours.

TH-2868_156302003

The development of this novel ageing regression model by using the FDS measurement technique combined with the ageing assessment helps to analyze the insulating oil samples. Since the chemical degradation and the dielectric integrity of the insulating oil are interrelated, this analysis is important. The FDS technique method helps in condition monitoring of any dielectric, however the reported works are not much focused on the relation of the ageing duration with the dielectric parameters and how it alters the integrity of the oil. Thus, this study will give a new insight into the usage of FDS measurement technique combined with the ageing assessment and help analyze the insulating oil samples.

In this work, section 3.2 deals with the materials and methods, the concept behind FDS is addressed in section 3.3, section 3.4 focuses on the results and discussions; section 3.5 establishes a quantitative relationship between ageing duration and the dielectric properties and the conclusions are included in section 3.6.

3.2 Materials and methods

The properties of insulation are dependent on many factors such as frequency, time, temperature, moisture and the inherent nature of the material itself [107-109]. The basic properties of MO and JAT are given in Table 2.1 of chapter 2. As seen from the table, JAT has superior thermophysical and electrical properties compared to MO, therefore JAT is considered for the present study. The relative permittivity and the tan δ are the critical properties to look for when analyzing the condition of the particular dielectric. So, in this work open beaker oxidative ageing of JAT is carried out and the variation of frequency response with ageing time is analyzed. Also, the characterization of the oil is done by FTIR and UV-Vis spectroscopy at various ageing duration.

3.2.1 Ageing of the oil

The ageing effect on JAT is achieved with an open beaker oxidative ageing apparatus developed in the laboratory as per ASTM D1934 [149]. This ageing oven shown in Figure 3.1 comprises of 4 open beakers, each with volume capacity of 300 ml. It also has a timer and a temperature controller. The stand with the 4 open beakers is rotated at 2 rpm with the aid of a motor fixed below. An equivalent amount of solid insulation, plus a copper catalyst is placed in the oil samples. The oven temperature is kept constant at 115±1^{o}C and ageing is carried out for duration of 500 hours maintaining a uniform ageing environment. The JAT samples are collected after ageing of each batch of samples for 100, 200, 300, 400 and 500 hours. The samples are then taken for conducting the further analysis.

TH-2868_156302003

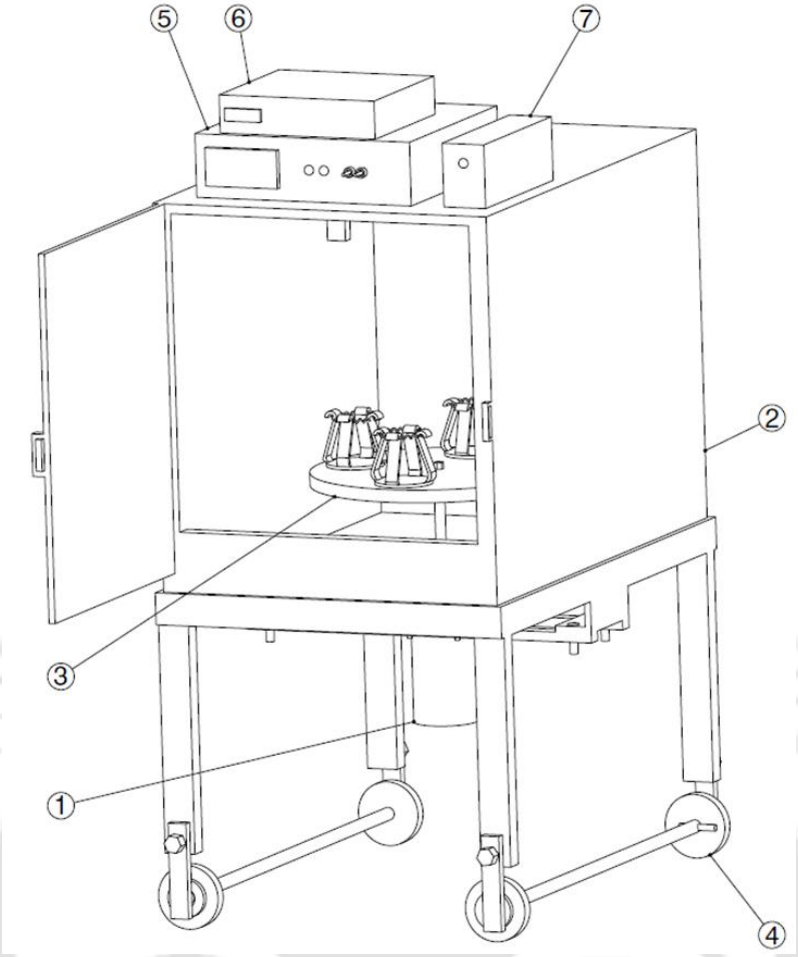

(a)

(b)

Figure 3.1: (a) Schematic diagram of the oxidative ageing complete setup and (b) the oxidative ageing complete setup developed in laboratory.

TH-2868_156302003

The operating conditions of the transformer is responsible for ageing of the TO, which experience thermal, chemical and electrical stress causing alteration in its properties. The ageing stress on the TO and the presence of polar contaminants in the oil accelerates the degradation process in the oil. Ageing by-products such as acids, oxides, sludge, and moisture are generated which further accelerate the ageing of oil and hence service life of the transformer decreases. Thus, ageing study is important to analyze the integrity of the insulating liquid. The different parts of the oxidative ageing setup developed in the laboratory for ageing study of JAT are described in the Table 3.1.

Table 3.1: Different functional parts of the oxidative ageing test set up as in Fig. 3.1.

Parts of the oxidative ageing	Description
1	DC motor attachment with driven shaft
2	Hot air oven with temperature sensor, where the samples are kept for testing
3	The beaker stand to hold the sample for testing, which is placed inside the oven
4	The oven stand which is drafted in such a way, that it can hold the motor
5	Temperature controller and indicator
6	Speed and a time control unit containing relay module, DC driver and Arduino boards.
7	The UPS for power backup to the Arduino UNO boards and DC driver.
8	The coupler link fitted with the beaker stand with driver shaft

3.2.2 Experimental setup for FDS

For measuring the frequency response of the oil samples, a frequency response analyzer (Solartron 1260A) in conjunction with a dielectric interface (Solartron 1296A) is considered as seen in Figure 3.2. An alternating voltage is applied to the oil sample in an electrode configuration. On the application of an external field, one part of energy is put in storage by the capacitance, and other part is dissipated by the resistance effects. The frequency range considered is from 10^0 to 10^5 Hz. The data is recorded by using the SMaRT software. Impedance spectroscopy is a widespread procedure for investigating dielectrics by

TH-2868_156302003

determining the electrical impedance over a wide frequency range. This impedance is associated with the capacitance and conductivity of the dielectric, and these attributes, in turn, are connected to the molecular motion in the dielectric. The experiments are carried out at ambient temperature.

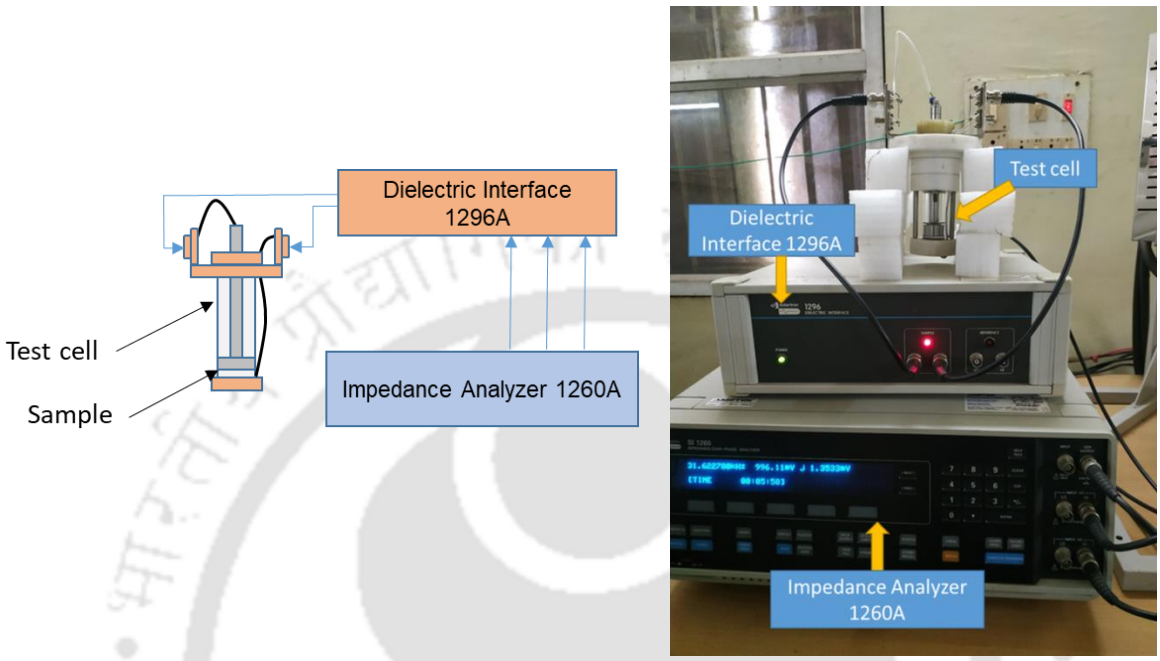

(a) (b)

Figure 3.2: (a) Schematic diagram for FDS test and (b) FDS set up.

3.2.3 Ultraviolet Visible (UV-Vis) spectroscopy

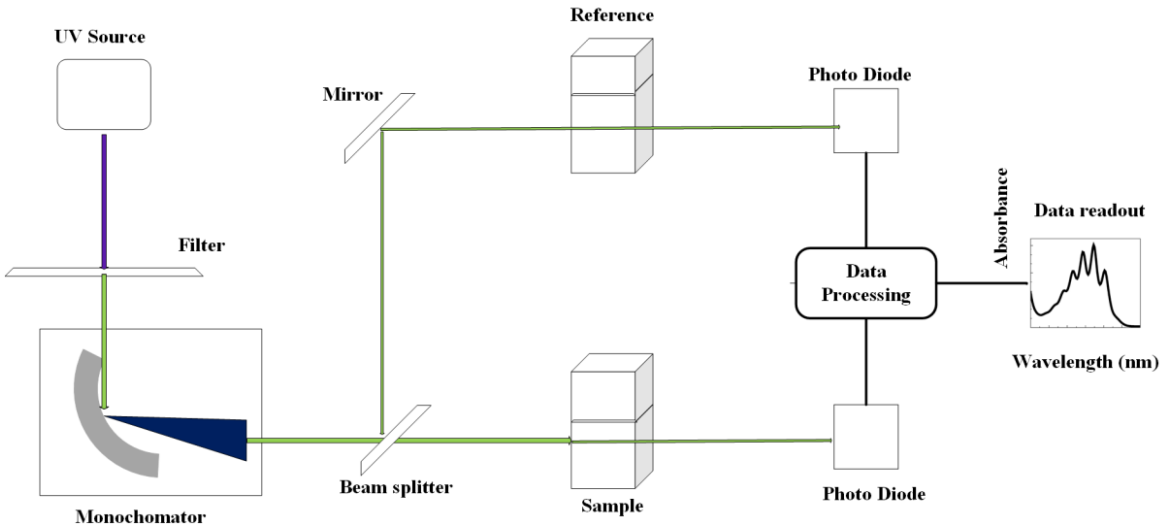

Figure 3.3: Mechanism of UV-Vis spectroscopy.

TH-2868_156302003

The UV-Visible absorption spectra of JAT at all ageing durations are obtained using Agilent Technologies, Model: Cary 100 UV-Vis spectrophotometer. In this kind of absorption spectroscopy, light of the UV-Vis region 350-800 nm is absorbed by the molecule which excites the electrons from the ground state to higher energy state. This method helps to analyze the ageing process of the insulating liquid. The mechanism of UV-Vis spectroscopy is depicted in Figure 3.3. The instrument has a UV-Vis source, a monochromator, a beam splitter, a mirror to get the beam to a reference sample, the sample under analysis and a detector. The reference and sample are kept in two quartz cuvettes. The light emitted from the monochromator is split into two beams: one is the reference beam and another is the sample beam. Each beam enters the sample chamber through separate optical paths. The reference beam intensity is taken as 100% Transmittance (or zero Absorbance), and the measurement is displayed as the ratio of the sample beam to the reference beam. The photo diodes are the detectors which are used to measure the transmitted or reflected light from a sample and convert it into a signal. The transmittance represents how much light is absorbed at each wavelength and the highest peak is observed for qualitative analysis of the samples. From the transmittance (T), the absorbance can be calculated as A=-log (T). An absorbance spectrum is obtained for the material at different wavelengths. The amount of absorbance at any wavelength is attributed to the chemical structure of the molecule.

The UV-Vis spectroscopy follows the Beer-Lambert law, which states that the absorbance of the solution is proportional to the concentration and the path length. This enables the concentration of a solution to be calculated by measuring its absorbance. If the path length is constant, UV-Vis spectroscopy defines the concentration of the absorber in any fluid. The absorbance varies with concentration and colour variation of the sample. The Beer-Lambert law is given in (3.1),

$$Abs = \log_{10}\left(\frac{I_o}{I_t}\right) = \varepsilon_{abs} cL \tag{3.1}$$

where Abs is the measured absorbance, I_o is the incident light intensity at a given wavelength, I_t is the transmitted light intensity, L is the length of the cuvette, and c is the concentration of the sample. ε_{abs} is the molar absorptivity or extinction coefficient.

TH-2868_156302003

3.3 Frequency domain spectroscopy (FDS)

Measuring the dielectric properties at a particular frequency is not sufficient to assess the overall condition of the dielectric. Therefore, FDS provides an insight into the variation of the dielectric properties over a wide range of frequencies. On application of a voltage across the dielectric, the charges orient themselves forming dipoles with positive and negative charges, ± q which are separated by a distance d. The dipole moment is given by $\mu_c = \alpha_0 E = qd$, where α_0 is the "polarizability" of the dielectric and E is the applied field. Depending on the nature of the material, the polarization will vary and so will the polarizability. This permanent dipole is formed because of the interactions between dissimilar atoms in a molecule. The dipoles are randomly oriented within the dielectric, when there is no external field. The dielectric polarization results because of the orientation of both types of charges in the material, on application of an electric field. The charges are confined within the material, so there is no probability of inherent conduction. The dielectric response methods are used to study the interactions between the fundamental electric quantities [46].

The polarization vector $\boldsymbol{P}$ and the electric field $\boldsymbol{E}$ of a dielectric material are related as in (3.2),

$$\boldsymbol{P} = \chi \varepsilon_0 \boldsymbol{E} \tag{3.2}$$

where χ is the electric susceptibility of the dielectric, which explains all kinds of polarization processes within the dielectric and ε_0 is the permittivity of free space. In any dielectric material, χ is always a positive number, hence reducing the value of $\boldsymbol{E}$, will lead to depolarization or relaxation process. This process happens with a delay relative to the decrease in $\boldsymbol{E}$. Thus, it is essential to analyze the behaviour of the dielectrics in time as well as frequency domain. In this work, only the frequency domain response of the insulating liquid is studied.

In any dielectric, the electric displacement $\boldsymbol{D}$ is given by,

$$\boldsymbol{D} = \varepsilon_0 \boldsymbol{E} + \boldsymbol{P} = \varepsilon_0 (1 + \chi) \boldsymbol{E} \tag{3.3}$$

Further, the complex dielectric displacement is directly related to the complex relative permittivity $\varepsilon_r^*(\omega)$,

$$\boldsymbol{D}(\omega) = \varepsilon_0 \varepsilon_r^*(\omega) \boldsymbol{E}(\omega) \tag{3.4}$$

where
$$\varepsilon_r^*(\omega) = \varepsilon_r'(\omega) - i\varepsilon_r''(\omega) \tag{3.5}$$

In (3.5), ε_r' is the real part of relative permittivity and ε_r'' is the imaginary part of relative permittivity. The ε_r'' is given by,

$$\varepsilon_r''(\omega) = \varepsilon_p''(\omega) + \frac{\sigma_{dc}}{\omega \varepsilon_0} \tag{3.6}$$

TH-2868_156302003

The ε_r'' is divided into two terms: ε_p'' which denotes the absorption and dissipation associated with the dielectric relaxation processes and $\sigma_{dc}/\omega\varepsilon_0$ denotes the dissipation of energy associated with ionic and charge transport. Substituting (3.6) in (3.5), $\varepsilon_r^*(\omega)$ is achieved as,

$$\varepsilon_r^*(\omega) = \varepsilon_r'(\omega) - i\left[\varepsilon_p''(\omega) + \frac{\sigma_{dc}}{\omega\varepsilon_0}\right] \tag{3.7}$$

and the dielectric dissipation factor, tan δ is given by,

$$\tan\delta = \frac{\varepsilon_r''(\omega)}{\varepsilon_r'(\omega)} = \frac{\varepsilon_p''(\omega) + \frac{\sigma_{dc}}{\omega\varepsilon_0}}{\varepsilon_r'(\omega)} \tag{3.8}$$

3.4 Results and discussion

The complex permittivity of any dielectric material defines the dielectric properties, i.e. the ability of the material to accumulate electrical energy, on the application of an external electric field. Under the effect of a voltage source, the dielectric material will polarize. The extent of polarization varies for different materials at different frequencies. This process depends on the integrity of the material, like, what quantity of polar contaminants is present, ageing of the dielectric, moisture, temperature and their relaxation mechanisms.

3.4.1 Relative permittivity

The real part ε_r' is the measure of how much energy is stored by the material, the ε_r'' represents how dissipative a material can be in reaction to an external electric field. The complex relative permittivity is given by (3.5).

The oil samples showed increase in the relative permittivity with more ageing duration as seen in Figure 3.4. This is related to the existence of polar contaminants and other ageing byproducts. These byproducts affect the dielectric losses and thus the overall values increase at low frequency regions for aged oils. The loss component also intensifies because of the presence of polarizable elements in the dielectric, which in turn increases the conductivity of the dielectric. These elements may originate from the cellulosic paper, oil degradation, and dissolved gas generation in the transformer oil. Figure 3.5 shows the variation of relative permittivity magnitude with both frequency and ageing time. For a clear indication of the byproducts generated due to ageing, total acid number (TAN) and moisture content are given for each ageing durations in Table 3.2. The acids present majorly comprise of low and high molecular weight acids. These acids are namely, formic acid, acetic acid, levulinic acid, oleic acid, linoleic acid, palmitic acid, and stearic acid [110].

TH-2868_156302003

Table 3.2: Total acid number and moisture content.

Ageing duration	TAN (mgKOH/g)	Moisture (ppm)
JAT-0 hr	0.257	650
JAT-100 hrs	0.261	723
JAT-200 hrs	0.263	795
JAT-300 hrs	0.266	844
JAT-400 hrs	0.270	912
JAT-500 hrs	0.272	988

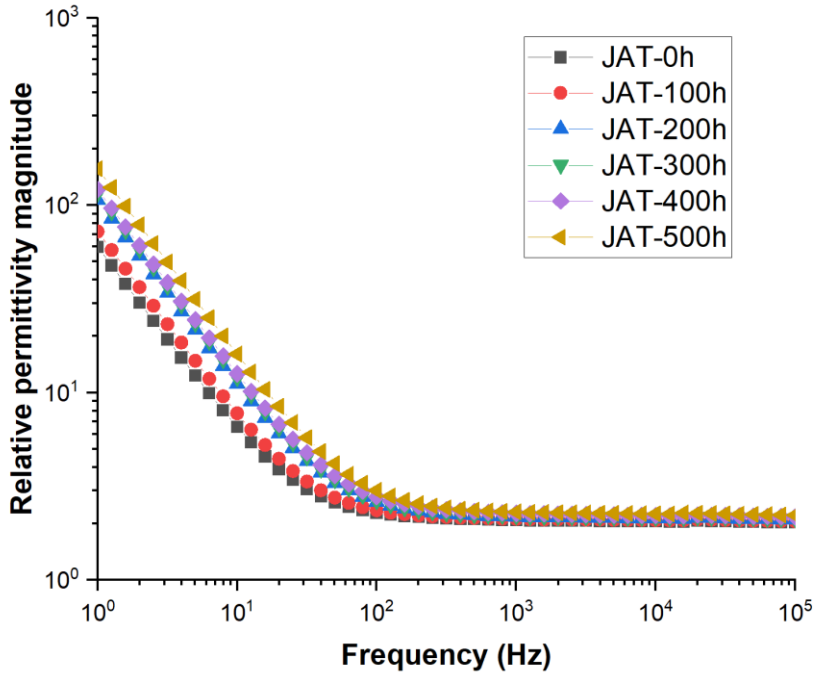

Figure 3.4: Variation of relative permittivity magnitude with frequency.

The changes in the permittivity values originate by the presence of polarizable or ionizable ageing byproducts within the dielectric. When the oil degradation occurs and the hydrocarbon chains dissociate, free radicals are generated in the oil. The collisions of the free radicals produce large masses of colloidal decay products, which are not soluble in oil and precipitate as sludge. Researchers noticed that ageing leads to higher amounts of polarization and depolarization currents, which in turn leads to higher permittivity, more so, in the lower frequency ranges [111].

TH-2868_156302003

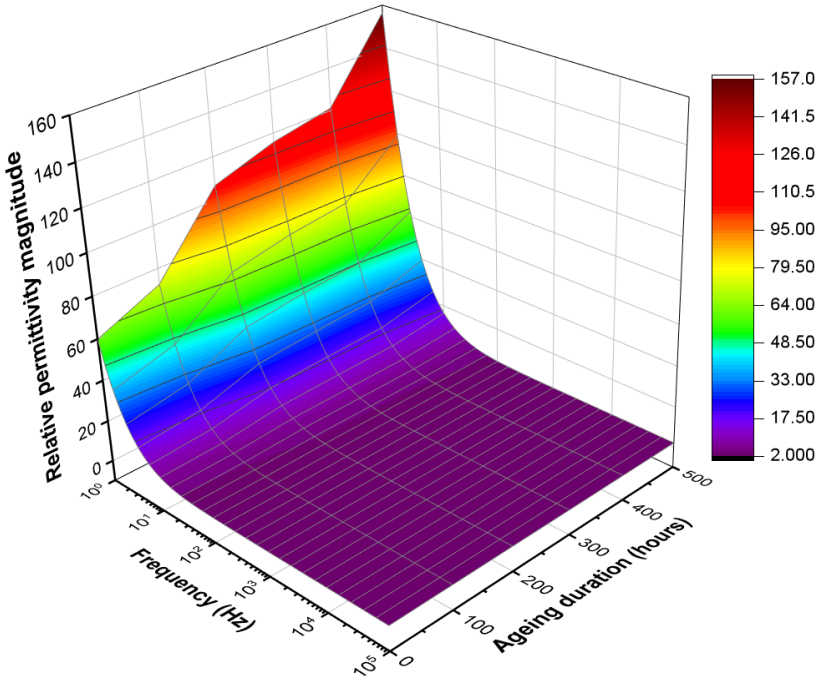

Figure 3.5: Variation of relative permittivity with frequency and ageing duration.

It is observed that the permittivity values are not much dependent on frequency above 10 kHz. However, at lower values of frequency the charge carriers react faster when there is an applied electric field. This results in a greater value of ε_r. At higher frequency ranges, the charge carriers do not have enough time to react to the quick variations in the applied electric field, which results in lower values of ε_r. This variation of the permittivity values with respect to frequency of the application of field is explained based on the polarization processes as below,

i. The electronic polarization occurs due to the displacement of the negative electron cloud of the atom with respect to the positive nucleus. Consequently, the atoms obtain the electric dipole moment, and finally each atom is characterized by an electronic polarizability. The electrons are light in weight and hence they have rapid response to the change in field. This process is fast and happens in the optical frequency range.

ii. The ionic polarization activates a relative displacement between the positive and the negative ions, and this phenomenon happens up to infrared frequency range. In this case of polarization, when atoms or ions in a set of molecules are exposed to an external electric field, they experience displacements from their equilibrium positions, giving rise to ionic or atomic polarizability. The significantly higher mass of ions or atoms compared to electrons leads to a considerably slower polarization process relative to electronic polarization. However, both processes are regarded as “fast,” compared to other

TH-2868_156302003

polarization processes as they are characterized by low relaxation times.

iii. The orientational or dipolar polarization arises when the permanent dipoles of the molecules orient in the direction of the applied field. This process happens up to MHz range.

iv. The interfacial or space charge polarization is a very slow process and responsible for permittivity changes at low frequency values. This process is generally active in the power frequency range and below.

3.4.2 Dielectric dissipation factor (tan δ)

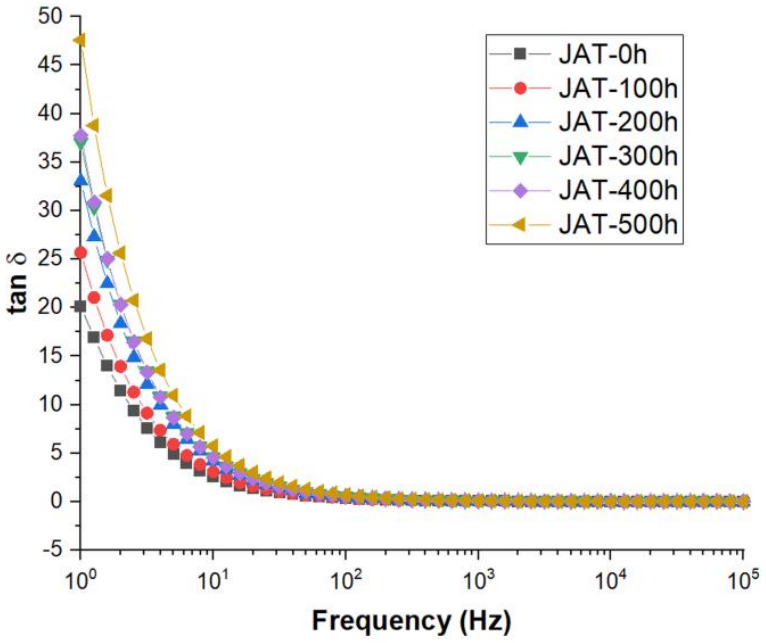

Figure 3.6: Variation of tan δ with frequency.

It is observed from the Figure 3.6, that the dielectric losses (tan δ) increase with ageing duration. This explains the moisture effect on the frequency domain spectra of the dielectric. The pattern of tan δ is much comparable to the permittivity magnitude. The dielectric loss obtained increases rapidly at lower levels of frequency, while being almost constant at higher frequencies. This behaviour of dielectric loss with respect to frequency establishes the fact that the ions travel in the interior the dielectric at low frequency values. The conduction losses are mainly associated with the movement of ions over substantial lengths. These ions leap over the highest barriers and as they move, some of their energy is given to the lattice as heat, which accounts for the dissipation of electrical energy as heat. Figure 3.7 gives the surface showing the variation of tan δ with both frequency and ageing duration.

TH-2868_156302003

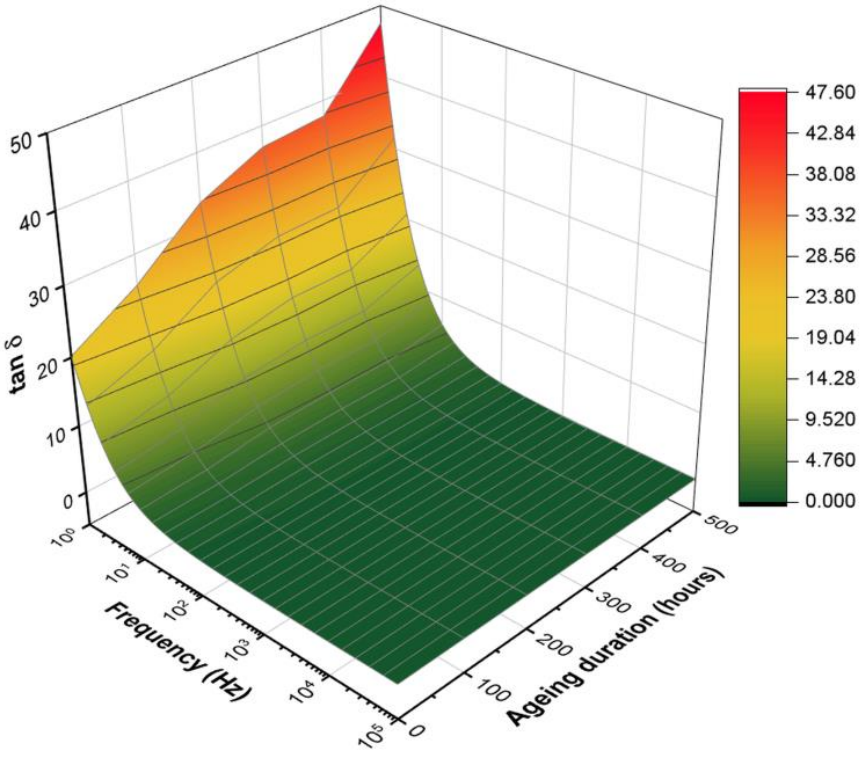

Figure 3.7: Variation of tan δ with frequency and ageing duration.

3.4.3 FTIR spectroscopy

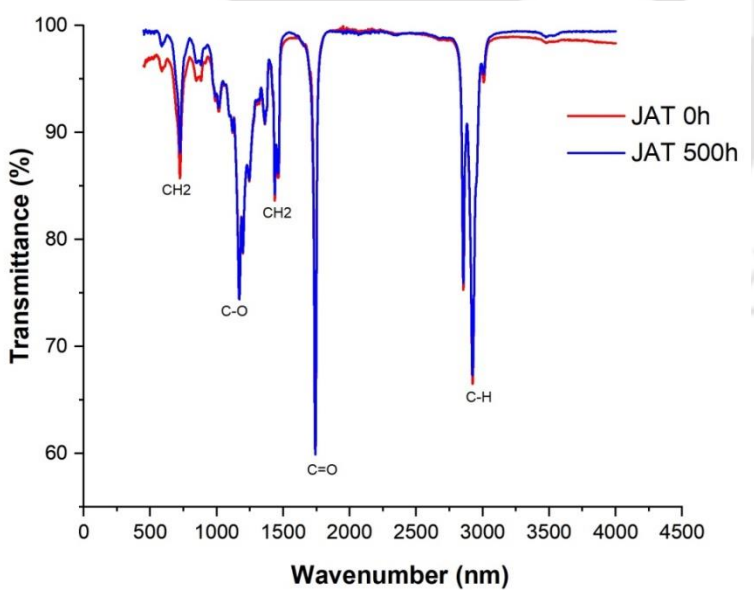

Figure 3.8: FTIR spectrum of fresh JAT and aged JAT for 500 hours.

It is observed from the FTIR study that the transmittance of the JAT is nearly unaffected after 500 hours of ageing. From Figure 3.8, two peaks are observed at wavenumbers of 2924 cm^{-1} and 2854 cm^{-1}, indicating the presence of C-H stretching for the existence of alkanes for both fresh and aged oil samples. The C=O stretching is observed at

TH-2868_156302003

the wavenumber of 1742 cm^{-1}. Some indication of CH_2 bending is there at wavenumber 1460 cm^{-1}. C-O stretching at wavenumbers of 1000-1260 cm^{-1} is observed indicating alcohol. The formation of carbonaceous particles is imperative with ageing for longer durations. However, the oil integrity is unharmed as all the functional groups exist even after 500 hours of ageing for JAT.

3.4.4 UV-Vis spectroscopy

It is observed from the Figure 3.9 that the fresh oil samples do not show any absorbance band. This technique helps to analyze the ageing process of the insulating liquid. At 100 hours ageing, a strong absorbance is observed for the JAT at 417 nm. Similarly, absorbance peaks are observed at 432, 445, 452 and 467 nm for JAT at 200, 300, 400 and 500 hours respectively. A steady red shift (Bathochromic Effect) is noticed in the maximum absorption as ageing time progresses. The change of colour happens because of ageing of the oil and the deposition of contaminants, and thus the spectra shows high absorbance peaks for more aged oils.

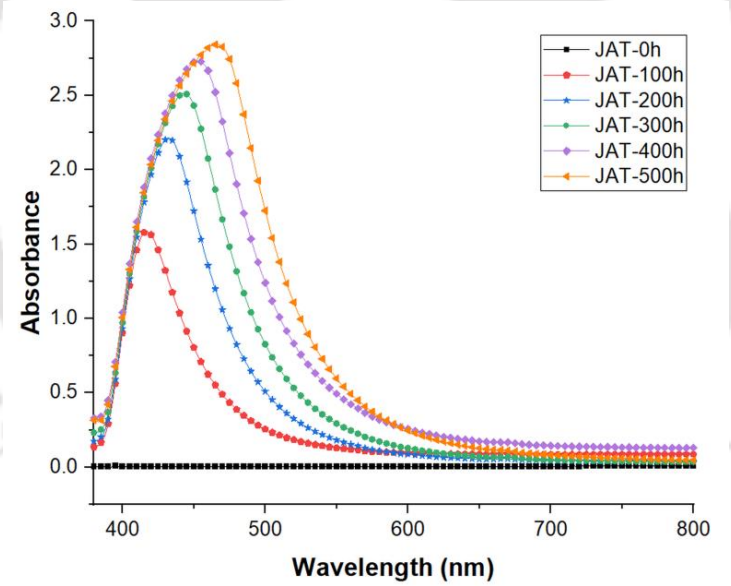

Figure 3.9: UV-Vis analysis of JAT for five different ageing durations along with fresh oil.

3.5 Quantitative effect of ageing duration

The ageing mechanism and the time duration play a major role in the variation of the dielectric properties with changing frequency. To understand the quantitative effect of ageing duration on the dielectric properties, statistical modeling is carried out on all parameters with respect to changing frequency and ageing time. The statistical analysis which is considered in

TH-2868_156302003

this work helps to predict the increase or decrease of a dependent variable with respect to another independent variable.

In this study, the duration of ageing in hours is considered as the independent variable, and the dielectric parameters at decades of frequency are considered as the dependent variable, as they change with the duration. The polynomial regression equation considered in the analysis is as follows:

$$y = b_0 + b_1 x + b_2 x^2 + b_3 x^3 + b_4 x^4 \tag{3.9}$$

where, b_0 is the intercept, b_1, b_2, b_3 and b_4 are coefficients, and x is the independent variable, also called the predictor variable, and y is the dependent variable, also called the criterion variable. Here, y denotes the dielectric parameters and x signifies the ageing time in hours. The regression models for permittivity and tan δ values are observed in Figure 3.10 and 3.11 respectively.

Considering the matrix form,

$$X = \begin{bmatrix} 1 & x_1 & x_1^2 & x_1^3 & x_1^4 \\ 1 & x_2 & x_2^2 & x_2^3 & x_2^4 \\ . & . & . & . & . \\ . & . & . & . & . \\ . & . & . & . & . \\ 1 & x_n & x_n^2 & x_n^3 & x_n^4 \end{bmatrix}, \quad y = \begin{bmatrix} y_1 \\ y_2 \\ . \\ . \\ . \\ y_n \end{bmatrix}, \quad b = \begin{bmatrix} b_0 \\ b_1 \\ b_2 \\ b_3 \\ b_4 \end{bmatrix} \tag{3.10}$$

$$\text{and, } y = Xb \tag{3.11}$$

The coefficients values are obtained by,

$$X^T y = X^T X b \tag{3.12}$$

$$(X^T X)^{-1} X^T y = b \tag{3.13}$$

The values of the statistical model achieved are given in Tables 3.3 and 3.4. The residual sum of squares (RSS) is the sum of the squared distances between your actual versus your predicted values. The R^2 or coefficient of determination (COD) always lies between 0 and 1, and its value tending towards 1 gives a better fit to the model.

TH-2868_156302003

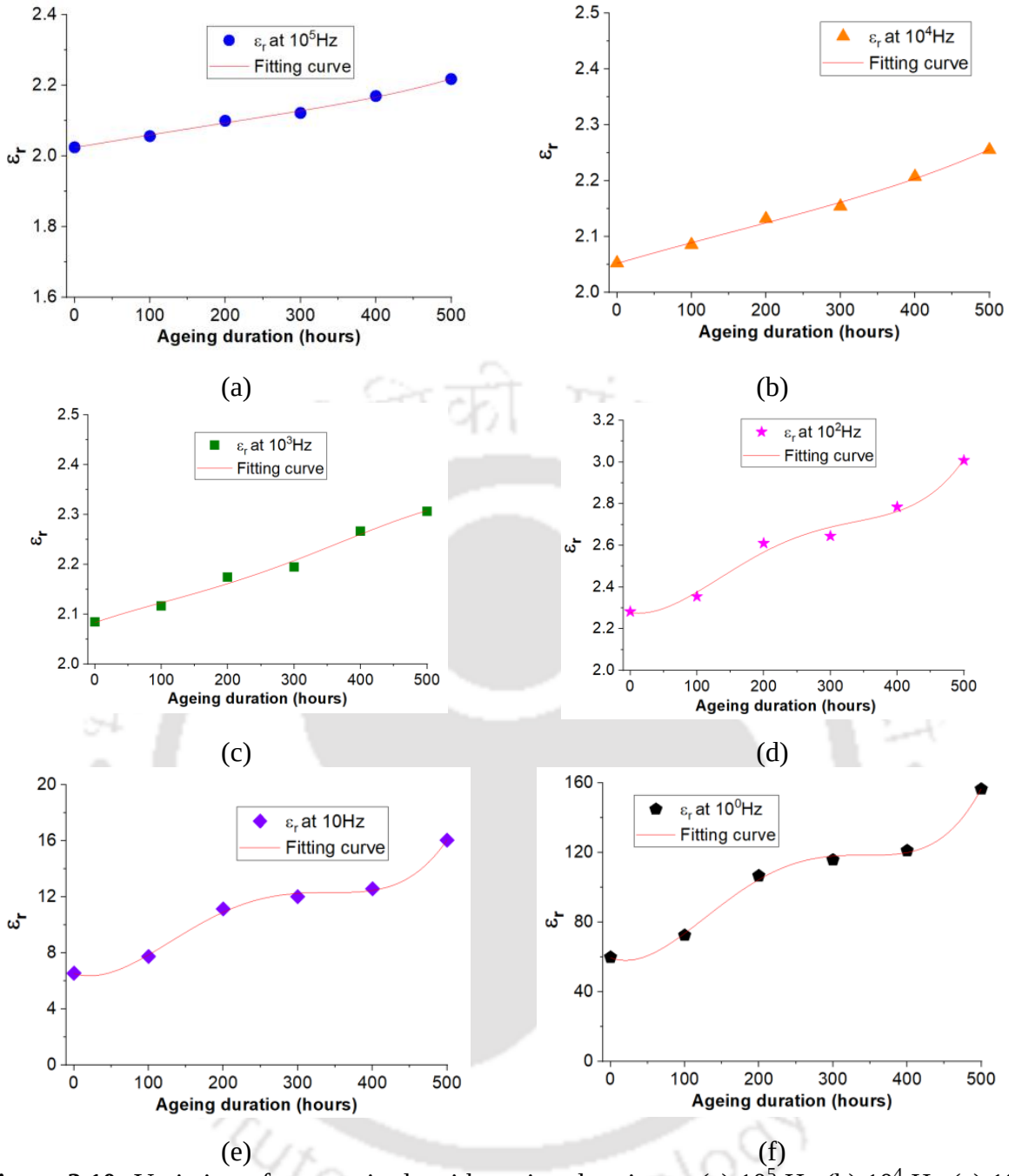

Figure 3.10: Variation of ε_r magnitude with ageing duration at (a) 10^5 Hz (b) 10^4 Hz (c) 10^3 Hz (d) 10^2 Hz (e) 10^1 Hz and (f) 10^0 Hz.

By analyzing the models and implementing the equations, the permittivity and tan δ values over a period of time are achieved and it is noted that these values rise with ageing time. At lower frequencies, this increase is more evident. To predict the behaviour of these parameters at other ageing durations, the curve fitting is done to obtain the regression models of all the parameters at decade frequencies, which closely relates to the other frequencies of that range. Considering all the coefficients and the intercept, and ignoring the minimal errors, they are further calculated as,

TH-2868_156302003

$$b_k = A_k e^{(-(f-p_k)/q_k)} + C_k \tag{3.13}$$

where A_k, p_k, q_k, C_k are constants, and f is the frequency. The values of the constants for relative permittivity and tan δ are given in Tables 3.5 and 3.6 respectively.

Equation (3.14) is applicable for ε_r along with tan δ. By combining all the major equations, an associative relationship among the parameters, ageing time and frequency is achieved as follows:

$$y(f,x) = \sum_{k=0}^{4} (A_k e^{(-(f-p_k)/q_k)} + C_k) x^k \tag{3.14}$$

Table 3.3: Model parameters for ε_r magnitude w.r.t ageing at different frequencies.

Parameters	10^5 Hz	10^4 Hz	10^3 Hz	10^2 Hz	10^1 Hz	10^0 Hz
Intercept, b_0	2.02	2.05	2.08	2.27	6.53	59.6
b_1	3.51×10^{-4}	3.88×10^{-4}	4.63×10^{-4}	-5.18×10^{-4}	-0.0165	-0.1606
b_2	8.91×10^{-8}	-2.04×10^{-7}	-1.03×10^{-6}	2.17×10^{-5}	4.37×10^{-4}	4.41×10^{-3}
b_3	-8.33×10^{-10}	3.29×10^{-10}	4.25×10^{-9}	-7.54×10^{-8}	-1.56×10^{-6}	-1.58×10^{-5}
b_4	1.61×10^{-12}	3.16×10^{-13}	-4.47×10^{-12}	7.98×10^{-11}	1.65×10^{-9}	1.68×10^{-8}
RSS	9.29E-05	1.32E-04	4.11E-04	0.00462	0.13915	12.27998
R^2 (COD)	0.99635	0.99534	0.98867	0.98728	0.99766	0.99799
Adjusted R^2	0.98177	0.9767	0.94333	0.93639	0.98828	0.98997

Table 3.4: Model parameters for tan δ w.r.t ageing at different frequencies.

Parameters	10^5 Hz	10^4 Hz	10^3 Hz	10^2 Hz	10^1 Hz	10^0 Hz
Intercept, b_0	0.0137	0.01168	0.0499	0.32688	2.55478	20.17965
b_1	2.714×10^{-6}	1.596×10^{-5}	-5.39×10^{-5}	-7.93×10^{-4}	-6.22×10^{-3}	-2.73×10^{-3}
b_2	3.71×10^{-9}	-4.724×10^{-9}	1.85×10^{-6}	2.00×10^{-5}	1.68×10^{-4}	8.60×10^{-4}
b_3	0	0	-6.36×10^{-9}	-7.14×10^{-8}	-6.09×10^{-7}	-3.32×10^{-6}
b_4	0	0	6.49×10^{-12}	7.50×10^{-11}	6.47×10^{-10}	3.66×10^{-9}
RSS	3.93×10^{-7}	3.2×10^{-6}	4.56×10^{-5}	2.31×10^{-4}	3.51×10^{-4}	0.17549
R^2 (COD)	0.9038	0.9103	0.97123	0.99755	0.99995	0.99963
Adjusted R^2	0.8398	0.8505	0.85615	0.98775	0.99973	0.99813

TH-2868_156302003

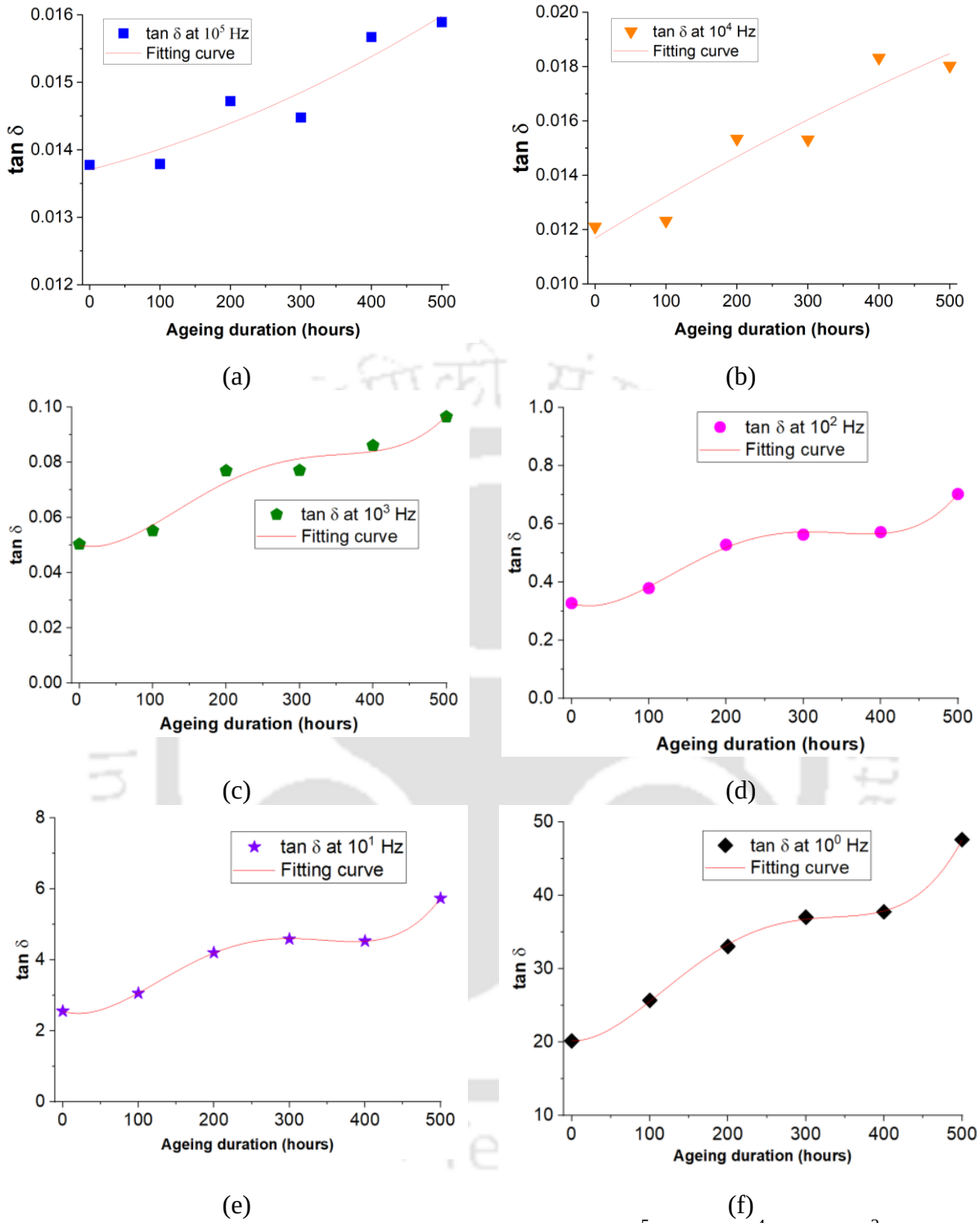

Figure 3.11: Variation of tan δ with ageing duration at (a) 10^5 Hz (b) 10^4 Hz (c) 10^3 Hz (d) 10^2 Hz (e) 10^1 Hz and (f) 10^0 Hz.

TH-2868_156302003

Table 3.5: Model parameters for b_0 to b_4 for ε_r magnitude w.r.t different frequencies.

Parameters	b_0	b_1	b_2	b_3	b_4
C_k	2.109	$1.17\text{x}10^{-4}$	$5.13\text{x}10^{-4}$	$-1.79\text{x}10^{-8}$	$1.93\text{ x }10^{-11}$
p_k	-22.81	-22.83	-21.48	-21.56	-21.59
A_k	76.55	-0.206	0.0057	$-2.04\text{x}10^{-5}$	$2.17\text{x}10^{-8}$
q_k	3.509	3.97	3.876	3.870	3.866

Table 3.6: Model parameters for b_0 to b_4 for tan δ w.r.t different frequencies.

Parameters	b_0	b_1	b_2	b_3	b_4
C_k	0.10054	$4.68\text{x}10^{-5}$	$5.47\text{x}10^{-6}$	$-1.94\text{x}10^{-8}$	$2.03\text{x}10^{-11}$
p_k	-22.40	62.18	-21.67	-4.41	-4.359
A_k	25.36	-0.00461	0.00103	$-3.99\text{ x}10^{-6}$	$4.42\text{x}10^{-9}$
q_k	4.281	84.57	5.424	5.226	5.116

The detailed steps followed to obtain the mathematical model are provided in the flowchart given in Figure 3.12.

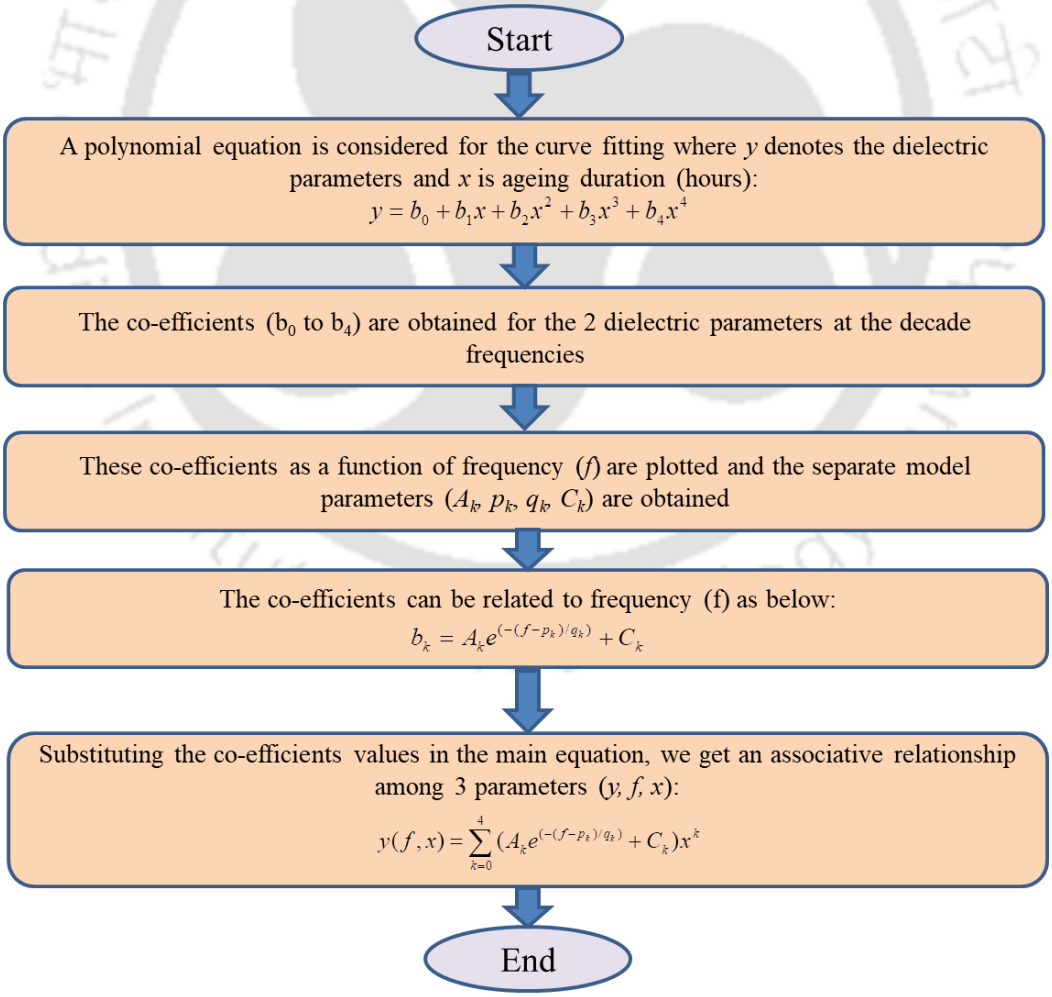

Figure 3.12: Flowchart for obtaining the mathematical model.

TH-2868_156302003

A correlation between variables signifies that the variation in one variable tends to change the value of the other variable in a specific direction. This relationship is useful as the value of one variable can be used to predict the value of the other variable. The relative permittivity curve for the frequency range from 10^0 to 10^5 Hz is being considered for all the ageing duration and correlation is implemented to assess the ageing effect at different durations of open beaker ageing over the given frequency range.

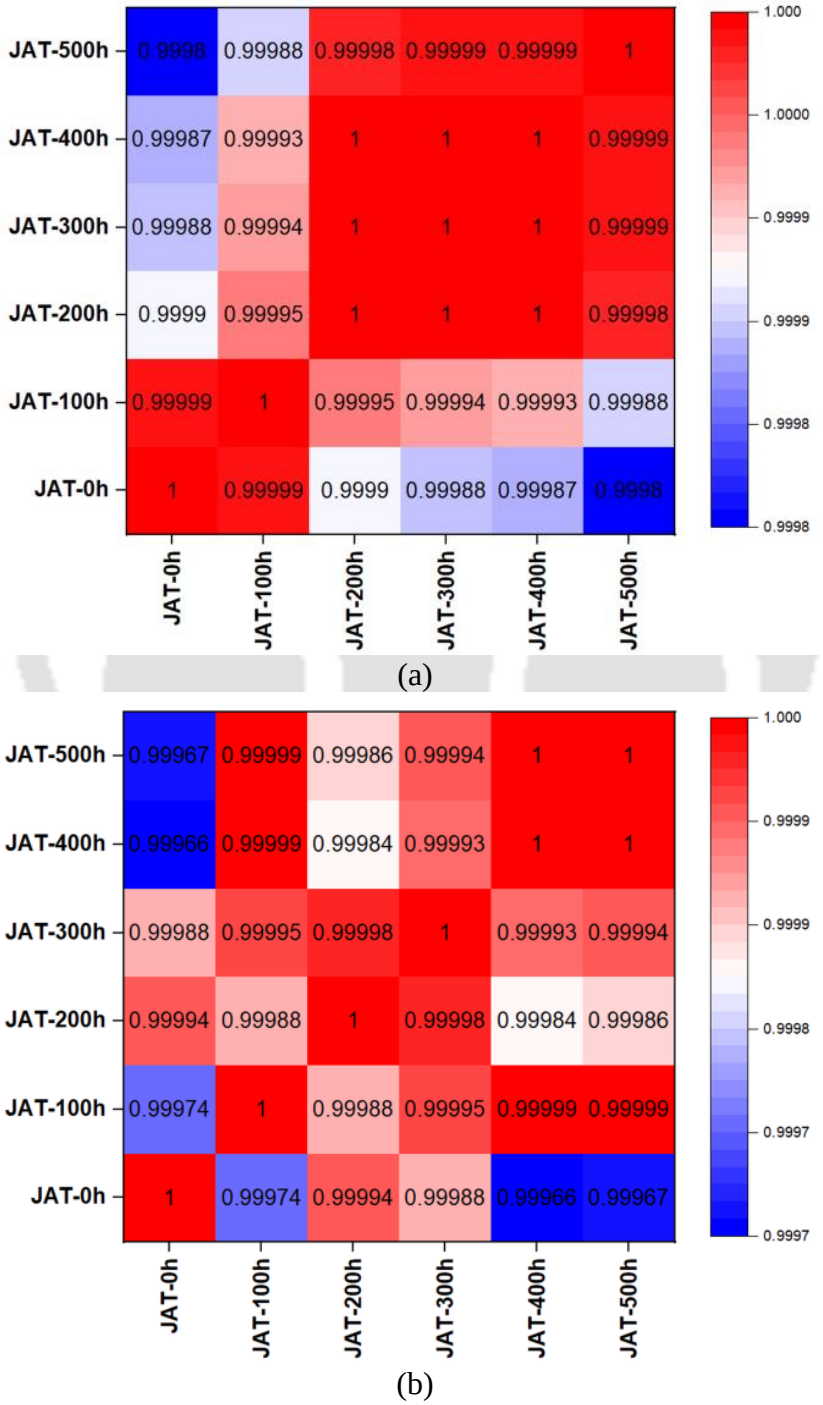

Figure 3.13: Heat maps at different ageing duration for (a) ε_r and (b) tan δ.

TH-2868_156302003

The correlation coefficients of the relative permittivity magnitude curves show that above 200 hours of ageing of the oil samples, there is a certain positive correlation of as seen in the heat map in Figure 3.13(a), which is almost equal to 1. The correlation coefficients of the tan δ curves show that for all ageing of the oil samples, there is a positive correlation of 99% as seen in Figure 3.13(b). The correlation plot gives an inference about the pattern of the data, which tends to be varying in a similar manner when compared related to the ageing durations.

3.6 Summary of the chapter

The main focus of this work is to analyze a new insulating liquid JAT under open beaker oxidative ageing using the FDS measurement technique which is not done yet. Thus this investigation helps to explore more into this NEO as a potential replacement for the other available insulating liquids used in power transformers. The ageing of the oil plays a major role in ascertaining the integrity of the oil in the long run. The main outcome of the present work is as below:

- The permittivity and tan δ of the natural ester oil JAT increases with ageing duration towards the lower frequency range which shows that the formation of polar contaminants hampers the condition of the oil.
- The FTIR results showed the composition of the oil to be intact even after 500 hours of ageing, as there is no significant change in the spectra.
- By analyzing the UV-Vis spectra, it is observed that the oil samples show a red shift in the spectra with increasing ageing duration and thus the samples are identified accordingly.
- A statistical modeling approach is proposed to understand the variation in the dielectric parameters of the oil and an expression relating all 3 parameters of frequency, ageing duration and dielectric parameters is developed. This will help to assess by how the oil properties degrade as time progresses.
- The correlation plots show that pattern of the data varies in a similar manner when compared related to the ageing durations.

To further study the temperature effects on the dielectric parameters when NPs are dispersed in base fluid, FDS is extended to NEO-NFs in the next chapter and predictive modeling technique is applied to determine the dielectric parameters. The semiconductive

TH-2868_156302003

TiO_2 NP which is reported to have shown enhanced thermophysical and electrical properties is used for this work along with the commercially available FR3 insulating fluid.

भारतीय प्रौद्योगिकी संस्थान गुवाहाटी
Indian Institute of Technology Guwahati

Note: This work, "Quantitative Effect of Ageing Duration on Dielectric Parameters based on Frequency Response," has been published in IEEE Transactions on Instrumentation and Measurement, 2021, DOI: 10.1109/TIM.2021.3127306.

TH-2868_156302003

4

Temperature dependence on dielectric parameters of NFs

Contents

TH-2868_156302003

4.1 Introduction

In this work, MO and FR3 are considered for the FDS analysis. For enhancing the performance of the NEOs further, the dispersion of NPs to the base fluid is considered. Many research works have reported that the addition of NPs in the NEOs as well as MOs tend to improve the dielectric properties [113, 114]. For upgrading the insulation performance and thermal conductivity in a dielectric, TiO_2 is an efficient NP. The breakdown strength also increases with the dispersion of TiO_2 due to its electron scavenging property [115]. The NF with TiO_2 NPs has also shown improvement of breakdown strength when aged NF is compared with aged base fluid [69]. Thus, in this study the semi-conductive TiO_2 NPs are considered for preparation of the NFs. The FDS response is calculated in the frequency range of 10^{-3} to 10^{4} Hz and the temperature range varies from 30 to 90^{o}C with an interval of 15^{o}C between two successive temperatures. The permittivity and the tan δ achieved from FDS are compared for all the oil samples. The temperature effects on the variation of parameters are also considered for all the oil samples. The Cole-Cole relaxation model is used to analyze the dielectric behaviour [53, 54]. The parameters of the models are obtained using curve fitting method and after that the influence of the NPs on the relaxation parameters is also discussed.

The present study also deals with the application of supervised ML techniques to predict and explain the trends in the dielectric properties of the oil samples with change in temperature. The predictive analysis of the dielectric properties like complex permittivity and tan δ of the samples is carried out considering its dielectric response using the FDS. For the study, the supervised ML models like DTR and KNN are used as they are powerful tools for prediction, and both these methods are used for both classification and regression. The advent of ML has led many researchers to use these predictive algorithms to evaluate the water content in oil-paper insulation system. Some of them used the genetic algorithm (GA) to obtain the equivalent circuit parameters of transformer and eliminated the influence of temperature on FDS curve through neural network [112]. Some studies used support vector machine (SVM) algorithm to estimate the water content in the transformers [116]. Supervised neural network (SNN) is used to evaluate the moisture content and define the effect of moisture and ageing on FDS curve [117]. A study showed how the SVM is used to identify the aging and moisture of bushing [118]. It is reported that a suitable kernel function for SVM is usually difficult to find which results in mediocre performance [119]. The reasons for using DTR are that it is easy to use and understand and it is resistant to outliers and require

TH-2868_156302003

no data preprocessing. DTR also works well with non-linearity and so suitable for use in FDS curves. DTR also gives better accuracy compared to linear regression. The advantage of KNN is that it is easy to interpret and has quick calculation time. It does also not make any assumptions about the dataset, so no need for any tuning of parameters for predictions. The evaluation accuracy of these models is determined to estimate how well the model performs for predicting dielectric properties. The model is developed using a dataset of 355 experimentally measured values of the dielectric properties.

In this work, section 4.2 deals with the materials and methods, section 4.3 focuses on the results and discussions; section 4.4 discusses the predictive modeling technique and the conclusions are included in section 4.5.

4.2 Materials and methods

4.2.1 Preparation of NF

The basic attributes of the MO and FR3 are specified in Table 2.1 of chapter 2, which are used for this study along with its NFs.

Table 4.1: Measured values of TiO_2 Nanoparticle.

Characteristic	Specification
Purity	>= 99.5 %
Size	21 nm
pH	3.5 – 4.5
Surface area	35 - 65 m^2/g
Appearance	White powder
Manufacturer	Sigma Aldrich

The specification of the TiO_2 NP is given in Table 4.1 and the NF formulation procedure is presented in Figure 4.1. For the preparation of the NF, a quantity of 0.01wt.% of TiO_2 NPs is chosen because of its better stability [120]. The mixture is then ultrasonicated for a two hours to evenly scatter the particles. This weight percentage of NPs gives a stable dispersion in the base fluid to form the NF. The prepared NF is vacuum heated to dry out the moisture as much as possible.

TH-2868_156302003

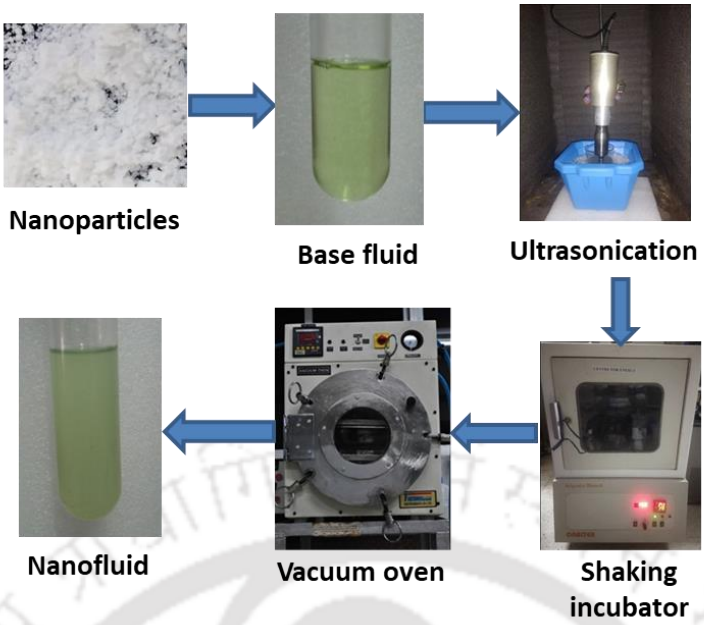

Figure 4.1: Nanofluid preparation with MO/NEO.

4.2.2 Experimental setup for FDS

An experimental setup is assembled in the laboratory for measuring the frequency response of the oil samples, a frequency response analyzer (Solartron 1260A) in conjunction with a dielectric interface (Solartron 1296A) as given in Figure 4.2.

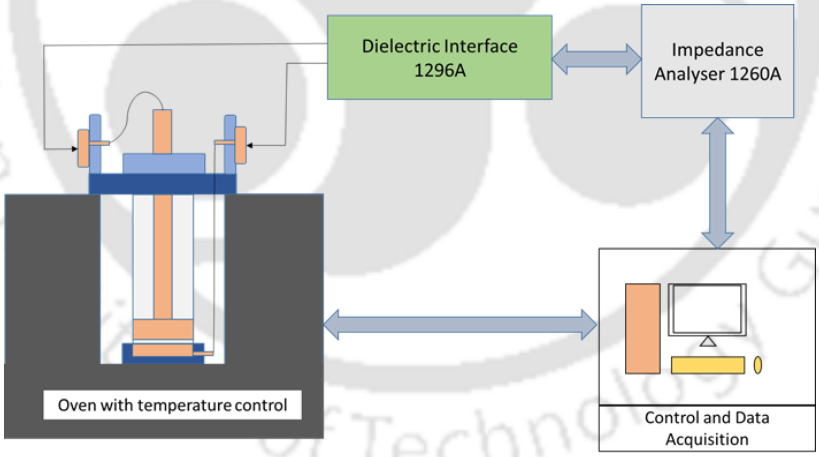

Figure 4.2: FDS test setup with heating oven and temperature controller.

For analyzing the effect of the temperature, a temperature controller along with a heating oven is considered and attached with the data acquisition computer. An alternating voltage is applied to the oil sample. On the application of an external field, one part of energy is put in storage by the capacitance, and other part is dissipated by the resistance effects. The frequency range considered is from 10^{-3} to 10^{4} Hz and the temperature is varied from 30 to 90^{o}C with an interval of 15^{o}C in between successive temperatures. The temperature is sensed

TH-2868_156302003

by using a thermal sensor in the heating oven where the test cell is placed. The data is recorded by using the SMaRT software.

4.3 Results and discussion

The relative permittivity and tan δ of all the oil samples are achieved by performing the FDS analysis. The complex permittivity of any dielectric material defines the dielectric properties, i.e. the ability of the material to accumulate electrical energy, on the application of an external electric field and also indicates the losses. Under the effect of a voltage, the dielectric material will polarize. The extent of polarization varies for different materials at different frequencies. This process depends on the integrity of the material, like, what quantity of polar contaminants is present, ageing of the dielectric, moisture, temperature and their relaxation mechanisms. In order to investigate the effect of temperature on the dielectric properties of MO, FR3 and their NFs, corresponding permittivity and tan δ profiles are evaluated from FDS measurement. The samples are freshly prepared for the experiments and hence no agglomeration of the NPs is observed for a day.

4.3.1 Cole-Cole double relaxation model

It has also been observed by many researchers that real dielectrics do not follow the standard Debye model which gives a semicircular arc with its centre on the x-axis. K. S. Cole and R. H. Cole developed a method to correlate the dielectric response of real materials with idealized Debye behaviour [53, 54]. They obtained a plot between real and imaginary components of complex permittivity (ε_r' and ε_r'') from the FDS over the entire range of frequency. It is found that during experimental observations on real dielectrics, the plot often formed only an arc of a circle, rather than a full semicircle, while its centre lying below the $\varepsilon_r'' = 0$ axis, which is a deviation from Debye model [53, 54]. Such deviation in the Cole–Cole plot is attributed to the distributed nature of relaxation process taking place in the complex dielectric material. These plots have been used by researchers for characterizing different materials and composites [121-123]. Researchers have investigated the dielectric response measurement results of transformer oil-paper insulation with Cole–Cole model and highlighted the fact that real dielectrics have more than one relaxation frequency and the intermolecular interactions should be considered while interpreting their dielectric response. Thus, to ascertain the number of relaxations in the oil samples, Cole-Cole plots between ε_r' (x-axis) and ε_r'' (y-axis) are plotted from the values obtained from the FDS measurement. It is observed from Figures 4.3 and 4.4 that there is more than one semi-circle for all the oil samples, one in the higher frequency range and another in the lower frequency range. Each

TH-2868_156302003

semicircle represents corresponding dominant relaxation mechanism in that particular range [124]. The shape of the plot exhibits the combination of two or more semicircles in lower frequency region. The overlapping of the semicircles causes the distortion in shape of Cole-Cole plot. This occurs when there are several relaxation mechanisms in existence with comparable relaxation time constants. The tail at the lower frequency region corresponds to the DC conductivity. Hence, the Cole-Cole double relaxation model is considered for further analysis of the oil samples.

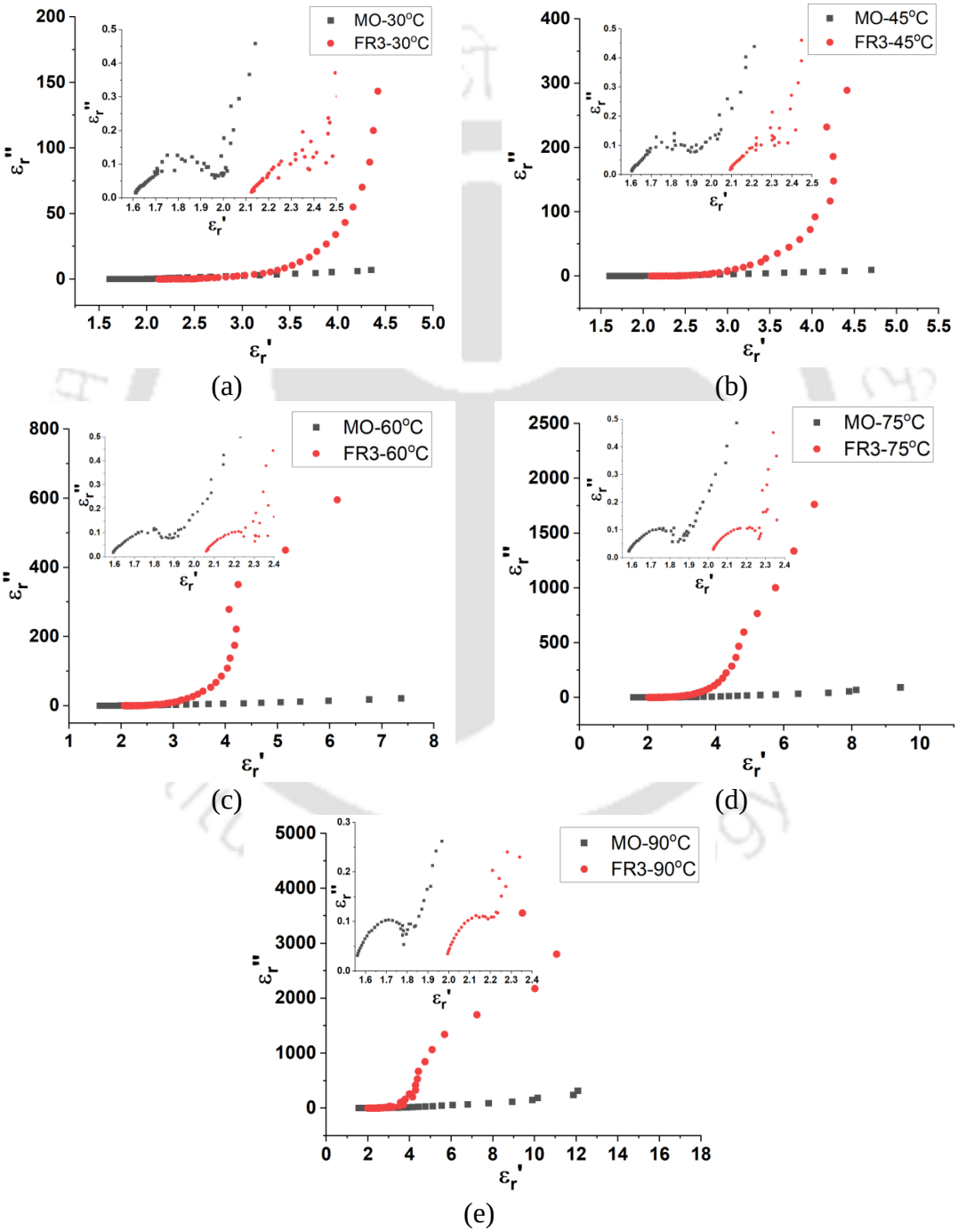

Figure 4.3: Cole-Cole plots for MO and FR3 at (a) 30°C (b) 45°C (c) 60°C (d) 75°C and (e) 90°C.

TH-2868_156302003

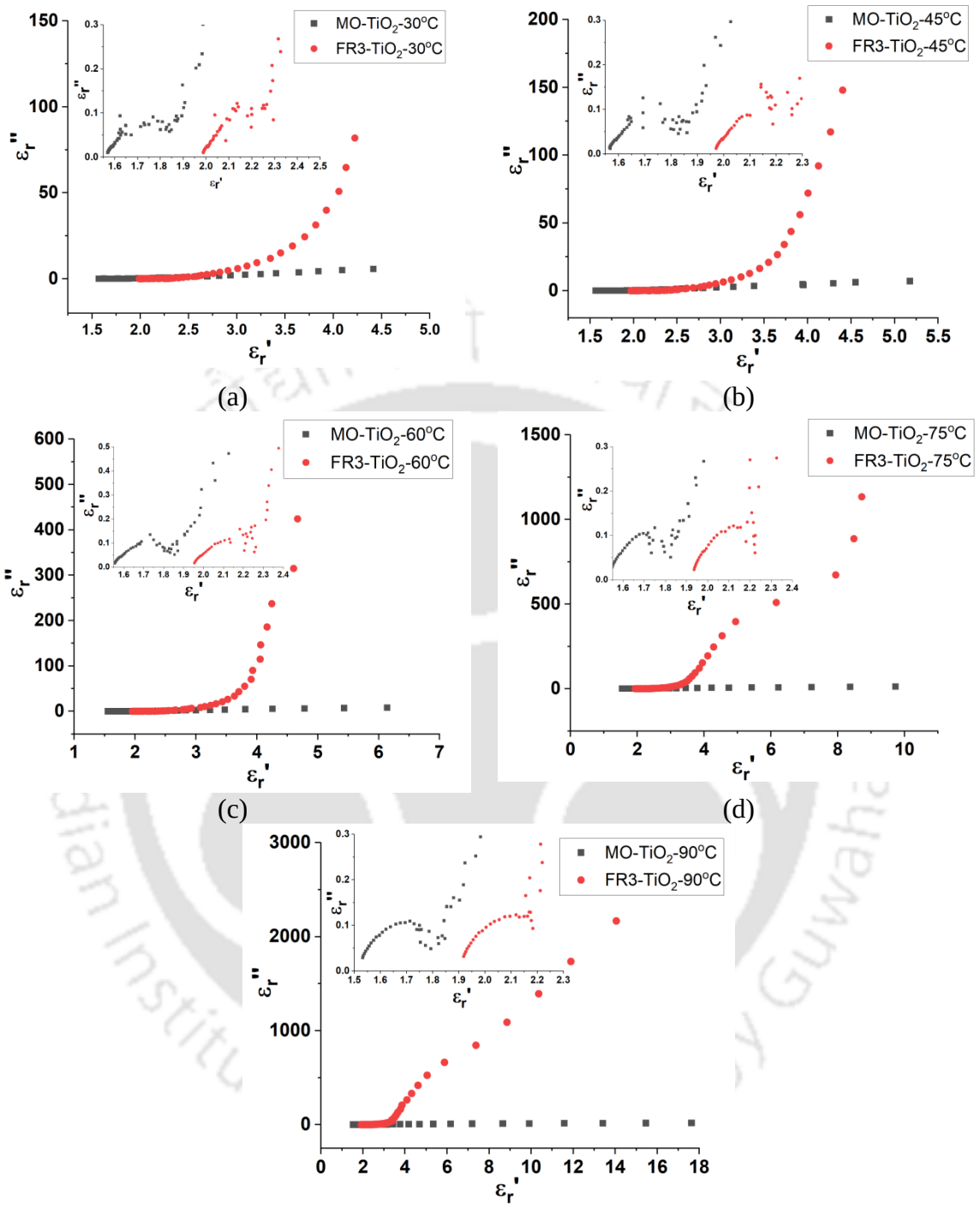

Figure 4.4: Cole-Cole plots for MO-NF and FR3-NF at (a) 30°C (b) 45°C (c) 60°C (d) 75°C and (e) 90°C.

By using least square method, curve fitting is done to the ε_r' and ε_r'' using (4.1) and (4.2), and obtain the model parameters (A, n, $\Delta\varepsilon_1$, τ_1, α_1, $\Delta\varepsilon_2$, τ_2, α_2, σ_{dc}).

$$\varepsilon_r' = \varepsilon_\infty + A\omega^{-n} + \mathrm{Re}\left\{\frac{\Delta\varepsilon_1}{1+(j\omega\tau_1)^{1-\alpha_1}} + \frac{\Delta\varepsilon_2}{1+(j\omega\tau_2)^{1-\alpha_2}}\right\} \quad (4.1)$$

TH-2868_156302003

$$\varepsilon_r'' = \frac{\sigma_{dc}}{\varepsilon_0 \omega} + A\omega^{-n} \cot\left((1-n)\frac{\pi}{2}\right) + \mathrm{Im}\left\{\frac{\Delta\varepsilon_1}{1+(j\omega\tau_1)^{1-\alpha_1}} + \frac{\Delta\varepsilon_2}{1+(j\omega\tau_2)^{1-\alpha_2}}\right\} \quad (4.2)$$

The decrease in permittivity with the increasing frequency at low frequency range is modeled by an $A\omega^{-n}$ which is the inverse power dependence on frequency, whereas the remaining part is modeled by Cole-Cole expression [115, 125] with two relaxation times. $\Delta\varepsilon_1$, τ_1 and α_1 represent the relaxation amplitude, time constant of relaxation and spread of the first relaxation respectively. $\Delta\varepsilon_2$, τ_2 and α_2 represent the relaxation amplitude, time constant of relaxation and spread of the second relaxation respectively and σ_{dc} represents the DC conductivity.

4.3.2 Effect of temperature on permittivity and tan δ

4.3.2.1 Real and imaginary parts of permittivity

The parameters are estimated by means of the least square technique to obtain the best fit of the measured ε_r' *and* ε_r'', and they are plotted in Figures 4.5 and 4.6 for all the oil samples.

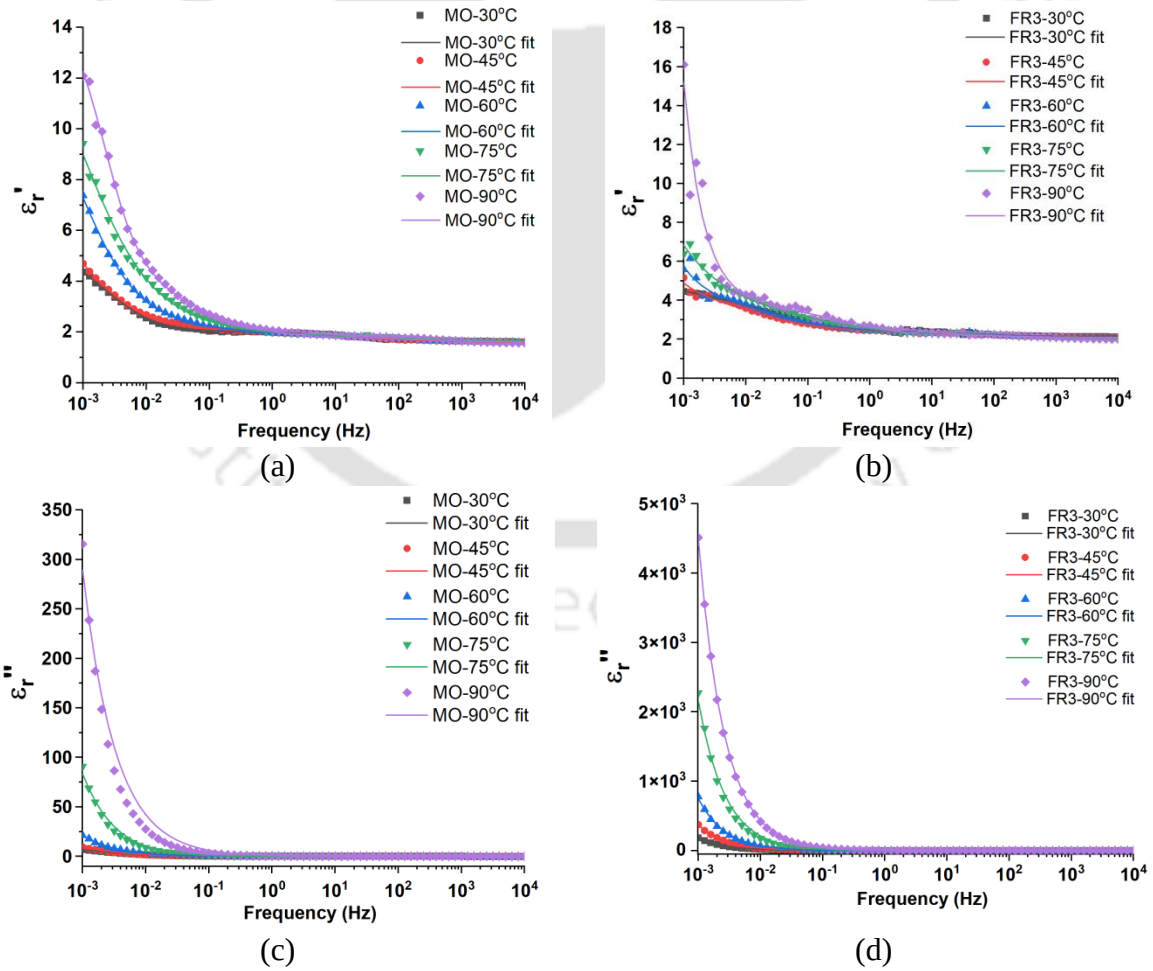

Figure 4.5: Variation of ε_r' and ε_r'' with frequency and temperature for (a) MO-ε_r' (b) FR3-ε_r' (c) MO-ε_r'' and (d) FR3-ε_r''.

TH-2868_156302003

Table 4.2: Estimated Cole-Cole model parameters of MO and FR3 at different temperatures.

MO

Temp / Parameters	30°C	45°C	60°C	75°C	90°C
A	0.009	0.413	0.487	0.161	1.215
n	0.851	0.139	0.110	0.391	0.313
$\Delta\varepsilon_1$	2.008	3.955	9.459	11.12	5.856
τ_1	42.76	129.73	149.72	132.59	63.101
α_1	0.184	0.261	0.282	0.373	0.028
$\Delta\varepsilon_2$	0.385	0.137	0.081	0.219	0.231
τ_2	0.0072	0.004	0.002	0.001	0.047
α_2	0.368	0.115	0.288	0.530	4.657
σ_{dc}	1.54×10^{-12}	1.36×10^{-12}	9.55×10^{-13}	5.87×10^{-11}	3.37×10^{-12}

FR3

Temp / Parameters	30°C	45°C	60°C	75°C	90°C
A	0.061	0.002	0.0085	0.1047	0.010
n	0.427	1.141	1.050	0.648	1.368
$\Delta\varepsilon_1$	1.723	1.929	1.798	3.084	2.186
τ_1	5.756	10.36	5.282	6.387	0.519
α_1	0.381	0.416	0.430	0.708	0.533
$\Delta\varepsilon_2$	0.200	0.258	0.247	0.210	0.168
τ_2	0.002	0.0015	0.0013	0.017	0.026
α_2	0.272	0.556	0.408	4.845	12.89
σ_{dc}	1.11×10^{-11}	2.07×10^{-11}	4.17×10^{-11}	1.19×10^{-10}	2.46×10^{-10}

A good fit is observed between the measured data and fitted response based on Cole-Cole expression with two relaxation times. The estimated parameters by the least squares for the dielectric responses of the oil samples are listed in Table 4.2. It is observed from Figure 4.5 that as the frequency increases there is decrease in the ε_r' and ε_r'' values of all the oil samples. It is observed from the Figures 4.5(a) and 4.5(b) that the ε_r', which gives an indication of the degree of polarization, increases with increase in temperature for both MO

TH-2868_156302003

and FR3. The ε_r'' which gives an indication of losses also increases with increase in temperature. With increased temperature, the mobility of polar molecules increases, which increases the permittivity. It is observed that the permittivity values are not much dependent on frequency above 10 kHz. However, at lower frequency the charge carriers react faster when there is an applied electric field which in turn enhances the value of permittivity. At higher frequency ranges, the charge carriers do not have enough time to react to the quick variations in the applied electric field, which results in lower values of permittivity.

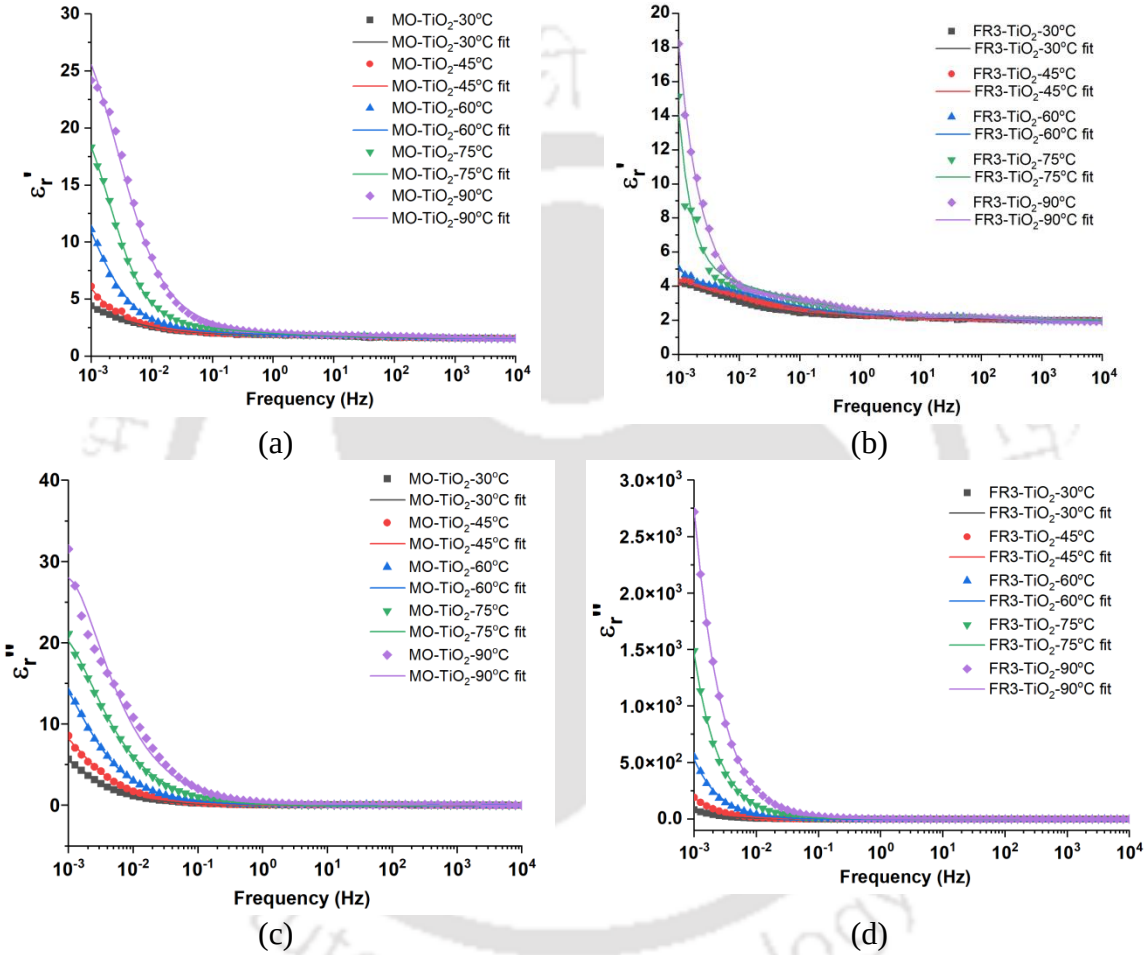

Figure 4.6: Variation of ε_r' and ε_r'' with frequency and temperature for (a) MO-TiO_2-ε_r' (b) FR3-TiO_2-ε_r' (c) MO-TiO_2-ε_r'' and (d) FR3-TiO_2-ε_r''.

The conductivity of the oils increases with increase in temperature as given by the below expression [126],

$$\sigma_{dc} = \sigma_o e^{\frac{-E_a}{kT}} \tag{4.3}$$

where T is the absolute temperature in Kelvin, σ_o is conductivity constant, k is the Boltzman constant and E_a is the activation energy. This indicates that at higher temperatures, the condition of insulation degrades. As observed from Table 4.3, there is a variation in the

TH-2868_156302003

relaxation times and spread of the distribution with change in temperature for MO. Also, the conductivity values for MO have increased from 30 to 90°C, with a slight fluctuation in the mid temperature range. For the FR3, the conductivity values show a gradual increase with increase in temperature. The relaxation times in case of FR3 are lower than MO because the conductivity of FR3 is higher.

Table 4.3: Estimated Cole-Cole model parameters of MO-TiO_2 and FR3-TiO_2 at different temperatures.

MO-TiO_2					
Temp / Parameters	30°C	45°C	60°C	75°C	90°C
A	0.125	0.008	0.006	0.0006	0.216
n	0.575	1.126	1.175	1.354	0.412
$\Delta\varepsilon_1$	0.251	1.657	9.553	19.72	27.98
τ_1	16.62	48.99	97.785	74.43	53.86
α_1	0.121	0.270	0.182	0.119	0.226
$\Delta\varepsilon_2$	0.255	0.979	0.853	1.415	0.745
τ_2	0.007	1.534	0.350	1.166	0.103
α_2	0.277	0.782	0.738	0.598	0.753
σ_{dc}	1.25×10^{-12}	1.56×10^{-12}	5.21×10^{-12}	5.74×10^{-12}	9.56×10^{-12}
FR3-TiO_2					
Temp / Parameters	30°C	45°C	60°C	75°C	90°C
A	0.0009	0.0138	0.000015	0.00034	0.0423
n	0.740	0.732	2.139	2.007	1.156
$\Delta\varepsilon_1$	2.558	2.238	2.278	5.093	0.805
τ_1	40.620	6.542	6.729	26.065	0.285
α_1	0.371	0.536	0.428	0.695	0.062
$\Delta\varepsilon_2$	0.301	0.016	0.261	0.198	0.521
τ_2	0.0109	0.038	0.0009	0.013	0.0007
α_2	0.485	0.732	0.201	2.097	0.561
σ_{dc}	4.72×10^{-12}	1.06×10^{-11}	6.28×10^{-11}	6.94×10^{-11}	1.56×10^{-10}

Similarly from Figure 4.6, it is observed that ε_r' and ε_r'' values increases with increase

TH-2868_156302003

in temperature for both MO-TiO_2 NF and FR3-TiO_2 NF. With increased temperature, the mobility of polar molecules increases, which increases the permittivity. The addition of NPs leads to an enhancement of the permittivity of the NFs corresponding to the same frequency and temperature levels. The polarization processes happening in the NPs affects the overall permittivity of the NFs. The higher permittivity of NFs is attributed to the inner polarization of the NPs and the effective permittivity of the NFs is mostly influenced by the permittivity of the base fluid [127]. It is observed from Table 4.3 that the conductivity values for both the NFs show a gradual increase with increase in the temperature. The temperature effects prevail at lower frequencies in which interfacial polarization is largely thermally activated. When the Figures. 4.5(c) and 4.5(d) are compared with Figures. 4.6(c) and 4.6(d), it is observed that the loss component ε_r'' has decreased with the addition of NPs for both MO and FR3. This happens because with the presence of NPs, the free electrons are captured, which in turn reduces the conduction current and thus reducing the losses.

4.3.2.2 Dielectric dissipation factor (tan δ)

As seen in Figure 4.7, the tan δ profile of all the oil samples decreases as the frequency increases and reverse occurs with the increment of temperature. The longer time available at lower frequencies makes the dipoles present in the dielectric acquire a particular polarity for a longer time. Therefore, the dipoles exhibits a tendency to arrange more in the direction of the applied field and the electrons too get abundant time to travel to the anode. These phenomena augment the interactions among the molecules, electrons and dipoles, which result in rise of the frictional loss and therefore increase the tan δ [128].

It is also observed from Figures 4.7 that the tan δ values for MO, FR3 and their NFs increase with temperature. It is reported that the rise of temperature augments the activation energy in the oil molecules [129]. With the increment of the activation energy, the conduction current increases and this eventually causes the conduction loss which leads to consequent augmentation of tan δ value. However, it is observed from Figures 4.7(c) and 4.7(d) that with the addition of NPs, the tan δ value at lower frequency levels is lower than the corresponding values of the base fluid. A study has reported that at lower frequency levels, Ti atom bonds with the hydroxyl (OH^-) group present within the water molecules in NFs. This hydroxyl group bonds with the cellulose chains in MO which makes the polarization capability of the NPs weak [130]. Consequently, the tan δ value reduces as the weakening of polarization of NPs leads to a decline in the interactions among the dipoles during the experiments. Also, this reduction in tan δ values may be because of capture of free electrons by the NPs thus

TH-2868_156302003

reducing the conduction current in the NF. There are also loss peaks observed in case of MO-NFs for all temperature ranges which may be because of space charge polarization phenomenon occurring at lower frequencies [129].

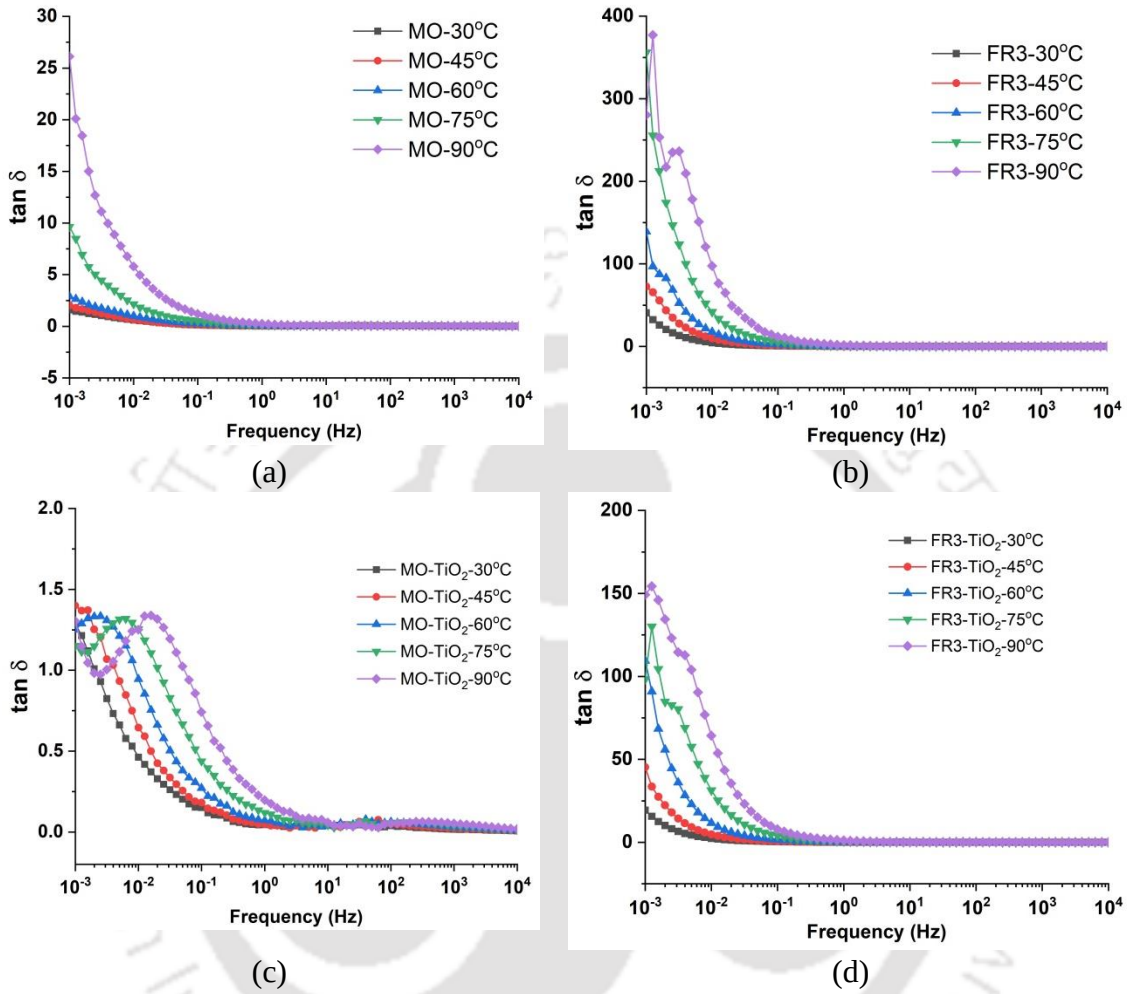

Figure 4.7: Variation of tan δ with frequency and temperature for (a) MO (b) FR3 (c) MO-TiO_2 NF, and (d) FR3-TiO_2 NF.

Figure 4.7(d) shows that the tan δ values of FR3-NF have reduced significantly compared to FR3, for the entire frequency range. It is stated that under the application of an external field in NEO, the conduction current tends to be higher than the polarization current [129]. Since the free electron in a dielectric generates the conduction current, this ultimately determines the tan δ in the NEO. In case of NFs, the NPs get polarized under the applied field and trap the free electron. The electron scavenging by the NPs leads to reduction of free electrons within the dielectric and thus the conduction current decreases. The decline in the conduction current leads to decrease in the corresponding tan δ value of NFs.

TH-2868_156302003

4.4 Predictive modeling using regressor

ML techniques offer a prospect to carry out predictive analysis for large amounts of data. Multiple output or multi-output regression is a type of regression problem that involves the prediction of two or more target variables given an input dataset. Many ML algorithms are designed to predict a single target variable known as simple regression. However, some ML algorithms support multi-output predictions inherently, like linear regression, DTR and KNN. In multi-output regression, the outputs may be inter-dependent and also are dependent on the input. There are a number of techniques for dealing with multi-output regression problems and in this work, DTR and KNN algorithms are implemented on a dataset, which consists of two input features temperature and frequency and the target variables are ε_r', ε_r'' and tan δ. The model is developed using a dataset of 355 experimentally measured values of the dielectric properties with temperature range of 30 to 90^{o}C in the frequency range of 10^{-3} to 10^{4} Hz. The training:testing sample size is considered with the ratio of 70:30. These results indicate the variation in the dielectric properties of both the oil samples and help to comprehend the changes in the oil properties at a wide range of frequencies. The reasons for using DTR are that it is easy to use and understand and it is resistant to outliers and require no data preprocessing. DTR also works well with non-linearity and so suitable for use in FDS curves. DTR also gives better accuracy compared to linear regression. The advantage of KNN is it is easy to interpret and has quick calculation time. It does also not make any assumptions about the dataset, so no need for any tuning of parameters for predictions.

4.4.1 Decision tree regressor

DTR is a predictive model based on supervised learning that uses a set of binary rules to estimate a target value. Each isolated tree is a simple model that has branches, nodes and leaves. A decision tree is arriving at an estimate by asking a series of questions to the data, each question narrowing our possible values until the model get confident enough to make a single prediction. A decision tree consists of three nodes as shown in Figure 4.8. The root node is the base node which signifies the complete dataset and it is divided further into additional nodes called the decision or interior nodes which represent the features of the data set and the branches signify the decision rules whether True/False. The interior nodes are further sub-divided into the leaf terminal nodes which represent the result.

For a particular sample data, DTR is run entirely through the whole tree by answering decision rules in the branches till it arrives at the leaf node. The final estimate is the mean of the dependent variable in that particular leaf node. The DTR predicts a good value for the

TH-2868_156302003

data value by means of numerous iterations. Figure 4.9 represents the implementation of a DTR algorithm.

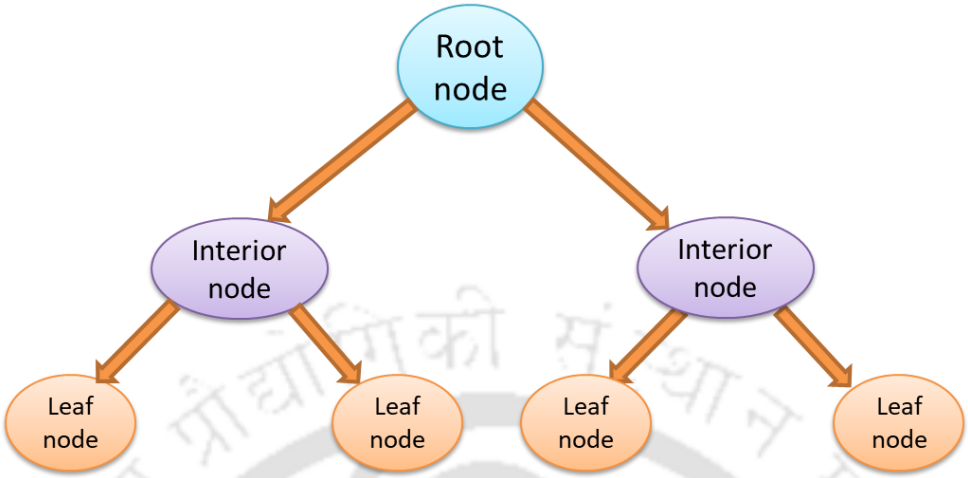

Figure 4.8: Decision tree algorithm.

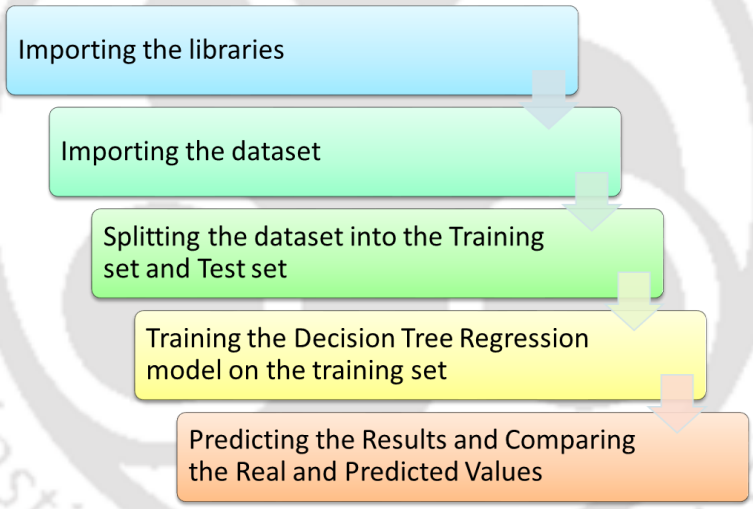

Figure 4.9: Decision tree regression flow chart.

The decision tree algorithm calculates the entropy which gives the measure of the information contained in the particular level/state. The level with minimum entropy is a pure node. The entropy (E_n) is given as,

$$E_n = \sum_{i=1}^{N_{ML}} -p_i \log_2(p_i) \tag{4.4}$$

where p_i is the probability of class i and N_{ML} is the number of classes.

The information gain (IG) feature is used to decide which feature to split on at each step in building the tree.

TH-2868_156302003

$$IG = (Entropy\_parent) - sum(Entropy\_children) \tag{4.5}$$

$$IG = \sum_{i=1}^{N_{ML}} -p_i \log(p_i) - \sum_{i=1}^{N_{ML}} w_i p_{i/a} \log(p_{i/a}) \tag{4.6}$$

where w_i are the weights attached to each class. The model compares all the possible splits and takes the one that maximizes the information gain. For the DTR, reduction in variance is used for splitting the node used when the target variable is continuous. It is so-called because it uses variance as a measure for deciding the feature on which node is split into child nodes. Variance is used for calculating the homogeneity of a node. If a node is entirely homogeneous, then the variance is zero. The variance of any dataset of N values is given by:

$$Var = \frac{1}{N}\sum_{i=1}^{N}(y_i - \bar{y})^2 \tag{4.7}$$

For the prediction of a target variable, the average of values at the leaf node is considered.

$$Var\_red = (Var\_parent) - sum(Var\_child) \tag{4.8}$$

$$Var\_red = \frac{1}{N}\sum_{i=1}^{N}(y_i - \bar{y})^2 - w_i \frac{1}{N}\sum_{i=1}^{N}(y_i - \bar{y})^2 \tag{4.9}$$

4.4.2 KNN regressor

The KNN is a supervised ML algorithm with easy implementation rules and is used for both classification and regression problems. The KNN algorithm assumes that similar things are near to each other. It is commonly used for its easy interpretation and low calculation time. The K in KNN is selected which is right for the dataset. The algorithm is run multiple times with different values of K and the value of K is chosen that reduces the number of errors which is encountered while maintaining the algorithm's ability to accurately make predictions when it is given data it has not seen before. The KNN algorithm uses 'feature similarity' to predict the values of any new data points. This means that the new point is assigned a value based on how closely it resembles the points in the training set.

Initially, the distance between the new point and each training point is calculated. A number of methods are available for calculating the distance, of which the most commonly used method, is the Euclidian for continuous variables. The scikit-learn KNN regressor uses the Euclidean distance which is calculated as the square root of the sum of the squared differences between a new point *u* and an existing point *v*, which is given by,

TH-2868_156302003

$$d(u,v)=\sqrt{\sum_{i=1}^{N}(u_i-v_i)^2} \tag{4.10}$$

These two methods are implemented on the dataset by using spyder which is an open source integrated development environment (IDE) for Python. First of all, the dataset is imported using pandas. After the data pre-processing, the data samples are randomly split into training set and test set ratio of 65:35, as it is giving better results.

Table 4.4: Accuracy of the ML models.

Accuracy of the predicted model with DTR					
		MO	FR3	MO-NF	FR3-NF
R^2	ε_r'	0.9452	0.8162	0.9222	0.9048
	ε_r''	0.9150	0.9200	0.9292	0.9180
	tan δ	0.9526	0.8758	0.9880	0.9421
MAE	ε_r'	0.1763	0.1940	0.4164	0.1899
	ε_r''	2.7292	46.28	0.5155	30.256
	tan δ	0.2314	6.2140	0.0299	3.007
Accuracy of the predicted model with KNN					
		MO	FR3	MO-NF	FR3-NF
R^2	ε_r'	0.9490	0.7376	0.9450	0.8606
	ε_r''	0.8291	0.8217	0.9404	0.8300
	tan δ	0.9008	0.8834	0.9916	0.8973
MAE	ε_r'	0.1455	0.2334	0.3393	0.1835
	ε_r''	3.0794	58.338	0.4300	36.373
	tan δ	0.2640	6.079	0.0233	3.201

After the training of the model, the predicted data samples are obtained and compared with the test data and accuracy is calculated. In order to analyze the evaluation accuracy of the DTR and KNN model, the comparison is done with R^2 and mean absolute error (MAE) and the values are given in Table 4.4. It is observed that the R^2 values for ε_r', ε_r'' and tan δ of all oil samples give quite favourable results as they are near to 1. Further, the MAE values are also acceptable as they are near to 0 for ε_r' and tan δ. However, for ε_r'' values are a bit higher because of the distribution of the data. This shows that both the models give a good accuracy of prediction for ε_r' and tan δ.

TH-2868_156302003

4.5 Summary of the chapter

In the present work, semi-conducting TiO_2 NP based NFs are prepared in laboratory for investigation of their dielectric properties and FDS is performed under varying temperature. The main outcome of this research work is as below:

- The Cole-Cole plots show that more than one relaxation exists in the oil samples when subjected to an electric field. Thus, Cole-Cole double relaxation model is considered for extracting the parameters by using least square method for curve fitting and it is observed that the conductivity increases with temperature for all oil samples.
- It is observed that the real part of relative permittivity increases with the presence of NPs. This is because of the polarization phenomenon happening in the NPs. The values of the permittivity also increase with rise in temperature levels because of the mobility of polar molecules increases.
- It is observed that the imaginary part of permittivity which gives an indication of losses also increases with increase in temperature. With increased temperature, the mobility of polar molecules increases, which increases the permittivity.
- It is observed that the presence of NPs in oils decreases the corresponding tan δ values compared to base fluids because of electron capture by the NPs. The values of tan δ also increase with increase in temperature levels because of increase in the activation energy of the oil molecules.
- The DTR and KNN model developed to predict the permittivity and tan δ values gives acceptable results as the MAE values are less and the R^2 value approaches 1.

To further study the NEO-NFs, a statistical investigation of the ACBDV is done in the next chapter considering fresh and aged FR3 and FR3-NFs.

TH-2868_156302003

5

Investigation of natural ester based insulating liquid using hypothesis testing

Contents

TH-2868_156302003

5.1 Introduction

NFs for application in high voltage apparatus is expansively studied by many investigators. Many studies have proposed that NP helps in enhancing the breakdown voltages of the NFs. The information of BDV of the NFs is very essential for any insulation system. BDV depends on many properties of oil and contaminations that can exist in the oil as well as the electrodes arrangement. In the present work, semi-conductive TiO_2 NPs are used in the NEO to prepare the NF with FR3 as base fluid considered in chapter 4. High temperature and moisture affects the thermophysical and electrical attributes of the insulating liquids, resulting in reduced life of the power and distribution transformers. So, the open beaker oxidative ageing study is performed on both the oils: NEO and NEO-NF, using the open beaker oxidative ageing setup developed in the laboratory as shown in Figure 3.1 of chapter 3.

Since the breakdown is a random occurrence, it is required to examine the reproducibility of experimental data on an adequate number of tests. In this work, ACBDV test results are performed for all the samples: NEO, NEO-NF, aged NEO and aged NEO-NF and a comparative examination is done among them to estimate the behaviour of the new and aged oils. To understand the statistical behaviour of the ACBDV of the oil samples, normal, 2-parameter Weibull and 3-parameter Weibull distributions are considered. It is important to confirm whether these distributions really belong to that specified distribution. To confirm this, hypothesis testing with Shapiro-Wilk test and Anderson-Darling test is used, which is a powerful technique to ascertain if the distribution of experimental data follows a theoretical distribution [131]. The goodness of fit is used to measure how well the data fits a specified distribution.

In this research work, section 5.2 deals with sample preparation and ageing, the ACBDV analysis is addressed in section 5.3, section 5.4 focuses on the statistical hypothesis testing, section 5.5 addresses the normal and Weibull test and the summary is included in section 5.6.

5.2 Sample preparation and ageing

The basic attributes of the MO and NEO measured in laboratory are specified in Table 2.1 of chapter 2. It is observed that the critical parameter like ACBDV is better for the NEO. For further enhancement of ACBDV, TiO_2 NPs are dispersed in FR3 to prepare the NFs and further investigation of ACBDV is carried out in this work.

TH-2868_156302003

5.2.1 Preparation of NF

For the preparation of NF, a quantity of 0.01wt.% of TiO_2 NPs is chosen because of its better stability [120]. The specification of the TiO_2 NP is given in Table 4.2 and the NF formulation procedure is presented in Figure 4.1 of chapter 4.

The mean ACBDV values of MO and FR3 are given in Table 2.1 of chapter 2. It is observed that the NEO has better properties in terms of ACBDV compared to MO, so this NEO is considered for ageing and other statistical investigations in this work.

5.2.2 Ageing using open beaker oxidative ageing

The effect of ageing on NEO and NEO-NF is done by using an open beaker oxidative ageing. There are 4 beakers, each of 300 ml volume capacity, inside the ageing oven, with a temperature sensor, speed recorder and timer as given in Figure 3.1 of chapter 3. The beakers are kept on a platform, which rotates at a speed of 2 rpm. An equivalent amount of kraft paper and pressboard (in the ratio of 20:1:1 for oil:paper:pressboard), along with a copper wire (of length 475±2 mm and 1mm diameter rolled into a spiral of 30 mm dia and 50 mm height) is inserted into the samples and the temperature of the oven is maintained at 115±1^{o}C as per standard [149]. The ageing is carried out for duration of 500 hours. After 500 hours of ageing, the oils samples are taken out for performing the ACBDV analysis.

5.3 ACBDV analysis

The ageing of the oil samples at raised temperatures for extended periods alters the dielectric properties significantly. Therefore, a comparative investigation of ACBDV is necessary to understand the changes for all the four types of oils. The distribution data of ACBDV are tested for normal and Weibull distributions. The hypothesis testing is considered to confirm whether or not the distribution follows the assumption.

A high ACBDV of any insulation is beneficial for the lifetime of the apparatus. The presence of moisture, conductive particles and bubbles in the oil is not desirable, as they tend to lower the BDV. The ACBDV test is done for all samples of new and aged oils at room temperature with a frequency of 50±0.5 Hz and voltage ramping rate of 2kV/sec with the Megger OTS 100AF test setup as show in Figure 5.1, which has a spherically capped brass electrodes of 12.5 mm diameter separated by 2.5 mm gap as per IEC 60156 [150]. A total of 30 breakdowns are performed out for new and 500 hours aged oil samples.

TH-2868_156302003

Figure 5.1: ACBDV test setup.

The mean ACBDV values of NEO, NEO-NF and their aged samples are given in Table 5.1 and it is observed from the table that the augmentation in the values for new NEO-NF to NEO is nearly 1.22% and in case of aged samples, a decrease in values of BDV is observed. However, the aged NEO-NF shows an increment of 2.85% when compared with aged NEO. The decrease in the mean ACBDV of aged NEO and aged NEO-NF is by 14.63% and 12.19% respectively compared to fresh NEO. This corroborates that NFs show lower degradation relative to base oil, as ageing time progresses. When NPs are added to an insulating liquid, the charge entrapment occurs on the exterior of the NPs on application of electric field [1]. This slows down the streamer development, resulting in higher values of BDV in the NF. With ageing, sludge formation takes place and other kinds of impurities also evolve in due course of time. The amount of moisture content also increases, which results in lower BDV values. Figure 5.2 shows the ACBDV distribution for NEO, NEO-NF, aged NEO and aged NEO-NF.

Table 5.1: Enhancement in mean ACBDV.

Oil samples	Mean ACBDV values (kV)	% increase in mean ACBDV
NEO	82.00	0
NEO-NF	83.00	+1.22
Aged NEO	70.00	-14.63
Aged NEO-NF	72.00	-12.19

TH-2868_156302003

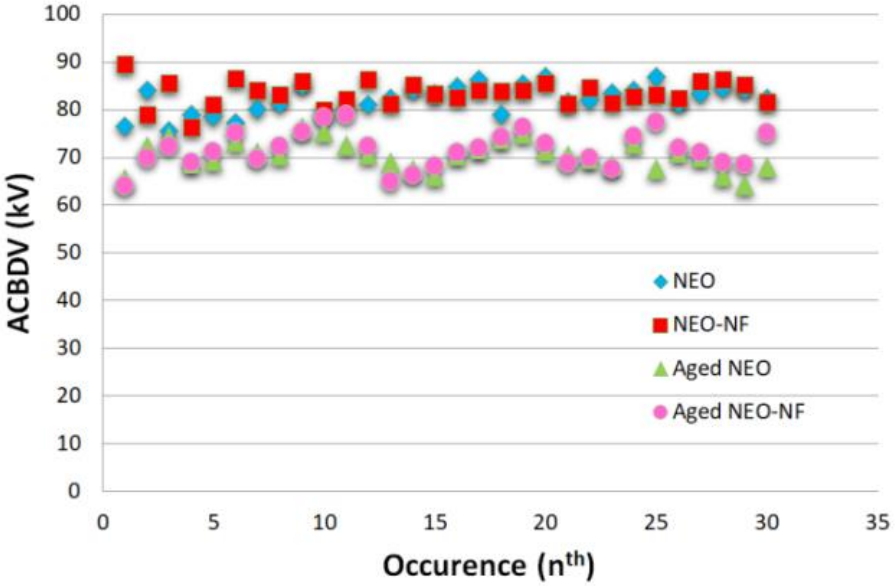

Figure 5.2: Distribution of ACBDV of the oil samples with 30 data values.

From the Figure 5.2, the frequency distribution of data appeared to be normal, so a probability distribution plot is considered relating to normal distribution for all the oils in Figure 5.3. The Bell curve is plotted along with the histogram of the distribution data. To ascertain and confirm whether these data follow a particular distribution, a statistical hypothesis testing is carried out for normal, 2-parameter and 3-parameter Weibull distributions.

5.4 Statistical hypothesis testing

Hypothesis testing is a statistical tool whereby an assumption is tested regarding a population parameter. The procedure employed is governed by the nature of the data used and the reason for the analysis. Hypothesis testing assesses the acceptability of a hypothesis by using a set of distributed sample data. There are two different hypotheses that are used: (i) the null hypothesis (H_O) and (ii) the alternative hypothesis (H_A). The null hypothesis is usually a hypothesis that states that a set of data follows a particular distribution or it is a hypothesis of equality between population parameters. The alternative hypothesis contradicts the null hypothesis and they are mutually exclusive. However, one of the two hypotheses will always be true. Distribution tests are hypothesis tests that determine whether your sample data are drawn from a population that follows a hypothesized probability distribution. The distribution tests also have a null hypothesis and an alternative hypothesis, to confirm whether or not the selected data follow a particular distribution.

TH-2868_156302003

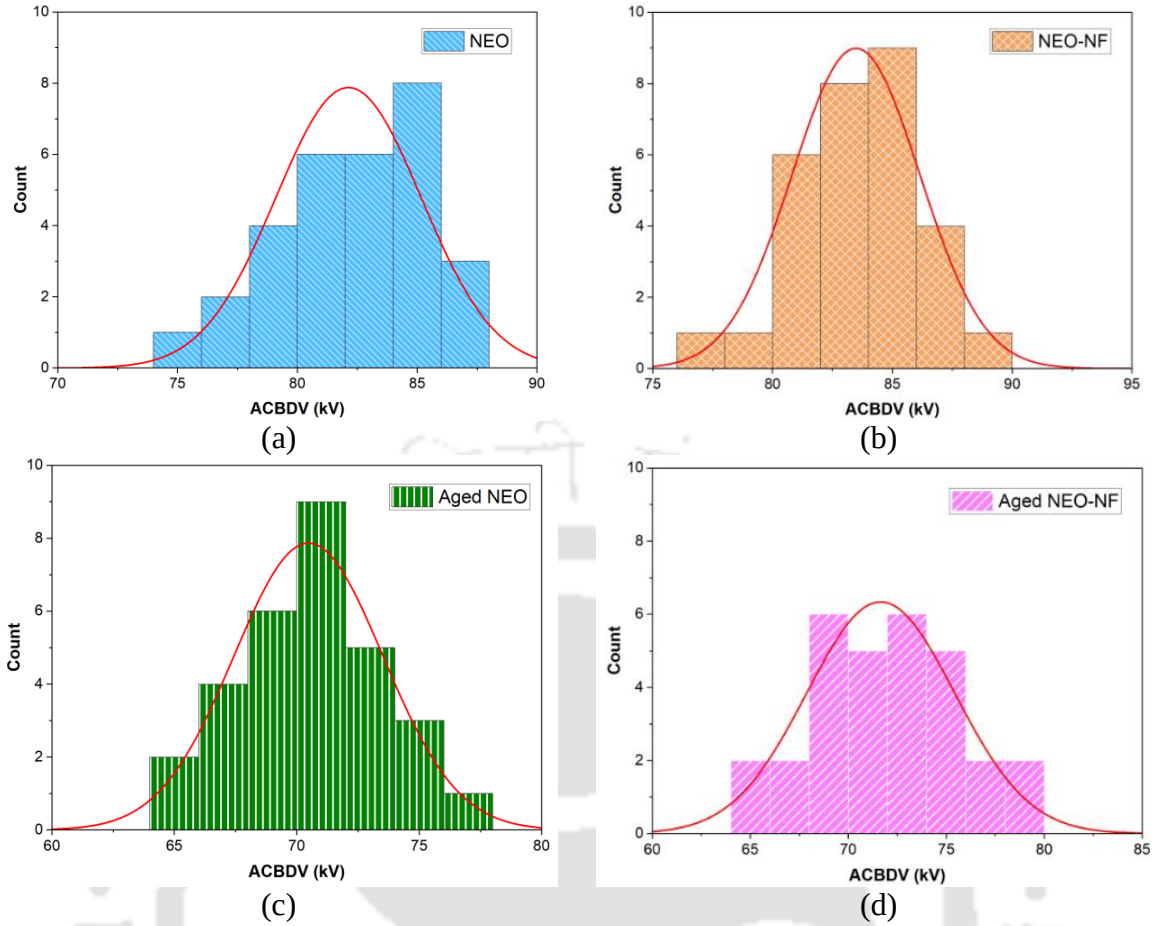

Figure 5.3: Histogram with bell curve of ACBDV of (a) NEO (b) NEO-NF (c) aged NEO, and (d) aged NEO-NF.

5.4.1 Shapiro-Wilk test for normality

The Shapiro-Wilk test is one kind of distribution test used to calculate W- and p-value which ascertain the normality of a dataset [22, 131]. In this statistical analysis, a significant level test of 5% (α_s = 0.05) is considered for a normal distribution. To check if a hypothesis is valid or not, p-value is used to weigh the strength of the hypothesis and see if it is statistically significant. If the null hypothesis is correct, then the p-value is the probability of gaining the results as extreme as the observed results of the statistical test. A higher p-value (greater than the significant level α_s =0.05) indicates that the null hypothesis is accepted, otherwise it is rejected.

The Shapiro-Wilk test is considered as a very powerful tool to ascertain the normality of a distribution. This technique calculates a W statistic that tests whether a random sample, $y_1, y_2, \ldots, y_n$ arises from a normal distribution. It always satisfies $0 < W \leqslant 1$. For values of W close enough to 1, the null hypothesis for normality is not rejected. For smaller values of W, it will be rejected. The W statistic is calculated as follows:

TH-2868_156302003

$$W = \frac{\left(\sum_{i=1}^{N} c_i y_i\right)^2}{\sum_{i=1}^{N}\left(y_i - \bar{y}\right)^2} \tag{5.1}$$

where the y_i are the data values, $\bar{y}$ is the sample mean, and the c_i are constants of the distribution set with N sample values. The H_O and alternate H_A for the Shapiro-Wilk test are considered as:

H_O: The distribution follows normality

H_A: The distribution does not follow normality

The Shapiro-Wilk test is run in the R-studio software and the results of test statistic and p-value are given in Table 5.2. Since, all the p-values are higher than the significance level of 0.05, so we fail to reject the null hypothesis. Also, the values of the test statistic W are close to unity, which indicates that there is negligible deviation from normality.

Table 5.2: Shapiro-Wilk test parameters.

Oil samples	p-value	W-value	Conformity to normal distribution
NEO	0.538	0.96874	Confirmed
NEO-NF	0.649	0.97531	Confirmed
Aged NEO	0.994	0.98942	Confirmed
Aged NEO-NF	0.922	0.98412	Confirmed

5.4.2 Anderson-Darling test

The Anderson-Darling test is one kind of distribution test used to calculate AD-value and p-value [22, 131] and ascertain the conformity to a distribution for a particular dataset. In this statistical analysis, a significant level test of 5% (α_s = 0.05) is considered. To check if a hypothesis is valid or not, p-value is used to weigh the strength of the hypothesis and see if it is statistically significant. If the null hypothesis is correct, then the p-value is the probability of gaining the results as extreme as the observed results of the statistical test. A higher p-value (greater than the significant level α_s =0.05) indicates that the null hypothesis is accepted, otherwise it is rejected. The Anderson-Darling test is considered as it is a very powerful tool to ascertain if a sample of data came from a population with a specific distribution. This technique calculates an *AD*-value that tests whether a random sample, x_1, x_2, …, x_n arises from a particular distribution.

TH-2868_156302003

The *AD*-value is calculated as follows:

$$AD = -N - \frac{1}{N}\sum_{i=1}^{N}(2i-1)[\ln F(x_i) + \ln(1 - F(x_{N-i+1}))] \tag{5.2}$$

where the x_i are the data values, N is the sample size, and $F(x)$ is the cumulative distribution function (CDF) for the specified distribution. The H_O and H_A for the Anderson-Darling test are considered as:

H_O: The distribution follows a specified distribution

H_A: The distribution does not follow the specified distribution

5.5 Normal and Weibull test

5.5.1 Normal distribution

Since all the p-values are higher than the significance level of 0.05, so we fail to reject the null hypothesis and confirm that the dataset belongs to normal distribution. The test parameters are given in Table 5.3. Figure 5.4 shows the cumulative probability of ACBDV of all the four oil samples. The straight lines are the references to which the values should be close. The probability plot also indicates the proximity of the predicted values and reference lines, which shows that the frequency distributions of ACBDV data are normal. The CDF of a standard normal distribution is given by (5.3),

$$F(x) = \int_{-\infty}^{x} \frac{e^{-x^2/2}}{\sqrt{2\pi}} dx \tag{5.3}$$

where x is the ACBDV data points in the present analysis.

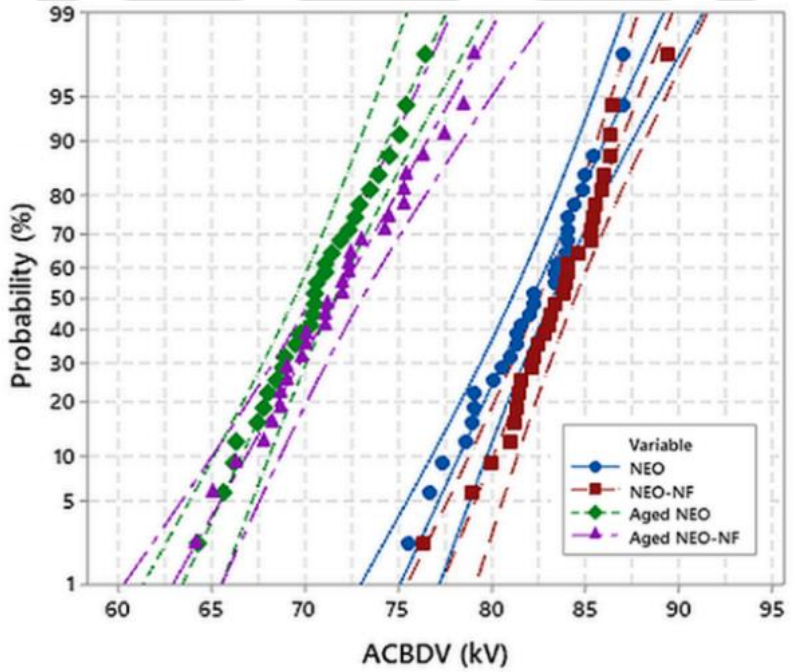

Figure 5.4: Normal probability plot of all oil samples.

TH-2868_156302003

The probability of occurrence of ACBDV at 5%, 10% and 50% are given in Table 5.3. The skewness and kurtosis data also govern whether a distribution data set is normal. In a perfectly normal distribution, the values of skew and kurtosis are zero. These values specify the deviance from normality. If the skewness value is positive, it is called positive skewed and it indicates that the values of the distribution are grouped at the lower end. Similarly, if the skewness value is negative, it is called negatively skewed and it indicates that the mean values of the distribution are grouped at the higher end. The skewness (S) is given as,

$$S = \frac{N}{(N-1)(N-2)} \sum_{i=1}^{N} \frac{(x_i - \bar{x})^3}{s^3} \tag{5.4}$$

where N is the sample size, x_i is the i^{th} value of the dataset, $\bar{x}$ is the average and s is the sample standard deviation.

Table 5.3: Normal distribution test parameters.

	Anderson-darling test parameters			ACBDV for different probability (kV)		
Oil samples	p-value	AD-value	Conformity to normal distribution	5%	10%	50%
NEO	0.538	0.309	Confirmed	76.70	78.00	82.30
NEO-NF	0.649	0.271	Confirmed	78.90	80.50	83.90
Aged NEO	0.994	0.106	Confirmed	65.00	66.10	70.50
Aged NEO-NF	0.922	0.172	Confirmed	64.80	67.00	71.7

The kurtosis value signifies the degree to which the values of the dataset cluster at the tails or at the peak of a distribution. The positive kurtosis signifies that the distribution has a sharper peak and heavier tails compared to a perfectly normal distribution. Whereas, distributions having negative kurtosis means that the distributions have a flatter peak and thinner tails compared to a perfectly normal distribution. The kurtosis (K) is given as,

$$K = \left\{ \frac{N(N+1)}{(N-1)(N-2)(N-3)} \sum_{i=1}^{N} \frac{(x_i - \bar{x})^4}{s^4} \right\} - \frac{3(N-1)^2}{(N-2)(N-3)} \tag{5.5}$$

where N is the sample size, x_i is the ith value of the dataset, $\bar{x}$ is the average and s is the sample standard deviation. The skewness and kurtosis which are calculated using (5.4) and (5.5) respectively, are shown in Table 5.4 and Figure 5.5. The standard deviation and variance of the distribution values are also given in Table 5.4. Ideally, the value of skewness

TH-2868_156302003

and kurtosis in a normally distributed dataset should be 0 and 3 respectively. Since the values of skewness and kurtosis vary from -0.406 to +0.076 and from -0.507 to+0.917 respectively, the experimental findings do not follow normality rigidly.

Table 5.4: Statistical parameters.

Oil samples	Skewness	Kurtosis	Standard deviation	Variance
NEO	-0.386	-0.507	3.039	9.235
NEO-NF	-0.406	0.917	2.663	7.092
Aged NEO	-0.035	-0.459	3.043	9.263
Aged NEO-NF	0.076	-0.409	3.777	14.263

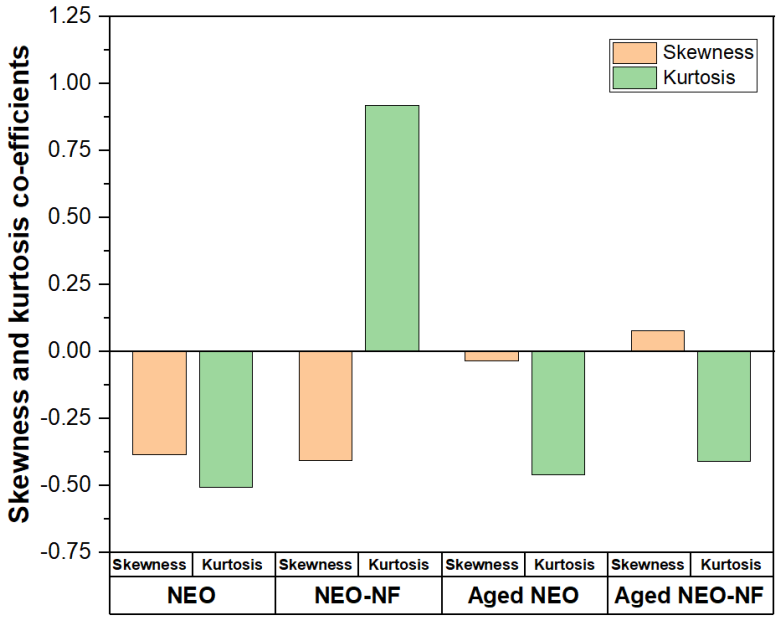

Figure 5.5: Skewness and kurtosis of the oil samples.

5.5.2 Weibull distribution

a) 2-parameter Weibull distribution

To understand the behaviour of the breakdown voltages, 2- and 3-parameter Weibull statistical analysis are also considered. Weibull statistical analysis is a very effective statistical tool to determine the probability of failure of all the oil samples. Firstly, the 2-parameter Weibull model is considered to plot the ACBDV data for fresh and aged NEO and NEO-NF in Figure 5.6 and the Weibull distribution parameters are presented in Table 5.5. The 2-parameter Weibull distribution is plotted with a confidence interval of 95% and the expression is given as,

TH-2868_156302003

$$F(x:\alpha,\beta)=1-\exp(-(x/\alpha))^{\beta};x>0 \tag{5.6}$$

where x is the ACBDV, $F(x)$ is the CDF, α is the scale parameter which gives the spread of the Weibull distribution, and β is the shape parameter which defines the shape of any distribution. It is equal to the slope of the line in the probability plot. The hypothesis test also showed that the p-values are greater than 0.05, thus all the four oils conforms to 2-parameter Weibull distribution. The failure probabilities in oil samples at 5, 10 and 50% are given in Table 5.6.

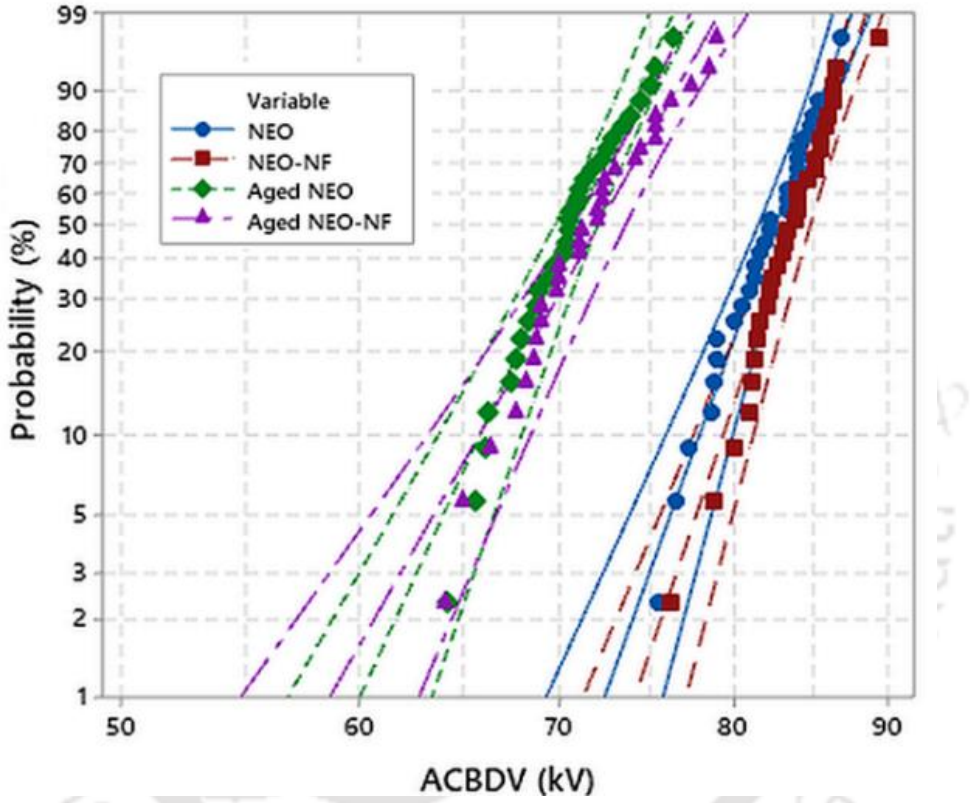

Figure 5.6: 2-parameter Weibull distribution of ACBDV of all oil samples.

Table 5.5: 2-parameter Weibull parameters.

Parameters	Oil Samples			
	NEO	NEO-NF	Aged NEO	Aged NEO-NF
α	83.53	84.71	71.91	73.43
β	32.28	34.44	25.46	20.48
γ	-	-	-	-
p-value	>0.25	>0.25	>0.25	0.246
AD-value	0.220	0.373	0.315	0.461
Conformity to Weibull	Confirmed for all cases			

TH-2868_156302003

Table 5.6: Failure probabilities of the oil Samples (kV).

Oil samples	2-parameter Weibull			3-parameter Weibull		
	50%	10%	5%	50%	10%	5%
NEO	82.55	77.88	76.17	82.32	77.90	76.56
NEO-NF	83.85	79.77	78.20	83.77	79.77	78.39
Aged NEO	70.88	66.28	64.61	70.52	66.34	65.23
Aged NEO-NF	72.13	66.51	64.48	71.67	66.59	65.25

The improvement in the ACBDV for NEO-NF compared to NEO at 50, 10 and 5% failure probability are 1.57, 2.42 and 2.66% respectively. Similarly, the % increase in ACBDV for the aged NEO-NF when compared to aged NEO at 50, 10 and 5% probabilities is 1.76%, 0.347% and -0.20% respectively.

b) 3-parameter Weibull distribution

Further, the 3-parameter Weibull model is considered to check how the dataset fits the distribution and understand the behaviour of the breakdown voltages when the threshold parameter is included. The 3-parameter Weibull method is used to plot the ACBDV data for fresh and aged oil samples in Figure 5.7. The Weibull distribution parameters are presented in Table 5.7. The Weibull distribution for the 3-parameter model is plotted with a confidence interval of 95%, and is expressed as below,

$$F(x:\alpha,\beta,\gamma) = 1 - \exp\left\{-\left[(x-\gamma)/\alpha\right]^{\beta}\right\}; x \geq \gamma \quad (5.7)$$

where x is the ACBDV, $F(x)$ is the CDF, α is the scale parameter, β is the shape parameter and γ is the threshold parameter. The threshold parameter gives the failure free region in dataset. The hypothesis test also showed that the p-values are greater than 0.05, thus all the four oils conforms to 3-parameter Weibull distribution.

The failure probabilities of oil samples at 5, 10 and 50% are given in Table 5.6. The improvement in the ACBDV for NEO-NF compared to NEO at 50%, 10% and 5% probabilities are 1.76%, 2.4% and 2.39% respectively. Similarly, the % increase in ACBDV for the aged NEO-NF when compared to aged NEO at 50%, 10% and 5% probabilities are 1.63%, 0.376% and 0.03% respectively.

TH-2868_156302003

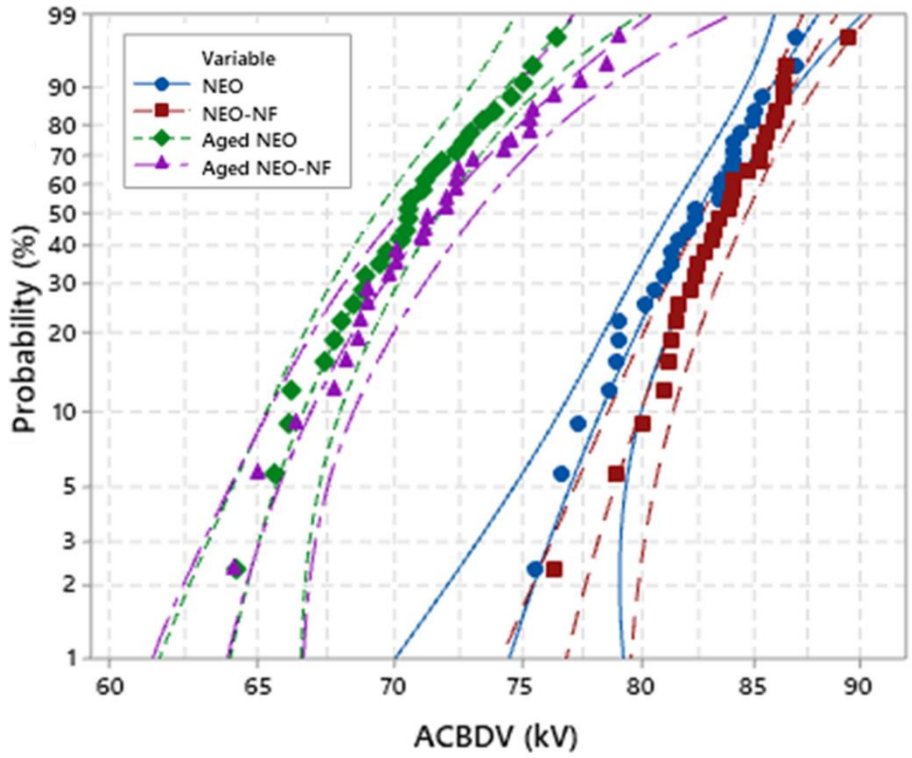

Figure 5.7: 3-parameter Weibull distribution of ACBDV of all oil samples.

Table 5.7: 3-parameter Weibull parameters.

Parameters	Oil samples			
	NEO	NEO-NF	Aged NEO	Aged NEO-NF
α	17.70	13.64	10.02	11.49
β	6.57	5.50	3.36	3.04
γ	65.65	70.86	61.48	61.38
p-value	>0.5	>0.5	>0.5	>0.5
AD-value	0.222	0.242	0.114	0.171
Conformity to Weibull	Confirmed for all cases			

5.5.3 Goodness of fit

The goodness of fit gives the measure of how well a dataset fits a distribution by giving the values of correlation coefficient (CC). The CC measures the strength of the linear relationship between the *x* and *y* variables on a probability plot. The correlation values range between -1 and 1. Higher the correlation values the better is the fit of the data. The expression of CC is given by,

TH-2868_156302003

$$\rho = \frac{\sum_{i=1}^{N}\left(x_i - \bar{x}\right)\left(y_i - \bar{y}\right)}{\left(N-1\right)s_x s_y} \tag{5.8}$$

where $\bar{x}$ is the sample mean for the first variable x_i, s_x is the sample standard deviation for the first variable, $\bar{y}$ is the sample mean for the second variable y_i, s_y is the sample standard deviation for the second variable and N is the number of rows with no missing data for the pair of variables. The nearer the value of CC is towards 1, the better is the fit of the data. The values for the CC are given in Table 5.8 for all the distributions. It is observed that NEO and NEO-NF dataset fits the 3-parameter Weibull plot better. However, for the aged NEO the dataset shows equal CC for both normal and 3-parameter Weibull plots. And the aged NEO-NF fits the normal distribution slightly better. Taking all the analysis into consideration, it can be confirmed that the 3-parameter Weibull distribution fits all the 4 breakdown datasets very well.

Table 5.8: Goodness-of-fit coefficients for different distributions.

Oil samples	Normal	2 parameter Weibull	3 parameter Weibull
	CC	CC	CC
NEO	0.988	0.991	0.995
NEO-NF	0.982	0.986	0.988
Aged NEO	0.997	0.983	0.997
Aged NEO-NF	0.995	0.977	0.994

5.6 Summary of the chapter

This work shows the statistical analysis of ACBDV of four oil samples-NEO, NEO-NF, aged NEO and aged NEO-NF. The main outcome of this research work is as below:

- The mean ACBDV of NEO-NF is found to be higher than NEO because of the addition of the semi-conductive TiO_2 NPs.
- With ageing, the ACBDV decreases because of the oxidation of the oils and deposition of sludge in the oil in due course of time. However, the degradation in aged NEO-NF is less compared to aged NEO.
- Shapiro-Wilk test provides an acceptable result regarding the conformity to normality of the samples. Anderson-Darling test provides an acceptable result regarding the conformity to the specified distributions by giving the *AD*-values and the p-values.

TH-2868_156302003

- The CC is chosen to analyze the goodness of fit which shows that all the 4 datasets follow a 3-parameter Weibull distribution quite well.

Considering the advantages of using NEO, a new non-edible variant of NEO is developed and compared with the existing NEOs in the next chapter. Although the semiconductive TiO_2 gives favourable results when dispersed in insulating oil with regards to its breakdown strength, the BDV is observed to be only marginally higher. Also, there is a tendency of the NPs to align in the direction of the field which may lead to the possible formation of a conducting channel, causing an inadvertent breakdown. Thus, an insulating NP is used to further enhance the dielectric properties of the new NEO for an alternative solution as discussed in the next chapter.

Note: This work, "Investigation of Natural Ester based Insulating Liquid using Statistical Hypothesis Testing," has been published in IEEJ Transactions on Fundamentals and Materials, 2021, vol. 141, no.10.

TH-2868_156302003

TH-2868_156302003

6

Performance analysis of natural ester based NFs

Contents

TH-2868_156302003

6.1 Introduction

The introduction of non-edible VOs in transformer application leads to an altogether environment-friendly alternative to MO used in transformers. The oil-paper interaction shows enhanced characteristics when VO is used in place of MO. Considering the advantages of non-edible VO, pongamia pinnata VO is developed for the study and to further enhance its properties NPs are introduced into the base fluid.

Pongamia pinnata oil (PPO) which is considered in this study is a non-edible oil, but it cannot be used in its crude form as an insulating fluid in transformers. Therefore, PPO is altered to pongamia oil methyl ester (POME) to achieve the desired properties of TO. Also, modifications are performed on both MO and POME for obtaining better dielectric and thermal properties by adding NPs. Studies have been carried out in recent times by dispersing different NPs in insulating liquids to obtain the NF. The addition of NPs into the oil for enhancing the thermal and dielectric properties has been an area of research for quite long. Hwang et al. have suggested that conductive NP Fe_3O_4 based NFs have superior positive breakdown levels with sluggish streamer velocities than that of pure TO. This is because of charging of the NPs and, thus fast electrons are converted to slow negatively charged NPs. Thus, the positive streamer velocity decreases due to electron trapping resulting in higher electrical breakdown strength [65, 81]. Studies have also shown that the molecular ionization in oil with NPs causes an electric field to develop and space charge wave propagates between electrodes, producing heat that forms vapours in the TO creating positive streamer. Research is carried out with exfoliated layers of hexagonal boron nitride (h-BN) in oil and it is found that they have high thermal conductivity compared to base oil [90]. The insulating NPs (h-BN) are considered for the present work because when an electric field is applied, there is a tendency of the NPs to align in the direction of the field and when these NPs are conducting or semiconducting, there is a possibility to form a conducting channel and cause an inadvertent breakdown. The insulating 3D h-BN NPs are exfoliated to get 2D exfoliated h-BN (Eh-BN) nanopowder. Then these NPs are added to both MO and VO. It is observed that both thermal and electrical properties are enhanced by the addition of Eh-BN NPs with the VO [91].

In this research work, section 6.2 addresses the preparation of the oil samples, section 6.3 addresses the results and discussions and the summary is included in section 6.4.

TH-2868_156302003

6.2 Materials and methods

6.2.1 Pongamia pinnata oil (PPO)

Pongamia pinnata belongs to a species of family Leguminosae and genus Pongamia. Commonly known as karanji, this plant is resistant to drought and has the property of nitrogen fixing. An investigation report shows that a single tree of karanji can produce 9-90 kg pongamia pinnata seeds per year [132]. In recent times, pongamia pinnata has been accepted as a practical source of non-edible oil for biofuel production [133].

The pongamia pinnata seeds collected from the trees located in IIT Guwahati campus are sun-dried for two to three days till the available moisture is removed. The kernel of the pongamia seeds is manually separated from the thick covering. The pongamia seeds are crushed into fine particles with the help of a grinder and the process of solvent extraction is followed, in which petroleum benzene is mixed with about 24 gm of ground seeds to extract the oil. Considering 5 samples of ground seeds of 24 gm each, the process of solvent extraction and condenser is followed to extract the oil. The percentage yield of oil obtained from 5 samples of ground seeds ranges from 25-30%.

The main component of VOs is triacylglycerol which constitutes 98% of the total and rest are fatty acid molecules linked to a single glycerol arrangement. The remaining constituents of VOs consist of free fatty acids, diglycerols, tocopherols and sterols, which are lesser in quantity. The triglyceride configuration is formed by condensation of three hydroxyl groups with carboxyl groups of three fatty acids, as shown in Figure 1.2 of chapter 1. The structure of triglyceride makes the VO highly viscous because of their high molecular weight. The properties of PPO are given in Table 6.1.

The crude PPO does not satisfy the specifications of transformer insulating liquid as per IEEE C.57.147 [147] and ASTM D6871 [151] standard for VO. So, PPO needs to be modified to POME because of its poor viscosity, acidity and pour point [98]. Crude oil is heated at 110-130^{o}C for 30 minutes for evaporation of contaminated moisture from the oil. For the production of POME, it is necessary to evaluate the value of the free fatty acid (FFA) and is measured by the titration method using 0.1N Potassium Hydroxide (KOH) solution. Since, the FFA value of PPO is 7.5%, which is more than 1%, two-step transesterification (including acid and base) process is required to form POME. FFA% is calculated as per standard ASTM D5555 [152].

TH-2868_156302003

Table 6.1: Specifications of MO, PPO, POME, JAT and FR3.

Characteristic	MO	PPO	POME	JAT	FR3
Density (kg/m^3)	0.825	0.93	0.9	0.879	0.91
Kinematic viscosity at 27^{o}C (cSt)	11.25	32	14	22	59
Interfacial tension at 27^{o}C (mN/m)	47	20	21.2	10.7	20.6
Flash point (^{o}C)	140	250	280	190	268
Pour point in (^{o}C)	-6	4	-1	0	-18
Dielectric dissipation factor at 90 ^{o}C	0.0089	0.0080	0.0045	0.0088	0.0086
Water content (ppm)	25	1080	586	650	53
ACBDV (kV)	35	89	82	79	82
Thermal conductivity (W/m-K)	0.128	0.160	0.152	0.162	0.163

Transesterification is the process which involves the production of POME from the crude oil to reduce the viscosity and acid levels and make it comparable to that of MO for transformer application. The reaction of the transesterification process is given in (6.1). In this process, the addition of methanol for the processing of triglyceride to Fatty Acid Methyl Ester (FAME) takes place. The alcohol reacts with the fatty acids to form three molecules of mono-alkyl ester and crude glycerol.

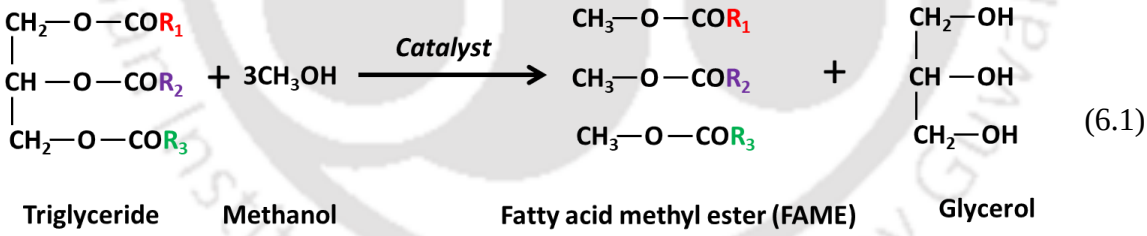

(6.1)

Two-step transesterification (acid esterification and base transesterification) set up is developed in the laboratory as shown in Figure 6.1. The FFA value in the crude oil is reduced by the acid esterification process to less than 1% using sulphuric acid (H_2SO_4) as a catalyst. The experiment is done in a round bottom flask with a reflux condenser along with a magnetic stirring hotplate with a temperature controller and a drain valve arrangement with a separating funnel. A molar ratio of 6:1 for methanol to crude oil is considered. When the temperature of the mixture reaches 60^{o}C, 1 vol.% of H_2SO_4 is poured into the round bottom flask as a catalyst [134, 135]. The solution is continuously stirred at 600 rpm for a period of 2

TH-2868_156302003

hours by using the magnetic stirrer. Then the prepared sample is transferred into a separating funnel and kept for 24 hours for the acid separation. The density variation of oil and water causes the water to precipitate in the lower part, lower fatty acid based oil forms the middle part and the mixture of sulphuric acid and methanol lies in the upper part. The settled water is taken out using a drain tap attached to the separating funnel and finally the lower FFA oil is collected. The FFA value is calculated to determine the decrease in acidity percentage of the crude oil. It is observed that the acid value is 1.47 mg KOH/g whose corresponding FFA level is 0.73%, which is desirable.

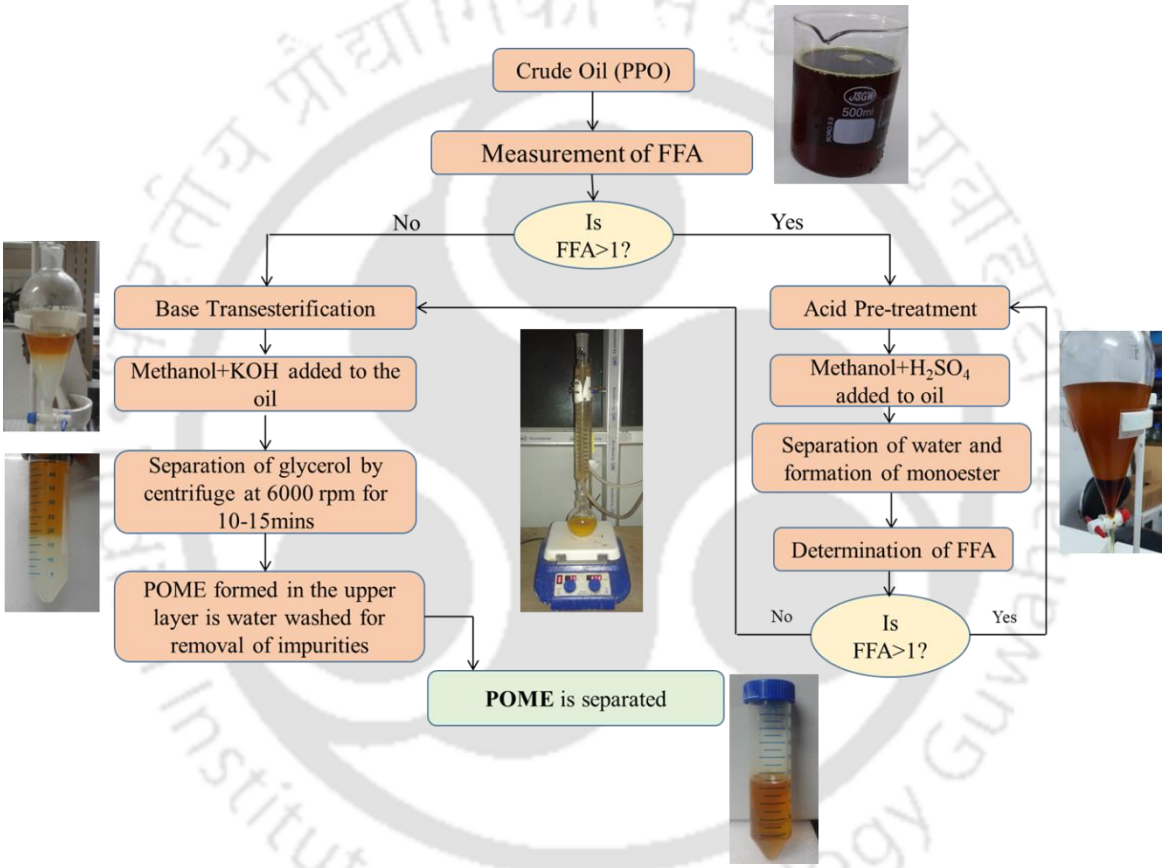

Figure 6.1: Transesterification process.

The next process is the base transesterification, in which the oil obtained from the previous step is transferred to a round bottom flask and heated up to a temperature of 60^{o}C. A molar ratio of 6:1 for methanol to oil is considered and a suitable amount of base catalyst potassium hydroxide (KOH, 1% by wt.) is poured into the mixture. The solution is heated and stirred for 3 hours. Then it is kept in separating funnel for 24 hours to settle the glycerol which has high density. Two layers are formed in the separating funnel, the upper one is the

TH-2868_156302003

FAME and the lower one is glycerol. The solution is continuously washed by using hot distilled water which removes the unwanted impurities. It is then centrifuged at 6000 rpm for 10-15 minutes to obtain the FAME. Due to the density difference, the crude PPO of low density floats on the top of the centrifuge tube while the unwanted glycerol settles down. The composition of all the fatty acids present in POME extracted from the GCMS study is given in Table 6.2. The liquids are dried in vacuum oven at 60^{o}C for 72 hours.

Table 6.2: Composition of POME.

FAME	Retention time (min)	Molecular formula	Molar mass, g/mol
Hexadecanoic acid	22.48	$C_{17}H_{34}O_2$	270
11-Octadecenoic acid	24.33	$C_{19}H_{36}O_2$	296
Octadecenoic acid	24.46	$C_{18}H_{34}O_2$	282.47
CIS-11-Eicosanoic acid	26.06	$C_{20}H_{38}O_2$	310.51

6.2.2 Preparation of NF

Two types of NFs such as MO-NF and POME-NF are prepared by dispersing the Eh-BN NPs with the MO and POME. The h-BN powder of primary size 1μm, purity 98% as nanofillers are considered for this purpose. The important properties of the fresh MO and POME are given in Table 6.1 along with the commercially available FR3 oil procured from Cargill India and the JAT procured from a govt. agency. The thermophysical and electrical properties of the h-BN NPs are given in Table 6.3. The h-BN NP has a high thermal conductivity of 300 W/m-k at 25^{o}C and high electrical resistivity, i.e. 10^{15} Ω-cm, therefore it is chosen to prepare the NF in this research work.

As the primary particles size of the nanopowder are approximately in the form of large spherical agglomerates so the surface modifications of the NPs are very much necessary to get enhanced dispersion behavior in the base fluid. The exfoliation process is followed to convert the 3D h-BN particle into 2D nanosheets which are seen in Figure 6.2 through the transmission electron microscopy (TEM) images. The average size of the Eh-BN powder is observed to be 50-100 nm as per TEM analysis. It is observed from Figure. 6.2 (b), around 10 to 12 layers of h-BN nanosheets are present in Eh-BN. Only 5gm of Eh-BN nanosheets are obtained that for the 8 gm of pure h-BN powder. It confirms that the size of the particles is

TH-2868_156302003

reduced from 1 μm to 50-100 nm. Enhancement of surface area to volume ratio occurs because of exfoliation of the h-BN-NPs. The process flow diagram is shown in Figure 6.3.

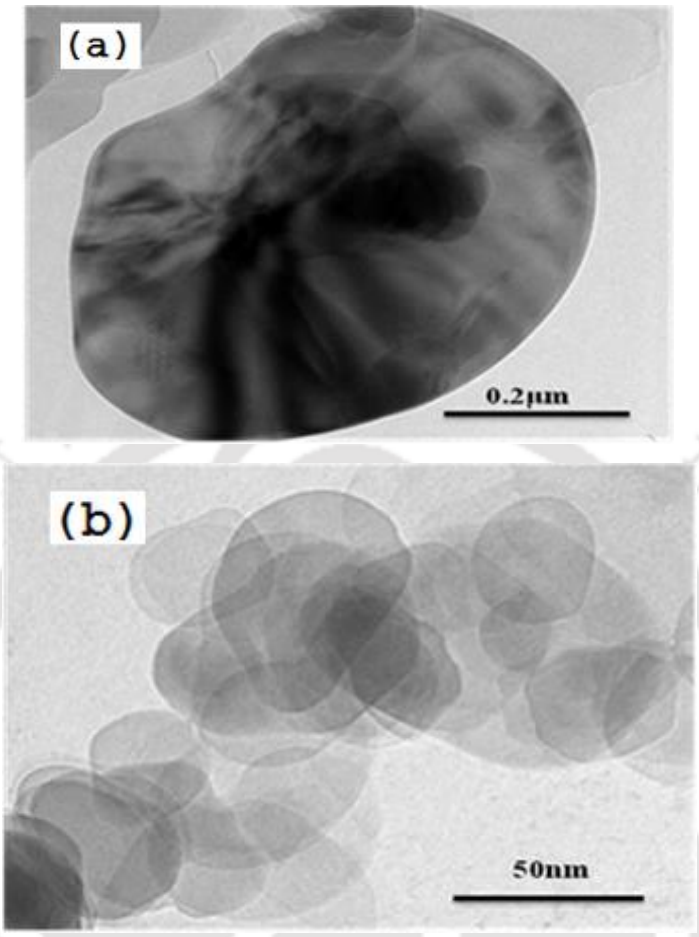

Figure 6.2: TEM results of (a) 3D structure of h-BN NP and (b) 2D nanosheets formed after exfoliation.

Table 6.3: Specifications of h-BN NP.

Characteristics	Specification
Purity	98 %
Size	1 μm
Density	2.29 g/cm^3
Dielectric constant	3-4
Thermal conductivity	300 W/m-K at 25^{o}C
Electrical resistivity	10^{15} Ω-cm
Thermal expansion coefficient	4×10^{-6}/^{o}C

TH-2868_156302003

In this process, the pure 5gm h-BN powder is mixed with isopropyl alcohol of 300 ml and then extensively sonicated for 2-3 hours using the probe sonicator. To maintain the solution at room temperature ice cubes are kept around the beaker so as to avoid a rise in temperature of the semi-prepared sample. Continuous monitoring of the sample temperature is carried out. The solution is centrifuged at 1500 rpm for 30 minutes after sonication, and the collected sample is vacuum filtered to get the Eh-BN particles. The isopropyl alcohol which is a better polar solvent is used to peel off the pure h-BN powder.

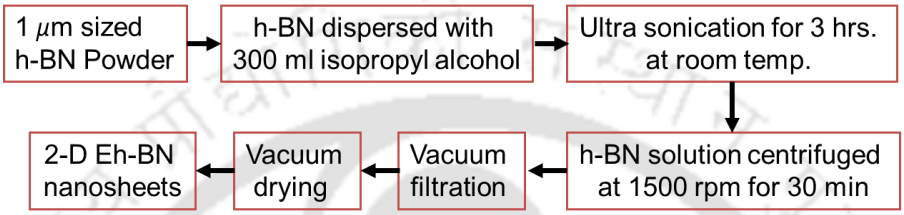

Figure 6.3: Exfoliation process of the h-BN powder.

The NF is prepared by dispersing the dielectric Eh-BN particles with 0.01 wt.% in the base fluid and the mixture is sonicated for 1-2 hours. The sonicated mixture is then put in a shaking incubator and finally a vacuum oven to dry out the moisture. The NF preparation process is depicted stepwise in Figure 6.4.

Figure 6.4: Nanofluid preparation with MO/POME.

TH-2868_156302003

6.3 Results and discussion

6.3.1 ACBDV analysis

The dielectric integrity of the insulating oil is studied by performing ACBDV test and it is measured in accordance with IEC 60156 standard at 50Hz and voltage ramping rate of 2kV/sec, using Meggar test kit shown in Figure 5.2 of chapter 5, with brass spherical electrodes set at 2.5 mm gap [150].

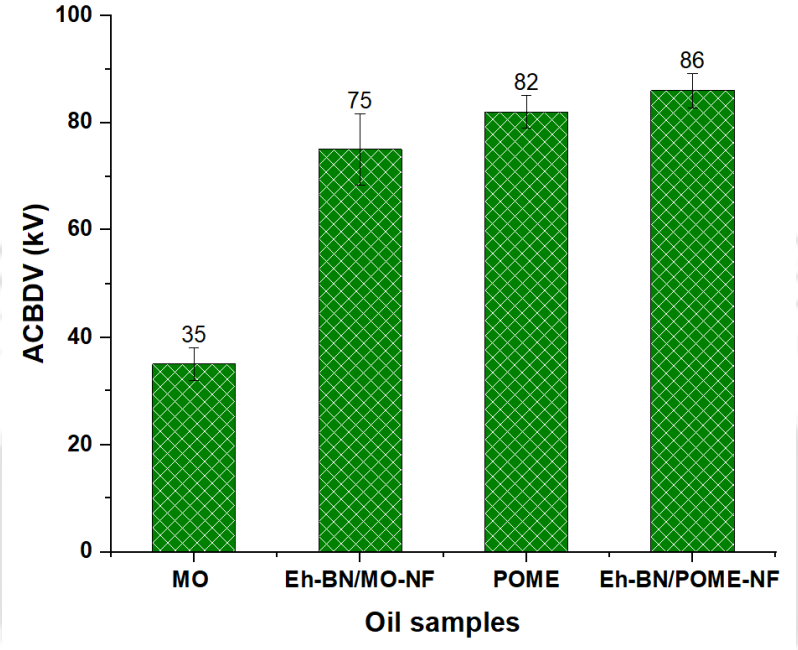

Figure 6.5: Mean ACBDV of oil samples.

Since MO is the major insulating oil for the transformer, a comparative analysis of the ACBDV of the MO, MO-NF, POME and POME-NF is carried out and presented in Figure 6.5. The moisture contents of all the insulating oils-MO, MO-NF, POME and POME NF as given in Table 6.4 are measured as per standard ASTM D6304. The value of mean ACBDV of POME-NF (86 kV), POME (82 kV) and MO-NF (75kV) are higher than that of MO (35kV) by 145.71%, 134.28% and 114.2% respectively, which are also given in Table 6.4. The POME has an ACBDV more than twice of MO, which means that this oil can better resist the high electrical stress compared to MO. The ACBDV of liquid insulating oils also highly depends on the moisture levels. The samples of VO tested have water content significantly higher than the conventional MO. Because of their chemical structure, VO has higher saturation limits in water content than that of MO. A 200 ppm water content level of VO has a relative humidity value of 26.7%, which is equivalent to 10 ppm of water content in

TH-2868_156302003

MO [136]. Thus, it is evident that the higher moisture levels of POME are comparable to MO, and thus the ACBDV of POME is observed to be higher than MO. It is obvious that the mean ACBDV of POME based NFs is greater than that of POME due to the addition of NPs. The breakdown strength is also dependent on charge trapping capacity. The addition of NPs to the insulating oil causes electron trapping on the surface of the NPs, thus suppressing the electric field and leading to an increase in breakdown strength.

Table 6.4: Enhancement in ACBDV.

Oil samples	ACBDV values (kV)	Moisture levels (ppm)	% increase in ACBDV
MO	35	25	0
Eh-BN/MO-NF	75	18	114.2
POME	82	586	134.28
Eh-BN/POME-NF	86	350	145.71

Statistical techniques are widely applied to understand dielectric failure data, out of which Weibull distribution is the most extensively used. From this study, the voltages at which the dielectric is most likely to breakdown is determined. Weibull distribution is an important tool for reliability analysis of the insulation performance. In this work, the ACBDV of 40 instances of each of the 4 oil samples are considered and statistical analysis is carried out by considering the 2-parameter Weibull model as shown in Figure 6.6.

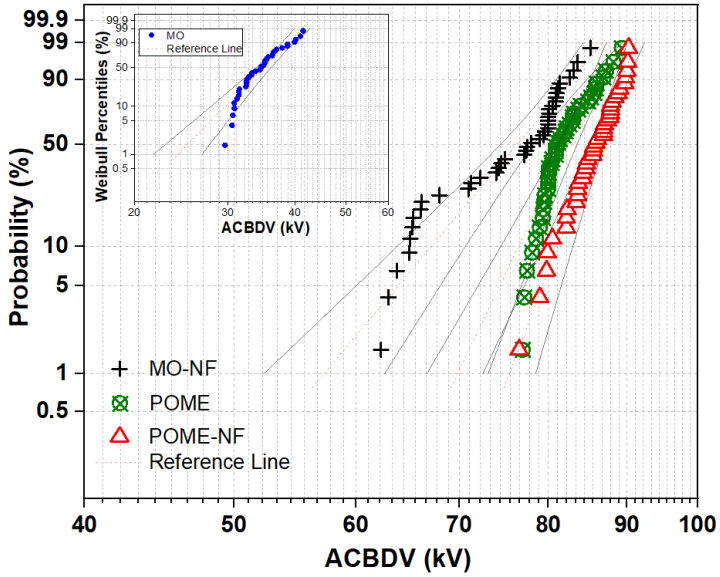

Figure 6.6: 2-parameter Weibull distribution of the ACBDV values.

TH-2868_156302003

The confidence interval considered for the distribution is 95%. In the 2-parameter model, the scale parameter α and the shape parameter β are fitted in the expression as below:

$$F(x:\alpha,\beta)=1-\exp\left\{-\left(\frac{x}{\alpha}\right)\right\}^{\beta};x>0 \quad (6.2)$$

where *F(x)* is the Weibull cumulative distribution function and *x* is the ACBDV. The Weibull parameters and the breakdown probabilities at 5, 10, 63.2% of failure instances are noted in Table 6.5. It is seen from the table that at each breakdown probability, there is a significant change in ACBDV values of Eh-BN/MO-NF, POME and POME-NF with respect to MO. Due to the presence of the NPs, there is an increase in the BDV values of MO-NF as compared to MO by 108.4%, 111.3% and 117.2% at 5%, 10% and 63.2% breakdown probabilities respectively. It is also seen from the table that the BDV values of POME are enhanced than MO by 152.2%, 154.8% and 131.6% at 5%, 10% and 63.2% breakdown probabilities respectively. This may be due to the structure of POME. Also, the BDV values of POME-NF are higher than MO by 158.1%, 161.3% and 141.6% at 5%, 10% and 63.2% breakdown probabilities respectively.

Table 6.5: Weibull parameters and ACBDV at different breakdown probabilities.

Oil samples	Weibull parameters		Withstand voltages					
	α	β	63.2%		10%		5%	
			BDV (kV)	Change (%)	BDV (kV)	Change (%)	BDV (kV)	Change (%)
MO	36	11.4	36	--	30.8	--	30.6	--
Eh-BN/MO-NF	78.2	14.7	78.2	117.2	65.1	111.3	63.8	108.4
POME	83.4	25.8	83.4	131.6	78.5	154.8	77.2	152.2
Eh-BN/POME-NF	87	32.4	87	141.6	80.5	161.3	79	158.1

To understand the enhancement of ACBDV of NF compared to the ACBDV of the base fluid, charge dynamics study of a NF is carried out. For the analysis, a spherical shape of Eh-BN NP is considered, with average radius *R* (= 75 nm), permittivity ε_2 (= $4\varepsilon_0$ F/m) and conductivity σ_2 (=10^{-13} S/m), which is bounded by MO with permittivity ε_1(= $2.03\varepsilon_0$ F/m) and conductivity σ_1 (= 10^{-12} S/m) or POME with permittivity ε_1(= $2.05\varepsilon_0$ F/m) and conductivity σ_1

TH-2868_156302003

(=1.26 × 10^{-13} S/m) is considered as shown in Figure 6.7(a). On the application of the electric field, E_0, the NP will undergo polarization as shown in Figure 6.7(b).

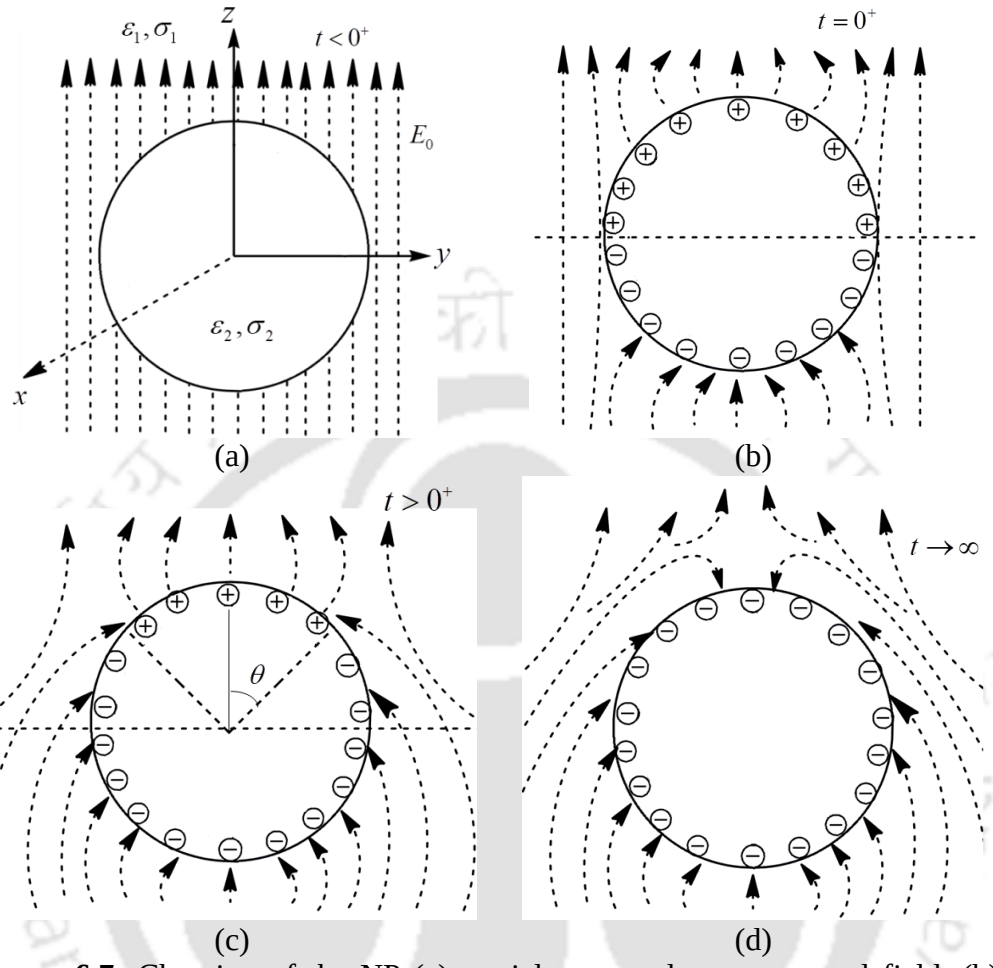

Figure 6.7: Charging of the NP (a) particle exposed to an external field, (b) ionization or polarization of the NP, (c) depletion of the positive ions, and (d) complete depletion of the positive ions.

The radial component of the electric filed in the oil outside the NP is [81],

$$E_r(r \geq R, \theta) = E_0\left[1 + \frac{2R^3}{r^3} C_\varepsilon e^{-t/\tau_r} + \frac{2R^3}{r^3} C_\sigma (1 - e^{-t/\tau_r})\right]\cos\theta \tag{6.3}$$

With time advancement, depletion of positive ions takes place as a higher number of electrons deposit on the surface of NP as shown in Figure 6.7(c). The expression of the electric field in the MO or POME on the surface of the NP in the presence of deposited electron charge *Q(t)* is [81],

$$E_r(r \geq R, \theta) = E_0\left[1 + \frac{2R^3}{r^3} C_\varepsilon e^{-t/\tau_r} + \frac{2R^3}{r^3} C_\sigma (1 - e^{-t/\tau_r})\right]\cos\theta + \frac{Q(t)}{4\pi\varepsilon_1 r^2} \tag{6.4}$$

TH-2868_156302003

where $C_\varepsilon = \frac{\varepsilon_2 - \varepsilon_1}{2\varepsilon_1 + \varepsilon_2}$, $C_\sigma = \frac{\sigma_2 - \sigma_1}{2\sigma_1 + \sigma_2}$ and $\tau_r = \frac{2\varepsilon_1 + \varepsilon_2}{2\sigma_1 + \sigma_2}$ is the relaxation time of the NPs.

The critical angle θ_c occurs at $E_r\ (r=R,\theta)=0$ and is,

$$\cos\theta_c = \frac{-Q(t)}{4\pi\varepsilon_1 R^2 E_0 C(t)} \tag{6.5}$$

where $$C(t) = 1 + \frac{2R^3}{r^3} C_\varepsilon e^{-t/\tau_r} + \frac{2R^3}{r^3} C_\sigma (1 - e^{-t/\tau_r}) \tag{6.6}$$

For an insulating NP, $\tau_r = \frac{2\varepsilon_1 + \varepsilon_2}{2\sigma_1 + \sigma_2}$ = 34 secs for MO-EhBN and 50 secs for POME-EhBN.

The dielectric relaxation in both the cases is negligible as the τ_r is quite long compared to the timescale for streamer growth (in nanosecond). Thus, the term $e^{-t/\tau r} \rightarrow 1$ and the $C(t)$ becomes,

$$C(t) = 1 + 2C_\varepsilon \times 1 + 2C_\sigma \times (1-1) = 1 + 2C_\varepsilon = \frac{3\varepsilon_2}{2\varepsilon_1 + \varepsilon_2} \tag{6.7}$$

The saturation charge Q_s for Eh-BN NP will be,

$$Q_s = -12\pi\varepsilon_1 R^2 E_0 \frac{\varepsilon_2}{2\varepsilon_1 + \varepsilon_2} \tag{6.8}$$

The current density charging the NP for $0 < \theta < \theta_c$ is,

$$J_r = -\rho_e \mu_e E_r (r = R) = -3\rho_e \mu_e E_0 \left[\frac{C(t)\cos\theta}{3} - \frac{\frac{Q(t)}{Q_s}}{\frac{\varepsilon_2}{2\varepsilon_1 + \varepsilon_2}} \right] \tag{6.9}$$

where ρ_e and μ_e represent the electron charge density and mobility respectively. The charging rate of the NP derived as:

$$\frac{dQ(t)}{dt} = -\int_{\theta=0^o}^{\theta=\theta_c} J_r 2\pi R^2 \sin\theta d\theta \tag{6.10}$$

$$\frac{dQ(t)}{dt} = \frac{3Q_s}{\tau_{pc} C(t)} \left[\frac{\frac{Q(t)}{Q_s}}{\frac{\varepsilon_2}{2\varepsilon_1 + \varepsilon_2}} - \frac{C(t)}{3} \right]^2 \tag{6.11}$$

TH-2868_156302003

where the charging time constant of the NP is expressed as:

$$\tau_{pc} = \frac{4\varepsilon_1}{|-\rho_e|\mu_e} \tag{6.12}$$

The particle is fully charged by a saturation charge Q_s as shown in Figure 6.7(d).

Solving (6.11) using MATHEMATICA, the expression of the charge accumulation *Q(t)* on the surface of Eh-BN NP with MO and POME are presented in (6.13) and (6.16) respectively. The number of electrons trapped by a single Eh-BN NP with MO and POME is 354 and 423 respectively, as shown in Figure 6.8 and Table 6.6. In the present work, 0.01wt.% (= 0.01/24.817 mol = 4.029×10^{-4} mol = $4.029 \times 10^{-4} \times 6.023 \times 10^{23}$ NPs = 2.43×10^{20} NPs) NPs are dispersed in MO and POME. Therefore, the total amount of electrons captured by NPs in MO and POME are 860.22×10^{20} (= $2.43 \times 10^{20} \times 354$) and 1027.89×10^{20} (= $2.43 \times 10^{20} \times 423$) respectively. Since the total number of electrons trapped by the NPs in POME is higher than the NPs in MO, the early streamer formation in POME-NF is arrested compared to MO-NF. This decelerates the ionization process in Eh-BN/POME-NF than Eh-BN/MO-NF and hence BDV with POME-NF increases.

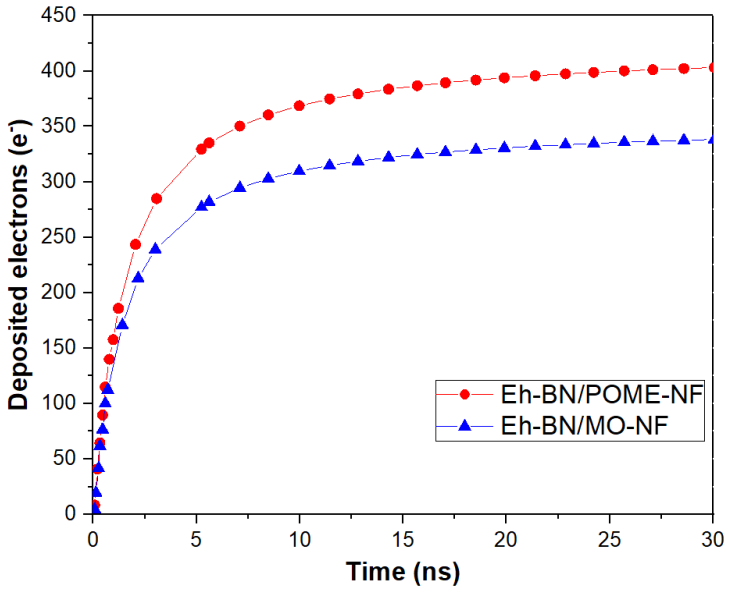

Figure 6.8: Charging characteristics of Eh-BN NP in MO and POME.

Table 6.6: Electron Captures by the NPs in MO and POME.

NPs in oil	Q_s per NP $\times10^{-17}$ (C)	*N_e per NP	*N_{np} in 100 gm of oil $\times10^{20}$	Total $N_e \times10^{20}$
Eh-BN/MO	-5.675	354	2.43	860.22
Eh-BN/ POME	-6.766	423	2.43	1027.89
*N_e and N_{np} are the number of electrons and the total number of NPs.				

TH-2868_156302003

$$Q(t)_{Eh-BN/MO} = \frac{M_1(t)}{M_2(t)} \tag{6.13}$$

where

$$M_1(t) = (6.90287\times10^{8}\ e^{-0.0588538\,t}\ (750.465\ e^{0.0294269\,t} + 79.6517\ e^{0.0588538\,t} + 9.42184\ e^{0.0294269\,t}\ t + 1.\ e^{0.0588538\,t}\ t - 320.178\ e^{0.0294269\,t} \log[9.42184\ e^{0.0294269\,t} + 1.\ e^{0.0588538\,t}] - 33.9825\ e^{0.0588538\,t} \log[9.42184\ e^{0.0294269\,t} + 1.\ e^{0.0588538\,t}])) \tag{6.14}$$

$$M_2(t) = (-1.00979\times10^{28} - 1.26776\times10^{26}\ t + 4.30818\times10^{27} \log[9.42184\ e^{0.0294269\,t} + 1.\ e^{0.0588538\,t}]) \tag{6.15}$$

and,

$$Q(t)_{Eh-BN/POME} = \frac{N_1(t)}{N_2(t)} \tag{6.16}$$

where

$$N_1(t) = (6.80176\times10^{8}\ e^{-0.00981631\,t}(83.1645\ e^{0.00490815\,t} + 112.648\ e^{0.00981631\,t} + 0.738272\ e^{0.00490815\,t}t + 1.\ e^{0.00981631\,t}\ t - 150.417\ e^{0.00490815\,t} \log[0.738272\ e^{0.00490815\,t} + 1.\ e^{0.00981631\,t}] - 203.743\ e^{0.00981631\,t} \log[0.738272\ e^{0.00490815\,t} + 1.\ e^{0.00981631\,t}])) \tag{6.17}$$

$$N_2(t) = (-1.96829\times10^{27} - 1.7473\times10^{25}\ t + 3.55999\times10^{27} \log[0.738272\ e^{0.00490815\,t} + 1.\ e^{0.00981631\,t}]) \tag{6.18}$$

6.3.2 Dielectric constant

The relative permittivity or dielectric constant of the insulating liquid is one of the key parameters of the dielectric spectroscopy analysis. The degradation in the properties makes the oil inappropriate to be used as an insulating liquid. It is seen from the Figure 6.9 that the permittivity of the insulating liquid such as MO, Eh-BN/MO-NF, POME and Eh-BN/POME-NF are 2.03, 2.06, 2.05 and 2.1 respectively. The results indicate that there is an increase in the dielectric constant of the NFs than that of base fluids by 1.47 and 2.43% respectively. This increase in dielectric constant in NFs is observed due to the polarization of the NPs in the oil under the effect of an external electric field. The measured and calculated values of the dielectric constant of all the fluids are calculated by the Maxwell-Garnett (MG) formula given below [127] and shown in Figure 6.9:

$$\frac{\varepsilon_{nf} - \varepsilon_{r1}}{\varepsilon_{nf} + 2\varepsilon_{r1}} = \varphi \frac{\varepsilon_{r2} - \varepsilon_{r1}}{\varepsilon_{r2} + 2\varepsilon_{r1}} \tag{6.19}$$

where ε_{r1}, ε_{r2} and ε_{nf} are the relative permittivities of the oil, NP and NF respectively. The

TH-2868_156302003

concentration of the NP added to the oil is represented by φ. The error % between measured and calculated values is given in Table 6.7.

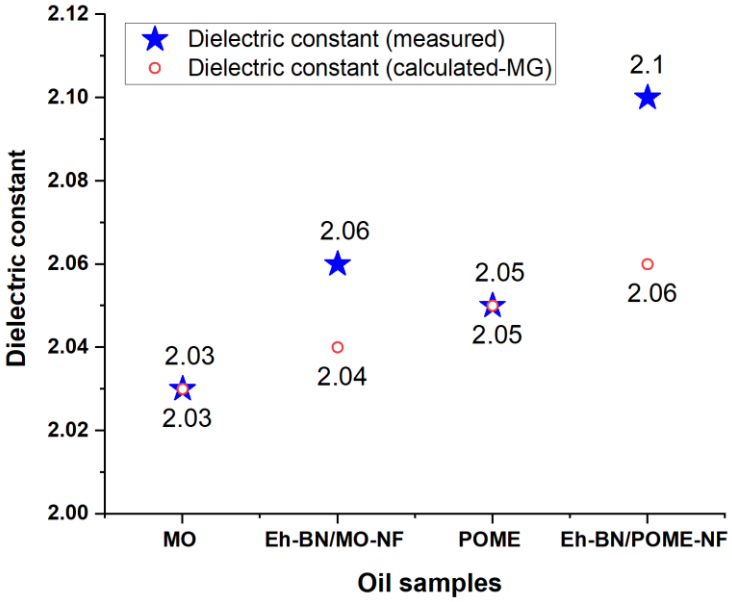

Figure 6.9: Dielectric constant of oil samples as per MG formula.

Table 6.7: Measurement of dielectric constant of all oils as per Maxwell-Garnett (MG) equation.

	Weight % of NP in base fluids			
	MO		POME	
	0%	0.01%	0%	0.01%
Measured	2.03	2.06	2.05	2.1
Calculated	2.03	2.04	2.05	2.064
% error	0	0.98	0	1.74

For NFs, the wt.% of NPs is very small, and the effect of NPs on NF relative permittivity is neglected in Maxwell-Garnett formula. Thus, to take the effect of NPs into consideration, NP polarization is looked into for the effective increase in the permittivity of the NFs by using Clausius-Mossotti (CM) equation in the next section [127].

6.3.2.1 Polarization in the NPs and oil molecules

When external electric field is applied, polarization happens in the NPs as well as the molecules present in the oil as shown in Figure 6.10. The NP gets divided into two halves with positive and negative charges.

TH-2868_156302003

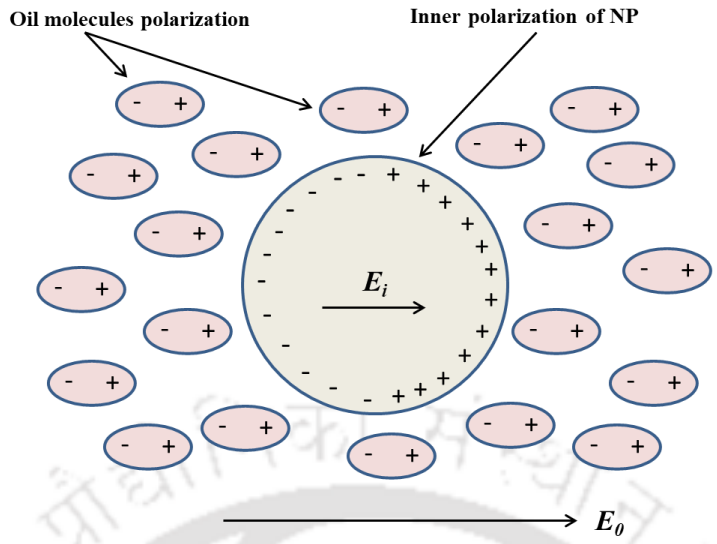

Figure 6.10: Polarization in oil molecules and NP.

Three types of polarization occur when a NF is subjected to electric field, namely:

i. polarization of the oil molecules,

ii. polarization within the NPs and,

iii. orientational polarization of the NPs.

The calculation of the dielectric constant by taking into account the polarization phenomenon given by the Clausius-Mossotti is given below [127]:

$$\frac{\varepsilon_{nf}-1}{\varepsilon_{nf}+2}=\frac{1}{3\varepsilon_o}\left(N_1\alpha_1+N_2\alpha_2+N_2\alpha_3\right) \tag{6.20}$$

where ε_0 is the permittivity of free space,

α_1 is the polarizability of the oil molecule,

α_2 is the polarizability caused by inner polarization of the NP,

α_3 is the orientational polarizability of the NP,

N_1 and N_2 are the numbers of oil molecules and NPs respectively.

The total charge Q_+, in the dipole, can be calculated as below [127],

$$Q_+=\pi R^2\varepsilon_o E_0\left(\frac{\varepsilon_{r2}-\varepsilon_{r1}}{2\varepsilon_{r1}+\varepsilon_{r2}}\right) \tag{6.21}$$

The negative charge Q_- has the same magnitude as the Q_+, the electric dipole moment μ_c (C.m) of the NP when it is orientational polarized is given by,

TH-2868_156302003

$$\mu_c = 2RQ_+ \tag{6.22}$$

a. Polarization of the oil molecules:

For base fluid, the Clausius-Mossotti equation becomes as given in (6.23) and substituting the values of dielectric constant of base fluid, the value of $N_1\alpha_1$ is achieved.

$$\frac{\varepsilon_{r1}-1}{\varepsilon_{r1}+2} = \frac{1}{3\varepsilon_0} N_1\alpha_1 \tag{6.23}$$

b. Inner Polarization of NPs

When an external electric field E_0 is applied, the electric field E_i inside the NP can be expressed as (6.21),

$$E_i = \frac{3\varepsilon_{r1}}{2\varepsilon_{r1}+\varepsilon_{r2}} E_0 \tag{6.24}$$

The polarization vector P_i (C/m^2) in the NP is given by,

$$P_i = \frac{\mu_i}{Vol} = \varepsilon_0 \left(\varepsilon_{r2}-1\right) E_i \tag{6.25}$$

where μ_i (C.m) is the vector sum of electric dipole moment inside the NP, and *Vol* is the volume of the NP. Thus, the polarizability of the NP, α_2 is given by,

$$\alpha_2 = \frac{\mu_i}{E_i} = \varepsilon_0 \left(\varepsilon_{r2}-1\right) Vol \tag{6.26}$$

The number of NP molecules N_2 is calculated with volumetric concentration φ and NP diameter $2R$ as follows:

$$N_2 = \frac{\varphi}{Vol} = \frac{3\varphi}{4\pi R^3} \tag{6.27}$$

c. Orientational polarization of NPs

The orientational polarizability α_3 of the NP is expressed as in (6.28):

$$\alpha_3 = \frac{\mu_c^{\,2}}{3kT} = \frac{4}{3kT} R^2 Q_+^{\,2} \tag{6.28}$$

TH-2868_156302003

where k is the Boltzmann constant and T is the temperature. Substituting the values from (6.23), (6.26), (6.27) and (6.28) in (6.20), the effective dielectric constant of the NF is obtained as below,

$$\frac{\varepsilon_{nf}-1}{\varepsilon_{nf}+2}=\frac{\varepsilon_{r1}-1}{\varepsilon_{r1}+2}+\frac{\varphi}{3}\left(\varepsilon_{r2}-1\right)+\frac{\varphi}{3kT}\pi\varepsilon_0 R^3 E_0^{\,2}\left(\frac{\varepsilon_{r2}-\varepsilon_{r1}}{2\varepsilon_{r1}+\varepsilon_{r2}}\right)^2 \tag{6.29}$$

The calculated values as per Clausius-Mossotti (CM) equation are shown in Figure 6.11 and the error% are given in Table 6.8.

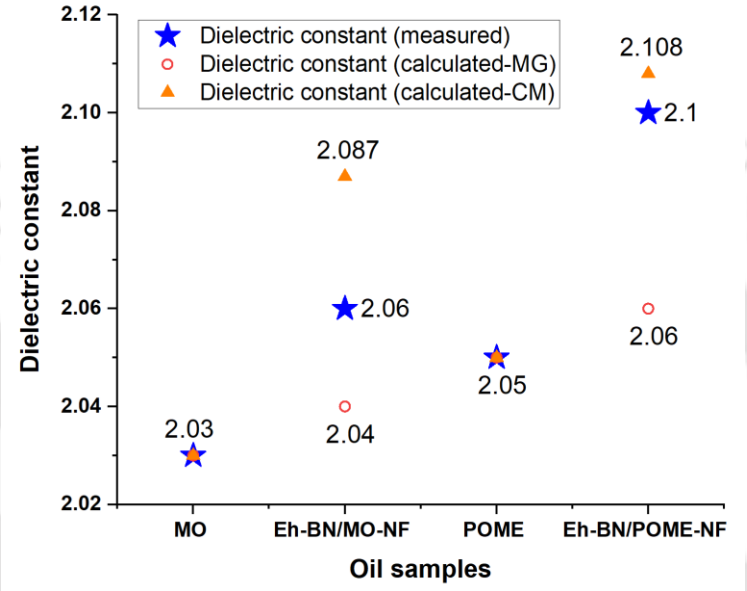

Figure 6.11: Dielectric constant of oil samples as per CM formula.

Table 6.8: Measurement of dielectric constant of all oils as per Cluasius-Mossotti (CM) equation.

	Weight % of NP in base fluids			
	MO		POME	
	0%	0.01%	0%	0.01%
Measured	2.03	2.06	2.05	2.1
Calculated	2.03	2.087	2.05	2.108
% error	0	1.31	0	0.377

From the above discussion, it is observed how the values of dielectric constant vary with the addition of NPs in the oil due to polarization phenomenon. The overall dielectric constant is more influenced by the permittivity of the base fluid and the higher relative

TH-2868_156302003

permittivity of NFs compared with that of base fluid is largely caused by the inner polarization of the NP. In case of POME-NF, the error % for permittivity has reduced using the Clausius-Mossotti equation.

6.3.3 Dielectric dissipation factor (tan δ)

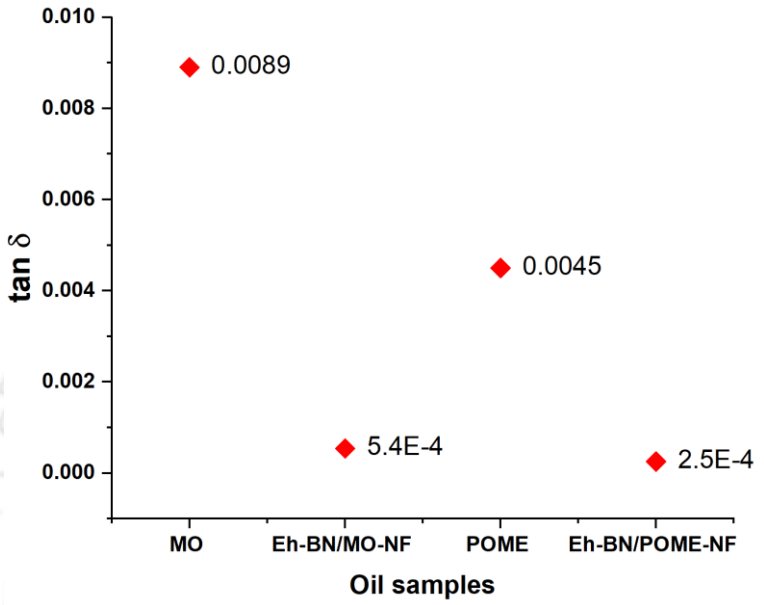

Figure 6.12: tan δ of oil samples.

The DDF, also known as loss factor or tan δ is the measure of the power loss when an external field is applied to an insulating medium. The temperature increases when power dissipation is more. Lower the value of DDF, the better is the integrity of the oil. High DDF values indicate the presence of contaminants in the oil. It is seen from the figure that DDF decreases with the addition of NPs which is desirable. Formation of sludge and water in due course of time increases the DDF value, hence dielectric properties decay. Better dielectric properties are achieved at minimum moisture contained insulating oil. As Eh-BN-based NF has less affinity towards water absorption, so better DDF value has been obtained, which is seen in the Figure 6.12.

6.3.4 Thermal conductivity

One of the most important characteristic to understand the heat transfer property of any insulating oil is thermal conductivity. In order to understand the property of cooling of the TO, thermal conductivity is evaluated by using the device Decagon KD2 Pro at room temperature. Single probe transient hot-wire method is followed to observe the thermal conductivity. The governing equation for thermal conductivity is as follows:

TH-2868_156302003

$$K = \frac{q_k}{4\pi(T_1 - T_2)} \ln \frac{t_1}{t_2} \tag{6.30}$$

where K is the thermal conductivity, q_k is the heat flow per unit length of the source and T_1 and T_2 are the temperatures of the heat source at times t_1 and t_2 respectively.

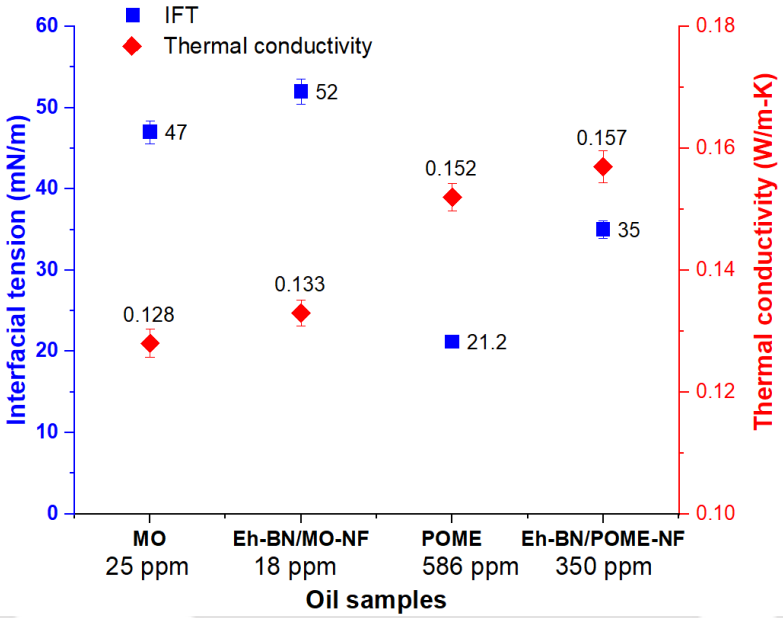

Figure 6.13: Thermal conductivity and IFT of oil samples at room temperature.

Table 6.9: Enhancement in thermal conductivity.

Oil samples	Thermal conductivity values (W/m-K)	% increase in thermal conductivity
MO	0.128	0
Eh-BN/MO-NF	0.133	3.9
POME	0.152	18.75
Eh-BN/POME-NF	0.157	22.65

A comparative analysis of the thermal conductivity of the various insulating oils such as MO, MO-NF, POME and POME-NF is carried out at room temperature and presented in Figure 6.13. It is seen from the figure that the thermal conductivity of the MO-NF is higher to MO, and that of POME-NF is further superior to POME and all the other liquids. The superior thermal conductivity value of the MO-NF is an evidence of the stable dispersion of Eh-BN NP into the MO [137]. The high surface area of the Eh-BN NPs due to exfoliation enhances the heat transfer abilities in the NF for enhanced thermal conductivity. The improvement in the thermal conductivity is due to the increase in Brownian motion of the

TH-2868_156302003

NPs [138, 139]. Keblinski et al. suggested that the remarkable augmentation in thermal conductivity can be credited to the ballistic phonons which originate in one particle can spread to a neighbouring particle [87, 140]. The thermal conductivity of POME is higher than MO because POME is derived from the PPO, which has higher thermal conductivity because of the triglyceride molecular structure. The mean value of thermal conductivity is calculated by conducting six number of experiments. The mean values of POME-NF (0.157 W/m-K), POME (0.152 W/m-K) and MO-NF (0.133 W/m-K) are higher than that of MO (0.128 W/m-K) by 22.65%, 18.75% and 3.9% respectively, which are given in Table 6.9.

6.3.5 Interfacial tension (IFT)

The IFT value for insulating oil provides sensitive data for detection of impurities or polar contaminations in the insulating oil. The poor value of the IFT leads to drop in the integrity of the oil which causes generation of oxides and peroxides in the insulating oil during service. The value of IFT is measured in accordance with ASTM D971. From the Figure 6.13, it is observed that the IFT value increases with the dispersion of NP. IFT is determined by the difference of the interactions between the molecules of one fluid with molecules of another fluid. So, the well-dispersed adequate NP concentration enhances IFT more than the MO, as the capillary forces between the particles oppose any deformation on the interface [141]. The adhesive forces come into play between the liquid and the solid NPs. It is also observed from the figure that the IFT of Eh-BN/POME-NF is lower than that of Eh-BN/MO-NF. This is because of the molecular structure of VO, which contains unsaturated fatty acid chains and the moisture content in the oil. The VOs have variances in the fatty acid structure which differ in their carbon chain lengths and in the number of double bonds or unsaturation. IFT is a physical attribute that is closely associated with the molecular configuration. The number of unsaturated fatty acids and the length of the fatty acid hydrocarbon chain affect the IFT. The tension also increases when the chain length increases.

6.3.6 Pour point and flash point

Pour point should be minimized in order to use the fluid at a very low temperature and is measured as per ASTM D97. It is noted from Figure 6.14 that the pour point of POME is -1^{o}C, which is higher than that of MO. This is because of the triglyceride structure.

TH-2868_156302003

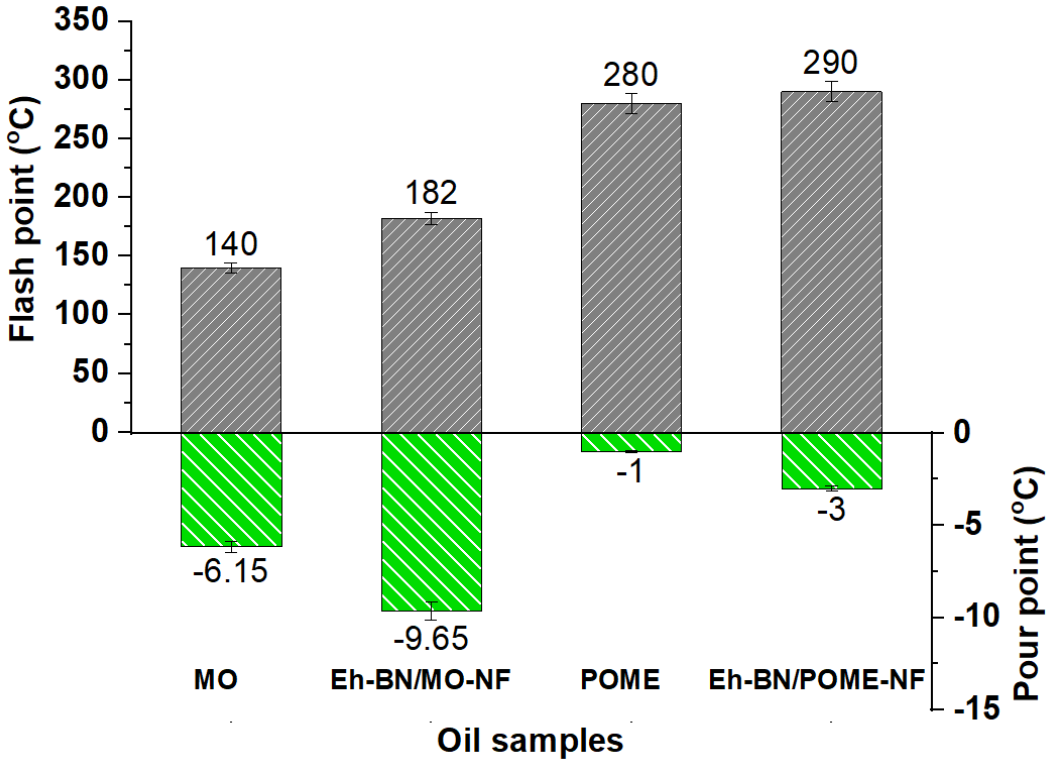

Figure 6.14: Pour point and flash point values of oil samples.

When esterification is performed, these triglycerides form mono-glycerides and thus assist in the flowability of the fluid and make it comparable to that of MO [136]. It is also seen from the figure that the NF having 0.01 wt. % of Eh-BN has a lower pour point temperature than the pure MO, which indicates the possible molecular interaction between Eh-BN and MO. The reason behind lowering the pour point temperature of NF may be associated with the nanoscale dimension of Eh-BN and high intermolecular interaction which disperses the wax present in the oil and hinders the formation of wax crystals [142]. The problem of high pour point can also be improved with the addition of pour point suppressants, winterization or blending with other fluids having lower pour points. Flash point of all the oil samples is determined as per ASTM D93. The POME-NF having 0.01wt% Eh-BN has the highest flash point temperature among all the liquids as seen in Figure 6.14. The enhancement in flash point in the NFs directly shows that the dispersed NP slows down the process of vapour generation.

6.3.7 Measurement uncertainty

The expression for combined uncertainty error for ACBDV and thermal conductivity is given in (6.31) and that for dielectric constant is given in (6.32):

TH-2868_156302003

$$U_{c1} = \sqrt{U_1^{\,2} + U_2^{\,2} + U_3^{\,2} + U_4^{\,2}} \tag{6.31}$$

$$U_{c2} = \sqrt{U_1^{\,2} + U_2^{\,2} + U_5^{\,2} + U_6^{\,2} + U_7^{\,2} + U_8^{\,2}} \tag{6.32}$$

where U_1 is the relative standard uncertainty due to repeatability (=($S/\sqrt{n}$)×100/X', n is the number of experiments, X' is the mean and S is the standard deviation of the data set), U_2 is the standard uncertainty of the instrument, U_3 is the standard uncertainty for gap gauge/probe, U_4 is the standard uncertainty of the electrode dimension/measurement, U_5 is the standard uncertainty for manufacturer's specification, U_6 is the standard uncertainty due to resolution, U_7 is the standard uncertainty for voltage and U_8 is the standard uncertainty for glass thermometer. The measurement uncertainty of ACBDV, thermal conductivity and dielectric constant values is shown in Table 6.10, 6.11 and 6.12 respectively.

Table 6.10: Measurement uncertainty for ACBDV.

	% Error(±)			
Uncertainty error	MO	MO-NF	POME	POME-NF
Repeatability (U_1)	1.0	1.01	0.57	0.38
Instrument accuracy (U_2)	0.916	0.916	0.916	0.916
Gap gauge (U_3)	0.44	0.44	0.44	0.44
Electrode (U_4)	0.168	0.168	0.168	0.168
Combined uncertainty (U_{c1})	1.43	1.44	1.17	1.09

Table 6.11: Measurement uncertainty for thermal conductivity.

	% Error(±)			
Uncertainty error	MO	MO-NF	POME	POME-NF
Repeatability (U_1)	0.45	0.70	0.88	0.80
Instrument accuracy (U_2)	0.5	0.5	0.5	0.5
Electrical probe (U_3)	0.2	0.2	0.2	0.2
Measurement (U_4)	0.1	0.1	0.1	0.1
Combined uncertainty (U_{c1})	0.71	0.88	0.98	0.97

TH-2868_156302003

Table 6.12: Measurement uncertainty for dielectric constant.

	% Error(±)			
Uncertainty error	MO	MO-NF	POME	POME-NF
Repeatability (U_1)	0.04926	0.0672	0.1485	0.2247
Instrument accuracy (U_2)	1.10	1.10	1.10	1.10
Manufacturer's specification (U_5)	0.5773	0.5773	0.5773	0.5773
Resolution (U_6)	0.000123	0.000121	0.000122	0.000119
Voltage (U_7)	0.5804	0.5804	0.5804	0.5804
Glass thermometer (U_8)	0.1666	0.1666	0.1666	0.1666
Combined uncertainty (U_{c2})	1.3822	1.383	1.3893	1.399

6.4 Summary of the chapter

This work introduces a new non-edible VO and presents the advantages of using it as an insulating liquid in transformer. Further, it intends to focus on the enhancement of the thermophysical and electrical properties by adding nanofillers to both MO and VO. In this work, the experimental and analytical analysis of the thermophysical and electrical properties of the oils are presented. The main conclusions are as below:

- The mechanism behind the better properties is apparently the molecular structure of the POME. The esterification of the POME helps in lowering the viscosity and pour point values, which make it suitable as a replacement for TO.
- Dispersion of NPs into the oil aids in enhanced ACBDV because of the electron capture on the surface of the NP and also the thermal conductivity increases.
- The variation in the permittivity is studied and a comparison of the calculated and measured values is performed and the cause for increase in permittivity may be attributed to the polarization of the NPs.
- The higher surface area of Eh-BN NP leads to improve the thermal conductivity of the NF significantly.
- The pour point of POME is comparable to that of MO, but still marginally higher, which can be improved by introducing additives or winterization.
- Flash point of POME is higher compared to MO, which is highly important parameter considering no fire risk in the event of a major fault in the electrical system.

TH-2868_156302003

Considering the aforementioned advantages of POME-NF and keeping some precautions in mind while processing, VO such as POME-NF can prove as a potential substitute to conventional MO in the transformer.

Note: This work, "Performance Analysis of Vegetable Oil based Nanofluids used in Transformers" has been published in IET Science, Measurement & Technology, 2019, Vol. 13, No. 7, pp. 995-1002.

TH-2868_156302003

7

Conclusion and future work

Contents

TH-2868_156302003

7.1 Summary of the present work

This thesis presents the condition assessment of transformer filled with alternative dielectric liquids with enhanced physicochemical, thermal and electrical performance. The ageing study of the alternative dielectric liquid along with statistical investigations is performed in this work.

The dissolved gas analysis (DGA) tool has been extended to two natural ester oils (NEOs), FR3 and JAT, to monitor their condition when in use in transformers. The oils along with an equivalent amount of solid insulation in the ratio of 20:1:1 for oil/paper/pressboard are thermally stressed with a temperature of 150^{o}C for duration of 500, 1000, 1500 and 2000 hours. After DGA of both NEOs, a comparative analysis is done between the two oils to understand the behaviour of the oils at accelerated thermal ageing for longer durations. The molecular structures of both NEOs are slightly different owing to the chemical structure. However, the types of gases generated by thermal faults in both NEOs are similar. It is observed from the results that the oil consistency remains unaltered for 2000 hours ageing for both FR3 and JAT, as confirmed by the fourier transform infrared (FTIR) and nuclear magnetic resonance (NMR) studies. FR3 generates a significant amount of C_2H_6 when thermal stress is applied. Also, the generation of H_2 in case of FR3 is higher compared to JAT, indicating FR3 is more prone to stray gassing at 150^{o}C. The JAT shows a higher generation of CO and CO_2, indicating FR3 keeps the paper insulation more intact. The different gas ratio methods are used to predict the fault types, however only the IEC method predicts the thermal faults for JAT correctly. Using the low temperature fault (LTF) Duval triangle 6, stray gassing is obtained in case of FR3 and overheating fault in case of JAT. It is observed that the total dissolved combustible gas (TDCG) generation for FR3 increases sharply with ageing time, which makes JAT fair better in terms of TDCG. Since the DGA for JAT under thermal ageing is not performed till now, this study will help to explore more into using JAT as a potential substitute to MO for real time transformer application.

Frequency domain spectroscopy (FDS) which is a non-invasive offline measurement technique is performed to see the variation in the relative permittivity and tan δ over a wide range of frequency, when the oil samples are subjected to ageing. This work investigates the change in the dielectric properties of JAT by considering ageing for 500 hours in an open beaker oxidative ageing test set up. It is observed that the permittivity and tan δ of the JAT increases with ageing duration towards the lower frequency range which shows that the

TH-2868_156302003

formation of polar contaminants which hampers the condition of the oil. The FTIR results showed the composition of the oil to be intact even after 500 hours of ageing, as there is no significant change in the spectra. By analyzing the UV-Vis spectra, it is observed that the oil samples show a red shift in the absorbance spectra with increasing ageing duration which indicates degradation of the oil. A statistical modeling approach is proposed to understand the variation in the dielectric parameters of the oil and an expression relating all three parameters of frequency, ageing duration and dielectric parameters (ε_r and tan δ) is developed. The proposed mathematical model may be applied to other insulating liquids for the estimation of dielectric parameters.

Further explained is the effect of temperature on the insulating oil with the addition of nanoparticles (NPs). The FDS response of TiO_2 based nanofluids (NFs) is studied in the frequency range of 10^{-3} to 10^{4} Hz and the temperature range varies from 30 to 90^{o}C with an interval of 15^{o}C between two successive temperatures. The Cole-Cole double relaxation model is used to ascertain the number of relaxations in the samples. The parameters of the Cole-Cole model are estimated by means of the least square technique to obtain the best fit of the measured ε_r' and ε_r''. The ε_r', ε_r'' and tan δ obtained from the FDS are compared for all the oil samples-MO, FR3, MO-NF and FR3-NF. Based on the experimental results, low frequency dispersion of the oils is investigated to obtain an insight into the integrity of the oil samples. It is observed that the conductivity increases with increase in temperature which in turn increases the tan δ for all oil samples. A predictive analysis model is proposed using ML algorithms DTR and KNN, to predict the dielectric properties like ε_r', ε_r'' and tan δ of all the oil samples considering its dielectric response using the FDS.

Statistical analysis is carried out to understand the breakdown probability of the fresh and aged NEO and NEO-NFs. High temperature and moisture affects the thermophysical and electrical attributes of the insulating liquids, resulting in reduced life of the power and distribution transformer. So, an open beaker oxidative ageing test setup is considered to comprehend the process of degradation. In this work AC breakdown voltage (ACBDV) test is performed for all the samples: NEO, NEO-NF, aged NEO and aged NEO-NF and a comparative examination is done among them to estimate the behaviour of the new and aged oils. The mean ACBDV of NEO-NF is found to be higher than NEO because of the addition of the semi-conductive TiO_2 NPs. With ageing, the ACBDV decreases because of the oxidation of the oils and deposition of sludge in the sample in due course of time. However, the degradation in aged NEO-NF is lesser when compared to aged NEO. To understand the

TH-2868_156302003

statistical behaviour of the ACBDV of the oil samples, normal, 2-parameter Weibull and 3-parameter Weibull distributions are considered. Through the Anderson-Darling hypothesis testing, it is ascertained that the distribution of experimental data follows a theoretical distribution. The correlation coefficients are chosen to analyze the goodness of fit which shows that all the 4 datasets follow a 3-parameter Weibull distribution quite well.

A new non-edible oil pongamia pinnata oil (PPO) is considered for study and it is altered to pongamia oil methyl ester (POME) to achieve the desired properties of TO. Also, modifications are performed on both MO and POME for obtaining better dielectric and thermal properties by adding insulating NPs. The 3D h-BN NPs are exfoliated to get 2D Eh-BN nanosheets and 0.01wt.% of Eh-BN is dispersed into the MO and POME to study the enhanced properties. It is observed that both thermal and electrical properties are enhanced by the addition of Eh-BN NPs with both the MO and the POME. The ACBDV enhancement of MO-NF, POME and POME-NF when compared to MO is 114.2, 134.28 and 145.71% respectively. The cause of enhancement in ACBDV of the NF compared to the base oils is analyzed with the help of charge dynamics and electron scavenging mechanism. The increase in the permittivity values of the NFs may be attributed to the effect of the NP polarization on the effective relative permittivity of the insulating medium. The thermal conductivity increment of MO-NF, POME and POME-NF when compared to MO is 3.9, 18.75 and 22.65% respectively. The flash point of POME is also higher than that of MO and MO-NF. However, the pour point and interfacial tension of POME needs to be improved. It is observed that the POME-NF has superior performance in terms of thermal as well as electrical performances. The results of the POME are also compared with two more NEOs, one is the FR3 and the other is JAT and the POME showed comparable results and thus may be used as a potential substitute to MO for transformer application.

7.2 Contribution of the thesis

The major contributions of the thesis for the condition assessment of transformer filled with alternative dielectric liquids are given as follows:

- DGA of two different NEOs has been done under different ageing durations using a sealed beaker test setup and a regression model is developed for TDCG prediction of the two oils to assess the condition of the insulation system.
- A statistical model has been developed to establish a relation between the dielectric parameters, frequency and ageing time for fresh and aged NEO based on FDS analysis.

TH-2868_156302003

- The temperature dependence on dielectric parameters of the MO and NEO along with their NFs has been studied based on FDS and a predictive ML model is developed to estimate the dielectric properties.
- A statistical investigation using hypothesis testing has been carried out for fresh and aged NEO and its NFs, to understand the failure probabilities for normal and Weibull distributions.
- Developed a nonedible VO based liquid dielectric POME doped with a thermally conducting and electrically insulating Eh-BN NP, which offers a potential substitute to the conventional MO.

.

7.3 Suggestions for future research work

The suggestions for further research are given as follows:

- The DGA of NEO based NFs can be carried out to check the concentration of the dissolved gases in the presence of NPs in the insulating oil.
- The time domain spectroscopic studies of the NEO along with its NFs may be investigated to understand the phenomenon of polarizing and depolarizing currents flowing through the material.
- The multistress ageing of the NEO and its NFs can be investigated to understand the effect of ageing duration on the base oil and its NFs.
- Studies related to the partial discharge formation in both the fresh and aged insulating oil can be carried out to understand the pre-breakdown phenomena of the NEO based TO.
- A multiphysics model can be developed to study the electro-thermal response of the MO, NEO and their NFs.

TH-2868_156302003

TH-2868_156302003

Bibliography

[1]. H. Jin, P. Morshuis, A. R. Mor, and J. J. Smit, "Partial discharge behaviour of mineral oil based nanofluids," *IEEE Trans. Dielectr. Electr. Insul.*, vol. 22, pp 2747-2753, 2015.

[2]. T. V. Oommen, "Vegetable oils for liquid-filled transformers," *IEEE Electr. Insul. Mag.*, vol. 18, no. 1, pp. 6-11, 2002.

[3]. C. P. McShane, "Vegetable-oil-based dielectric coolants," *IEEE Ind. Appl. Mag.*, vol. 8, no. 3, pp. 34-41, 2002.

[4]. T. V. Oommen, C. C. Claiborne, and J. T. Mullen, "Biodegradable electrical insulation fluids," in *IEEE Electr. Insul., Electr. Manufacturing and Coil Winding Conf.*, 1997, pp. 465-468.

[5]. D. M. Nail and P. H. Shoun, "Retrofilling-a technique to reduce polychlorinated biphenyls (pcb's)," *IEEE Power Engg. Rev.*, vol. 4, no. 3, pp. 26-26, 1984.

[6]. I. Webber, D. B. Pilgrim, and M. A. Thompson, "The safe disposal of polychlorinated biphenyls," *IEEE Trans. Ind. Appl.*, vol. IA-20, no. 1, pp. 159-166. 1984.

[7]. U. M. Rao, I. Fofana, T. Jaya, E. M. Rodriguez-Celis, J. Jalbert, and P. Picher, "Alternative dielectric fluids for transformer insulation system: progress, challenges, and future prospects," *IEEE Access*, vol. 7, pp. 184552 – 184571, 2019.

[8]. T. V. Oommen, C. C. Claiborne, E. J. Walsh, and J. P. Baker, "A new vegetable oil based transformer fluid: development and verification," in *IEEE Conf. Electr. Insul. Dielectr. Phenomena*, Victoria, BC, Canada, 2000, pp. 308-312.

[9]. C. P. McShane, "Relative properties of the new combustion-resist vegetable-oil-based dielectric coolants for distribution and power transformers," *IEEE Trans. Dielectr. Electr. Insul.*, vol. 37, no. 4, pp. 1132-1139, 2001.

[10]. M. Hrkac, P. Papageorgiou, I. Kosmoglou, and G. Miatto, "BIOTEMP® transformer technology for innovative compact substation,"in *7th Mediterranean Conference and Exhibition on Power Generation, Transmission, Distribution and Energy Conversion (MedPower 2010)*, Agia Napa, Cyprus, 2010, pp. 1-6.

[11]. C. P. McShane, "New dielectric coolant concepts for distribution and power transformers," in *IEEE Pulp and Paper, Ind. Technical Conf.*, 1999, pp. 55 –62.

[12]. M. Mazzaro, D. De Bartolomeo, L. Calcara, M. Pompili, F. Scatiggio, A. Vailant, M. Rebolini, E. Bemporad, S. Berardi, A. Ledda, M. Falconi, A. Vecchio, A. Sturchio, M. Salvadori, and F. Mauri, "Power transformer fire and environmental risk reduction by using natural esters," in *Int'l. Conf. Dielectr. Liquids (ICDL)*, Manchester, UK, 2017, pp. 1-4.

TH-2868_156302003

[13]. L. Pompili, A. Calcara, and C. F. Sturchio, "Natural esters distribution transformers: a solution for environmental and fire risk prevention," in *Int.l' Annu. Conf. Sustainable Development in the Mediterranean Area, Energy and ICT Networks of the Future*, Capri, Italy, 2017.

[14]. T. A. Prevost and T. V. Oommen, "Cellulose insulation in oil-filled power transformers: part I - history and development," *IEEE Electr. Insul. Mag.*, vol. 22, no. 1, pp. 28-35, 2006.

[15]. D. Martin and Z. D. Wang, "Statistical analysis of the AC breakdown voltages of ester based transformer oils," *IEEE Trans. Dielectr. Electr. Insul.*, vol.15, pp. 1044-1050, 2008.

[16]. P. Totzauer and P. Trnka, "Different ways to improve natural ester oils," *Transportation Research Procedia*, vol.40, pp. 102–106, 2019.

[17]. H. B. H. Sitorus, R. Setiabudy, S. Bismo, and A. Beroual, "Jatropha curcas methyl ester oil obtaining as vegetable insulating oil," *IEEE Trans. Dielectr. Electr. Insul.*, vol. 23, no. 4, pp. 2021-2028, 2016.

[18]. N. Beltrán, E. Palacios, and G. Blass, "Potential of jatropha curcas oil as a dielectric fluid for power transformers," *IEEE Electr. Insul. Mag.*, vol. 33, no. 2, pp. 8–15, 2017.

[19]. N. V. Dung and H. L. Huong, "The effect of antioxidants on the physical and chemical properties of rice oil, corn oil, peanut oil and kraft paper," *IEEE Trans. Dielectr. Electr. Insul.*, vol. 27, no. 5, pp. 1698–1706, 2020.

[20]. S. S. Kumar, M. W. Iruthayarajan, M. Bakrutheen, and S. G. Kannan, "Effect of antioxidants on critical properties of natural esters for liquid insulations," *IEEE Trans. Dielectr. Electr. Insul.*, vol. 23, no. 4, pp. 2068–2078, 2016.

[21]. D. M. Mehta, P. Kundu, A. Chowdhury, V.K. Lakhiani, and A.S. Jhala, "A review on critical evaluation of natural ester vis-a-vis mineral oil insulating liquid for use in transformers: part 1," *IEEE Trans. Dielectr. Electr. Insul.*, vol. 23, pp.873-880, 2016.

[22]. V-H. Dang, A. Beroual, and C. Perrier, "Comparative study of statistical breakdown in mineral, synthetic and natural ester oils under AC voltage," *IEEE Trans. Dielectr. Electr. Insul.*, vol. 19, pp. 1508-1513, 2012.

[23]. B. X. Diu and X. L. Li, "Dielectric and thermal characteristics of vegetable oil filled with BN nanoparticles," *IEEE Trans. Dielectr. Electr. Insul.*, vol. 24, no. 2, pp.956-963, 2017.

[24]. H. B. H. Sitorus, A. Beroual, and R. Setiabudy, "Pre-breakdown phenomena in new vegetable oil - based jatropha curcas seeds as substitute of mineral oil in high voltage equipment," *IEEE Trans. Dielectr. Electr. Insul.*, vol. 22, no. 5, pp. 2442-2448, 2015.

TH-2868_156302003

[25]. V-H. Dang, A. Beroual, and C. Perrier, "Investigations on streamers phenomena in mineral, synthetic and natural ester oils under lightning impulse voltage," *IEEE Trans. Dielectr. Electr. Insul.*, vol. 19, no. 5, pp. 1521-1527, 2012.

[26]. C. Perrier and A. Beroual, ''Experimental investigations on insulating liquids for power transformers: mineral, ester, and silicone oils," *IEEE Electr. Insul. Mag.*, vol. 25, no. 6, pp. 6–13, 2009.

[27]. D. Martin, N. Lelekakis, and W. Guo, "Further studies of a vegetable-oil-filled power transformer," *IEEE Electr. Insul. Mag.*, vol. 27, no. 5, pp. 6-13, 2011.

[28]. Y. Lijun, L. Ruijin, C. Sun, and Z. Mengzhao, "Influence of vegetable oil on the thermal aging of transformer paper and its mechanism," *IEEE Trans. Dielectr. Electr. Insul.*, vol.18, no. 3, pp. 692-700, 2011.

[29]. L. Ruijin, H. Jian, G. Chen, M. Zhiqin, and Y. Lijun, "A comparative study of physicochemical, dielectric and thermal properties of pressboard insulation impregnated with natural ester and mineral oil," *IEEE Trans. Dielectr. Electr. Insul.*, vol.18, no. 5, pp. 1626-1637, 2011.

[30]. R. Liao, H. Zheng, S. Grzybowski, L. Yang, Y. Zhang, and Y. Liao, "An integrated decision-making model for condition assessment of power transformers using fuzzy approach and evidential reasoning," *IEEE Trans. Power Del.*, vol. 26, no. 2, pp. 1111-1118, 2011.

[31]. W. H. Tang, K. Spurgeon, Q. H. Wu, and Z. J. Richardson, "An evidential reasoning approach to transformer condition assessments," *IEEE Trans. Power Del.*, vol. 19, no. 4, pp. 1696–1703, 2004.

[32]. R. A. Hooshmand, M. Parastegari, and Z. Forghani, "Adaptive neuro-fuzzy inference system approach for simultaneous diagnosis of the type and location of faults in power transformers," *IEEE Electr. Insul. Mag.*, vol. 28, no. 5, pp. 32-42, 2012.

[33]. N. A. Bakar and A. Abu-Siada, "A new method to detect dissolved gases in transformer oil using NIR-IR spectroscopy," *IEEE Trans. Dielectr. Electr. Insul.*, vol. 24, no. 1, pp. 409–419, 2017.

[34]. F. Scatiggio and M. Pompili, "Evaluation of vegetable ester for filling large power transformers," in *Proceedings of the 2016 IEEE International Conference on Dielectrics (ICD)*, Montpellier, France, 2016, pp. 1052-1056.

[35]. D. Martin, I. U. Khan, J. Dai, and Z. D. Wang, "An overview of the suitability of vegetable oil dielectrics for use in large power transformers," in *Proc. 5th Annual Euro TechCon*, Chester, UK, 2006.

[36]. K. Rapp, C. McShane, and J. Luksich, "Interaction mechanisms of natural ester dielectric fluid and kraft paper," in *Proc. IEEE Int. Conf. Dielect. Liquids*, Coimbra, Portugal, 2005, pp. 393–396.

TH-2868_156302003

[37]. I. Khan, Z. Wang, I. Cotton, and S. Northcote, "Dissolved gas analysis of alternative fluids for power transformers," *IEEE Electr. Insul. Mag.*, vol. 23, no. 5, pp. 5–14, Oct. 2007.

[38]. C. Perrier, M. Marugan, and A. Beroual, "DGA comparison between ester and mineral oils," *IEEE Trans. Dielectr. Electr. Insul.*, vol. 19, no. 5, pp. 1609-1614, 2012.

[39]. S. Singha, R. Asano Jr., G. Frimpong, C. C. Claiborne, and D. Cherry, "Comparative aging characteristics between a high oleic natural ester dielectric liquid and mineral oil," *IEEE Trans. Dielectr. Electr. Insul.*, vol. 21, no. 1, pp. 149-158, 2014.

[40]. H. M. Wilhelm, M. B. C. Stocco, L. Tulio, W. Uhren, and S.G. Batista, Jr., "Edible natural ester oils as potential insulating fluids," *IEEE Trans. Dielectr. Electr. Insul.*, vol. 20, no. 4, pp.1395-1401, 2013.

[41]. F. Murdiya, R. Hanaoka, H. Akiyama, K. Miyagi, K. Takamoto, and T. Kano, "Creeping discharge developing on vegetable based oil/pressboard interface under AC voltage," *IEEE Trans. Dielectr. Electr. Insul.*, vol. 21, no. 5, pp. 2102-2110, 2014.

[42]. M. H. A. Hamid, M. T. Ishak, M. M. Arifin, N. A. M. Amin, N. I. A. Katim, N. Azis, F. R. Hashim, and M. F. Md. Din, "Dissolved gas analysis (DGA) of natural ester oils under arcing faults," *J. Fundam. Appl.Sci.*, vol. 9, no.3S, pp.105-115, 2017.

[43]. A. Beroual, H. B. H. Sitorus, R. Setiabudy, and S. Bismo "Comparative study of AC and DC breakdown voltages in jatropha methyl ester oil, mineral oil, and their mixtures," *IEEE Trans. Dielectr. Electr. Insul.*, vol. 25, no. 5, pp. 1831-1836, 2018.

[44]. C. T. Dervos, C. D. Paraskevas, P. D. Skafidas, and P. Vassiliou, "A complex permittivity based sensor for the electrical characterization of high-voltage transformer oils," *Sensors*, vol. 5, no. 4, pp. 302-316, May. 2015.

[45]. T. K. Saha, "Review of modern diagnostic techniques for assessing insulation condition in aged transformers," *IEEE Trans. Dielectr. Electr. Insul.*, vol. 10, no. 5, pp. 903-917, Oct 2003.

[46]. W. S. Zaengl, "Dielectric spectroscopy in time and frequency domain for HV power equipment, part I: theoretical considerations," *IEEE Electr. Insul. Mag.*, vol. 19, no. 5, pp. 5-19, Sept/Oct. 2003.

[47]. J. Fal, A. Barylyak, K. Besaha, Y. V. Bobitski, M. Cholewa, I. Zawlik, K. Szmuc, J. Cebulski, and G. żyła, "Experimental investigation of electrical conductivity and permittivity of SC-TiO_2-EG nanofluids," *Nanoscale Research Letters*, vol.11:375, pp.1-9, 2016.

[48]. M.Dong, J. Dai, Y. Li, J. Xie, M. Ren, and Z. Dang, "Insight into the dielectric response of transformer oil-based nanofluids," *AIP Advances*, vol. 7, pp. 025307(1-7), 2017.

TH-2868_156302003

[49]. J. Dai, M. Dong, Y. Li, J. Zhou, and F. Wen, "Influence of nanoparticle concentration on the frequency domain spectroscopy properties of transformer oil-based nanofluids," in *IEEE Conference on Electrical Insulation and Dielectric Phenomena (CEIDP)*, Toronto, Ontario, Canada, 2016, pp. 587-590.

[50]. M. Grossi, G. D. Lecce, T. G. Toschi, and B. Ricco, "Fast and accurate determination of olive oil acidity by electrochemical impedance spectroscopy," *IEEE Sensors J.*, vol. 14, no. 9, pp. 2947-2954, Sept. 2014.

[51]. D. Wang, L. Zhou, W. Liao, A. Wang, X. Xu, and L. Guo, "Moisture estimation for oil-immersed bushing based on FDS method: field application," *IET Gener. Transm. Distrib.*, vol. 12, no. 11, pp. 2762-2769, 2018.

[52]. Y. Zhang, J. Liu, H. Zheng, and K. Wang, "Feasibility of a universal approach for temperature correction in frequency domain spectroscopy of transformer insulation," *IEEE Trans. Dielectr. Electr. Insul.*, vol. 25, no.5, pp. 1766-1773, 2018.

[53]. K. S. Cole and R. H. Cole, "Dispersion and absorption in dielectrics – I: alternating current characteristics," *J. Chem. Phys.*, vol. 9, no. 4, p. 341-351, 1941.

[54]. K. S. Cole and R. H. Cole, "Dispersion and absorption in dielectrics – II: direct current characteristics," *J. Chem. Phys.*, vol. 10, no. 2, p. 98-105, 1942.

[55]. E. Tuncer, Y. V. Serdyuk, and S. M. Gubanski, "Dielectric mixtures: electrical properties and modeling," *IEEE Trans. Electr. Insul.*, vol. 9, no. 5, pp. 809– 828, 2002.

[56]. K. Kondo, T. Chiba, S. Ando, S. Yoshida, Y. Shimada, T. Nakamura, N. Matsushita, and M. Abe, "Cole-Cole impedance analysis on spin sprayed Ni-Zn-Co ferrite films exhibiting strong magnetic loss in gigahertz range," *IEEE Trans. Magnetics*, vol. 39, no. 5, pp. 3130–3132, 2003.

[57]. R. M. Hakim, "Distribution of relaxation times in an insulating oil," *IEEE Trans. Electr. Insul.*, vol. 6, no. 4, pp. 158–164, 1971.

[58]. S. Martin, M. Valcav, T. Pavel, B. Jiri, P. Josef, and M. Petr, "Cole-Cole diagram as diagnostic tool for dielectric liquids," *in 2011 IEEE International Conference on Dielectric Liquids*, Trondheim, Norway, 2011.

[59]. S. K. Das, S. U. S. Choi, W. Yu, and T. Pradeep, "Conduction heat transfer in nano-fluids," in *Nanofluids: Science and Technology*, John Wiley & Sons, Inc., Dec. 2007.

[60]. Y. Du, Y. Lv, Z. Jian-quan, X. Li, and C. Li, "Breakdown properties of transformer oil-based TiO_2 nanofluid," in *IEEE Conf. Electr. Insul. Dielectr. Phenomena (CEIDP)*, West Lafayette, IN, 2010, pp. 1-4.

[61]. D. Wen and Y. Ding, "Natural convective heat transfer of suspensions of titanium dioxide nanoparticles (nanofluids)," *IEEE Trans. Nanotech.*, vol. 5, no. 3, pp. 220-227, 2006.

TH-2868_156302003

[62]. D. Liu, Y. Zhou, Y. Yang, L. Zhang, and F. Jin, "Characterization of high performance AlN nanoparticle-based transformer oil nanofluids," *IEEE Trans. Dielectr. Electr. Insul.*, vol. 23, no. 5, pp. 2757-2767, 2016.

[63]. T. V. Oommen, C. C. Claiborne, E. J. Walsh, and J. P. Baker, "A new vegetable oil based transformer fluid: development and verification," in *IEEE Conf. Electr. Insul. Dielectr. Phenomena (CEIDP)*, Victoria, BC, Canada, 2000, pp. 308-312.

[64]. V. A. Primo, B. Garcia, and R. Albarracin, "Improvement of transformer liquid insulation using nanodielectric fluids: A review," *IEEE Electr. Insul. Mag.*, vol. 34, no. 3, pp. 13-26, 2018.

[65]. W. Sima, J. Shi, Q. Yang, S. Huang, and X. Cao, "Effects of conductivity and permittivity of nanoparticle on transformer oil insulation performance: Experiment and theory," *IEEE Trans. Dielectr. Electr. Insul.*, vol. 22, no. 1, pp. 380–390, 2015.

[66]. Y. Lv, Y. Zhou, C. Li, Q. Wang, and B. Qi, "Recent progress in nanofluids based on transformer oil: Preparation and electrical insulation properties," *IEEE Electr. Insul. Mag.*, vol. 30, no. 5, pp. 23–32, 2014.

[67]. G. D. P. Mahidhar, R. Sarathi, N. Taylor, and H. Edin, "Dielectric properties of silica based synthetic ester nanofluid," *IEEE Trans. Dielectr. Electr. Insul.*, vol. 27, no. 5, pp. 1508-1515, 2020.

[68]. J. Li, R. Liao, and L. Yang, "Investigation of natural ester based liquid dielectrics and nanofluids," in *2012 Int. Conf. High Volt. Eng. Appl.*, Shanghai, China, 2012, pp. 16–21.

[69]. Y. Zhong, Y. Lv, C. Li, Y. Du, M. Chen, S. Zhang, Y. Zhou, and L. Chen, "Insulating properties and charge characteristics of natural ester fluid modified by TiO_2 semiconductive nanoparticles," *IEEE Trans. Dielectr. Electr.Insul.*, vol. 20, no. 1, pp. 135–140, 2013.

[70]. G. Dombek, Z. Nadolny, and P. Przybylek, "The study of thermal properties of mineral oil and synthetic ester modified by nanoparticles TiO_2 and C60," in *Int. Conf. High Volt. Eng. Appl. (ICHVE)*, Poznan, Poland, 2014.

[71]. B. Wang, J. Li, B. Du, and Z. Zhang, "Study on the stability and viscosity of Fe_3O_4 nano-particles vegetable insulating oils," in *Int'l. Conf. High Volt. Eng. Appl.*, 2012, pp. 307–310.

[72]. A. Raymon, S. Sakthibalan, C. Cinthal, R. Subramaniaraja, and M. Yuvaraj, "Enhancement and comparison of nano-ester insulating fluids," *IEEE Trans. Dielectr. Electr. Insul.*, vol. 23, no. 2, pp. 892–900, 2016.

[73]. M. G. Danikas, A. Bakandritsos, G. D. Peppas, V. P. Charalampakos, E. C. Pyrgioti, and I. F. Gonos, "Statistical investigation of AC breakdown voltage of nanofluids compared with mineral and natural ester oil," *IET Sci. Meas. Technol.*, vol. 10, no. 6, pp. 644–652, 2016.

TH-2868_156302003

[74]. C. Choi, H. S. Yoo, and J. M. Oh, "Preparation and heat transfer properties of nanoparticle-in-transformer oil dispersions as advanced energy-efficient coolants," *Current Applied Physics*, vol. 8, pp.710–712, 2007.

[75]. H. Jin, T. Andritsch, P. H. F. Morshuis, and J. J. Smit, "AC breakdown voltage and viscosity of mineral oil based SiO_2 nanofluids," in *Conference on Electrical Insulation and Dielectric Phenomena (CEIDP)*, Montreal, QC, Canada, 2012, pp. 902-905.

[76]. D-E A. Mansour, E. G. Atiyal, R. M. Khattab, and Ahmed M. Azmy1, "Effect of titania nanoparticles on the dielectric properties of transformer oil-based nanofluids," in *Conference on Electrical Insulation and Dielectric Phenomena (CEIDP)*, Montreal, QC, Canada, 2012, pp. 295-298.

[77]. M. Liu, M. C. Lin, and C. Wang, "Enhancements of thermal conductivities with Cu, CuO, and carbon nanotube nanofluids and application of MWNT/water nanofluid on a water chiller system," *Nanoscale Res. Lett.*, vol. 6, no. 1, pp. 1-13, 2011.

[78]. J-H. Lee, K. S. Hwang, S. P. Jang, B. H. Lee, J. H. Kim, S. U. S. Choi, and C. J. Choi, "Effective viscosities and thermal conductivities of aqueous nanofluids containing low volume concentrations of Al_2O_3 nanoparticles," *Int'l. J. of Heat and Mass Transfer*, vol. 51, pp. 2651–2656, 2008.

[79]. J. A. Eastman, S. U. S. Choi, L. J. Thompson, and S. Lee, "Enhanced thermal conductivity through the development of nanofluids," *Materials Research Society Sympos.*, Boston, MA, USA, 1996, pp. 3-11.

[80]. W. H. Lee, W. S. Lee, and J. C. Lee, "Influence of magnetic nanoparticles on the breakdown voltage of transformer oil," in *17th Int'l. Sympos. on High Volt. Eng. (ISH)*, Hannover, Germany, 2011.

[81]. J. G. Hwang, M. Zahn, F. M. O'Sullivan, L. A. A. Pettersson, O. Hjortstam, and R. Liu, "Effects of nanoparticle charging on streamer development in transformer oil-based nanofluids," *Journal of Appl. Phy.*, vol. 107, p. 014310, 2010.

[82]. M. Zahn, N. Lavesson, O. Widlund, and Borg, "Effects of impulse voltage polarity, peak amplitude, and rise time on streamers initiated from a needle electrode in transformer oil," *IEEE Trans. Plasma Sci.*, vol. 40, no 3, pp. 909 – 918, 2012.

[83]. Y. Z. Lv, X. Li, Y. F. Du, F. C. Wang, and R. Li, "Preparation and breakdown strength of TiO_2 fluids based on transformer oil," in *IEEE Conf. Electr. Insul. Dielectr. Phenomena*, West Lafayette, IN, 2010, pp. 1-3.

[84]. D. E. Mansour, E. G. Atiya, R. M. Khattab, and A. M. A. Azmy, "Effect of titania nanoparticles on the dielectric properties of transformer oil-based nanofluids," in *IEEE Conf. Electr. Insul. Dielectr. Phenomena*, Montreal, Canada, 2012, pp. 295-298.

[85]. Y. F. Du, Y. Z. Lv, F. C. Wang, and C. R. Li, "Effect of TiO_2 nanoparticles on the breakdown strength of transformer oil," in *IEEE Int'l. Sympos. on Electr. Insul.*, 2010, pp.1-3.

TH-2868_156302003

[86]. H. Jin, T. Andritsch, P. H. F. Morshuis, J.J. Smit, "AC breakdown voltage and viscosity of mineral oil based SiO_2 nanofluids," *IEEE Trans. Dielectr. Electr. Insul.*, vol. 978, pp. 1252-1255, 2012.

[87]. B. X. Du and X. L. Li, "High thermal conductivity transformer oil filled with BN nanoparticles," *IEEE Trans. Dielectr. Electr. Insul.*, vol. 22, no. 2, pp. 851-858, 2015.

[88]. Y. Lv, W. Wang, K. Ma, S. Zhang, Y. Zhou, C. Li, and Q. Wang, "Nanoparticle effect on dielectric breakdown strength of transformer oil-based nanofluids," in *IEEE Conf. Electr. Insul. Dielectr. Phenomena (CEIDP)*, Chenzhen, China, 2013, pp. 680-682.

[89]. S. Ponmania, J. K. M. Williama, R. Samuelb, R. Nagarajanc, and J. S. Sangwaia, "Formation and characterization of thermal and electrical properties of CuO and ZnO nanofluids in xanthan gum," *Colloids and Surfaces A: Physicochemical and Engineering Aspects*, vol. 443, no. 20 pp. 37–43, 2014.

[90]. J. N. Colleman, M. Lotya, O. A. Neill, S. D. Bergin, P. J. King, U. Khan, K. Young, A. Gaucher, and R. J. Smith, "Two-dimensional nanosheets produced by liquid exfoliation of layered materials," *Science*, vol. 331, no. 6017, pp. 568–571, 2011.

[91]. J. Taha-Tijerina, T. N. Narayanan, G. Gao, M. Rohde, D. A. Tsentalovich, M. Pasquali, and P. M. Ajayan, "Electrically insulating thermal nano-oils using 2D fillers," *ACS Nano*, vol. 6, no. 2, pp. 1214-1220, 2012.

[92]. A. Pakdel, C. Zhi, Y. Bando, T. Nakayama, and D. Golberg, "Boron nitride nanosheet coatings with controllable water repellency," *ACS Nano*, vol. 5, no. 8, pp. 6507–6515, 2011.

[93]. C. Zhi, Y. Xu, Y. Bando, and D. Golberg, "Boron nitride nanotube," *Mater. Sci. Eng. Res.*, vol.70, no. 3-6, pp. 92–111, 2010.

[94]. J. Yu, L. Qin, Y. Hao, S. Kuang, X. Bai, Y. Chong, W. Zhang, and E. Wang, "Vertically aligned boron nitride nanosheets: chemical vapor synthesis, ultraviolet light emission, and super hydrophobicity," *ACS Nano*, vol. 4, no. 1, pp. 414-422, 2010.

[95]. P. K. Sahoo and L.M. Das, "Combustion analysis of jatropha, karanja and polanga based biodiesel as fuel in a diesel engine," *Fuel*, vol. 88, pp. 994–999, 2009.

[96]. M. S. Rao and R. B. Anand, "Production characterization and working characteristics in DICI engine of Pongamia biodiesel," *Ecotox. Environ. Safe.*, vol. 121, pp. 16–21, 2015.

[97]. B. Baiju, M.K. Naik, and L.M. Das, "A comparative evaluation of compression ignition engine characteristics using methyl and ethyl esters of Karanja oil," *Rene. Ene.*, vol. 34, pp. 1616–1621, 2009.

TH-2868_156302003

[98]. M. Maharana, S. K. Nayak, and N. Sahoo, "Karanji oil as a potential dielectrics liquid for transformer," *IEEE Trans. Dielectr. Electr. Insul.*, vol. 25, no. 5, pp. 1871 - 1879, 2018.

[99]. M. Duval, "The Duval triangle for load tap changers, non-mineral oils and low temperature faults in transformers," *IEEE Electr. Insul. Mag.*, vol. 24, no. 6, pp. 22–29, 2008.

[100]. S. A. Khan, Md. D. Equbal, and T. Islam, "A comprehensive comparative study of DGA based transformer fault diagnosis using fuzzy logic and ANFIS models," *IEEE Trans. Dielectr. Electr. Insul.*, vol. 22, no. 1, pp. 590-596, Feb. 2015.

[101]. M. Duval, "A review of faults detectable by gas-in-oil analysis in transformer," *IEEE Electr. Insul. Mag.*, vol. 18, no. 3, pp. 8–17, Jun. 2002.

[102]. N. A. Gomez, R. Abonia, H. Cadavid, and I. H. Vargas, "Chemical and spectroscopic characterization of a vegetable oil used as dielectric coolant in distribution transformers," *J. Braz. Chem. Soc.*, vol. 22, no. 12, pp. 2292-2303, 2011.

[103]. M. Maharana, "Development of alternative dielectric fluid for power and distribution transformer," Ph.D dissertation, Indian Institute of Technology, Guwahati, Assam, India, Nov. 2018.

[104]. Y.-M. Wi, S.-K. Joo, and K.-B. Song, "Holiday load forecasting using fuzzy polynomial regression with weather feature selection and adjustment," *IEEE Trans. Power Sys.*, vol. 27, no. 2, pp. 596-603, May. 2012.

[105]. W. M. F. Al-Masri, M. F. Abdel-Hafez, and A. H. El-Hag, "Toward high accuracy estimation of partial discharge location," *IEEE Trans. Instrum. Meas.*, vol. 65, no. 9, pp. 2145–2153, Sep. 2016.

[106]. D. Mishra, A. Baral, N. Haque, and S. Chakravorti, "Condition assessment of power transformer insulation using short-duration time-domain dielectric spectroscopy measurement data," *IEEE Trans. Instrum. Meas.*, vol. 69, no. 7, pp. 4404–4411, Jul. 2020.

[107]. F. Chetibi, H. Moulai, and O. Idir, "Temporal and frequency-domain assessment of thermal and electrical ageing of mineral and vegetable oils," *IET Sci. Meas. Technol.*, vol. 13, no. 8, pp. 1139 – 1149, Oct. 2019.

[108]. S. Thakur. R. Sarathi, and M. G. Danikas, "Investigation on thermal ageing impact on dielectric properties of natural ester oil," *Electrical Engineering*, vol. 101, pp. 1007-1018, Oct. 2019.

[109]. T. K. Saha, P. Purkait, and F. Müller, "Deriving an equivalent circuit of transformers insulation for understanding the dielectric response measurements," *IEEE Trans. Power Del.*, vol. 20, no. 1, pp. 149–157, Jan. 2005.

TH-2868_156302003

[110]. W. Yao, J. Li, Z. Huang, X. Li, and C. Xiang, "Acids generated and influence on electrical lifetime of natural ester impregnated paper insulation," *IEEE Trans. Dielectr. Electr. Insul.*, vol. 25, no. 5, pp.1904-1914, 2018.

[111]. S. Wang, G. Zhang, J. Wei, S. Yang, and M. Dong, "Investigation on dielectric response characteristics of thermally aged insulating pressboard in vacuum and oil-impregnated ambient," *IEEE Trans. Dielectr. Electr. Insul.*, vol. 17, no. 6, pp.1853–1862, 2010.

[112]. S. Chatterjee, N. Haque, A. K. Pradhan, S. Dalai, and B. Chatterjee," Estimation of conductivity at reduced time for sensing moisture content of oil-paper insulation," *IEEE Sensors J.*, vol. 20, no. 21, pp. 12999-13006, 2020.

[113]. G. D. Peppas, V. P. Charalampakos, E. C. Pyrgioti, M. G. Danikas, A. Bakandritsos, and I. F. Gonos, "Statistical investigation of AC breakdown voltage of nanofluids compared with mineral and natural ester oil," *IET Sci. Meas. Technol.*, vol.10, no.6, pp.644–652, 2016.

[114]. M. K. Moraveji, F. Talebkeikhah, and M. Arjmanda, "On evaluation of thermophysical properties of transformer oil-based nanofluids: A comprehensive modeling and experimental study," *J. Mol. Liquids*, vol. 300 (112249), pp. 1-17, 2020.

[115]. J. Liu, L. Zhou, G. Wu, Y. Zhao, P. Liu, and Q. Peng, "Dielectric frequency response of oilpaper composite insulation modified by nanoparticles," *IEEE Trans. Dielectr. Electr. Insul.*, vol.19, no.2, pp.510–520, 2012.

[116]. H. Ma, T. K. Saha, and C. Ekanayake, "Machine learning techniques for power transformer insulation diagnosis," in *AUPEC 2011*, Brisbane, 2011, pp. 1–6.

[117]. A. Betie, F. Meghnefi, I. Fofana, Z. Yeo, and H. Ezzaidi, "Neural network approach to separate aging and moisture from the dielectric response of oil impregnated paper insulation," *IEEE Trans. Dielectr. Electr. Insul.*, vol.22, no.4, pp.2176–2184, 2015.

[118]. D. Wang, L. Zhou, C. Dai, L. Guo, and W. Liao, "Insulation defect diagnostic method for OIP bushing based on multiclass LS-SVM and Cuckoo Search," *IEEE Trans. Instrum. Meas.*, vol. 69, no. 1, pp.163–172, 2019.

[119]. H. Yao, H. Mu, N. Ding, D. Zhang, Z. Liang, J. Tian, and G. Zhang, "Evaluation method for moisture content of oil-paper insulation based on segmented frequency domain spectroscopy: from curve fitting to machine learning," *IET Sci. Meas. Technol.*, vol. 15, no. 6, pp. 517-526, 2021.

[120]. M. Maharana, M. Bordeori, S. K. Nayak, and N. Sahoo, "Nanofluid based transformer oil: effect of aging on thermal, electrical and physio-chemical properties," *IET Sci. Meas. Technol.*, vol. 12, no. 7, pp. 878–885, 2018.

[121]. E. Tuncer, Y. V. Serdyuk, and S. M. Gubanski, "Dielectric mixtures: electrical properties and modeling," *IEEE Trans. Electr. Insul.*, vol. 9, no. 5, pp. 809– 828, 2002.

TH-2868_156302003

[122]. K. Kondo, T. Chiba, S. Ando, S. Yoshida, Y. Shimada, T. Nakamura, N. Matsushita, and M. Abe, "Cole-Cole impedance analysis on spin sprayed Ni-Zn-Co ferrite films exhibiting strong magnetic loss in gigahertz range," *IEEE Trans. Magnetics*, vol. 39, no. 5, pp. 3130–3132, 2003.

[123]. S. Martin, M. Valcav, T. Pavel, B. Jiri, P. Josef, and M. Petr, "Cole-Cole diagram as diagnostic tool for dielectric liquids," *in 2011 IEEE International Conference on Dielectric Liquids*, Trondheim, Norway, 2011.

[124]. A. N. Asokan, A. P. Anagha, P. Preetha, and K. Sunitha, "Effect of interphase on dielectric relaxation mechanisms in epoxy-alumina nanocomposite," *IEEE Trans. Dielectr. Electr. Insul.*, vol. 26, no. 4, pp. 1211–1219, 2019.

[125]. B. S. H. M. S. Y. Matharage, M. A. R. M. Fernando, M. A. A. P. Bandara, G. A. Jayantha, and C. S. Kalpage, "Performance of coconut oil as an alternative transformer liquid insulation," *IEEE Trans. Dielectr. Electr. Insul.*, vol. 20, no. 3, pp. 887-898, 2013.

[126]. T. K. Saha and P. Purkait, "Effects of temperature on time-domain dielectric diagnostics of transformers," in *Proc. of the 2003 Australasian Universities Power Engineering Conf. (AUPEC)*, Christchurch, New Zealand, 2003.

[127]. J. Miao, M. Dong, M. Ren, X. Wu, L. Shen, and H. Wang, "Effect of nanoparticle polarization on relative permittivity of transformer oil-based nanofluids," *J. Curr. Appl. Phys*., vol. 113, pp. 204103 (1-5), 2013.

[128]. A. K. Pradhan, C. Koley, B. Chatterjee, and S. Chakravorti, "Determination of optimized slope of triangular excitation for condition assessment of oil-paper insulation by frequency domain spectroscopy," *IEEE Trans. Dielectr. Electr. Insul.*, vol. 23, no. 3, pp. 1303–1312, 2016.

[129]. B. Chakraborty, K. Y. Raj, A. K. Pradhan, B. Chatterjee, S. Chakravorti, and S. Dalai, "Investigation of dielectric properties of TiO_2 and Al_2O_3 nanofluids by frequency domain spectroscopy at different temperatures," *J. of Molecular Liquids*, vol. 330, 115642, 2021.

[130]. P. Sun, W. Sima, X. Jiang, D. Zhang, J. He, and Q. Chen, "Failure of nano-modified oil impregnated paper under repeated impulse voltage: effects of TiO_2 nanoparticles on space charge characteristics," *IEEE Trans. Dielectr. Electr. Insul.*, vol. 25, no. 6, 2103–2111, 2018.

[131]. L. Jäntschi and S. D. Bolboacă, "Computation of probability associated with Anderson–Darling statistic," *Mathematics*, vol. 6, no. 8, 2018.

[132]. V. H. Masarakall, C. D. Sikdar, S. B. Madalageri, M. R. Nitture, J. C. Naidu, "Development of new dielectric liquid from pongamia oil as alternative for transformer oil," *Int'l. J. Tech. Res. and Appl.*, vol. 3, pp. 304-309, 2015.

TH-2868_156302003

[133]. S. N. Bobade and V. B. Khyade, "Detail study on the properties of pongamia pinnata (Karanja) for the production of biofuel," *Res. J. Chem. Sc.*, vol. 2, no. 7, pp. 16-20, 2012.

[134]. M. N. Nabi, S. M. N. Hoque, M. S. Akhter, "Karanja (pongamia pinnata) biodiesel production in Bangladesh, characterization of karanja biodiesel and its effect on diesel emissions," *Fuel Proces. Technol.*, vol. 90, pp. 1080–1086, 2009.

[135]. I. A. Musa, "The effects of alcohol to oil molar ratios and the type of alcohol on biodiesel production using transesterification process," *Egyptian J. Petroleum*, vol. 25, pp. 21-31, 2016.

[136]. Y. Bertrand, L. C. Hoang, "Vegetable oils as substitute for mineral insulating oils in medium-voltage equipments," in *CIGRE Session*, 2004, pp.1-6.

[137]. Y. Lv, C. Li, Q. Sun, M. Huang, C. Li, and B. Qi, "Effect of dispersion method on stability and dielectric strength of transformer oil-based TiO_2 nanofluids," *Nanoscale Res. Lett.*, vol. 11, pp. 1-6, 2016.

[138]. D. H. Kumar, H. E. Patel, V. R. Kumar, T. Sundararajan, T. Pradeep, and S. K. Das, "Model for heat conduction in nanofluids," *Phys. Rev. Lett.*, vol. 93, no. 14, pp. 144301 (1-4), 2014.

[139]. R. K. Shukla and V. K. Dhir, "Effect of brownian motion on thermal conductivity of nanofluids," *J. Heat Transf.*, vol. 130, pp. 1-13, 2008.

[140]. P. Keblinski, S. R. Phillpot, S. U. S. Choi, J. A. Eastman, "Mechanisms of heat flow in suspensions of nano-sized particles (nanofluids)," *Int'l. J. Heat Mass Transf.*, vol. 45, no. 4, pp. 855-863, 2002.

[141]. L. Dong and D. Johnson, "Surface tension of charge-stabilized colloidal suspensions at the water-air interface," *Langmuir*, vol. 19, pp. 10205-10209, 2003.

[142]. N. Li, G. Mao, X. Shi, S. Tian, and Y. Liu, "Advances in the research of polymeric pour point depressant for waxy crude oil," *J. Disp. Science and Tech.*, vol. 38, pp. 1-7, 2017.

[143]. IEEE 60567, "Oil-filled electrical equipment – Sampling of gases and of oil for analysis of free and dissolved gases – Guidance", 2011.

[144]. IEEE 60599, "Mineral oil-filled electrical equipment in service - Guidance on the interpretation of dissolved and free gases analysis", 2015.

[145]. IEEE C57.104, "IEEE Guide for the Interpretation of Gases Generated in Mineral Oil-Immersed Transformers", 2019.

[146]. IEEE C57.155, "IEEE Guide for Interpretation of Gases Generated in Natural Ester and Synthetic Ester-Immersed Transformers", 2014.

TH-2868_156302003

[147]. IEEE C57.147, "IEEE Guide for Acceptance and Maintenance of Natural Ester Insulating Liquid in Transformers", 2018.

[148]. ASTM D3612, "Standard Test Method for Analysis of Gases Dissolved in Electrical Insulating Oil by Gas Chromatography", 2017.

[149]. ASTM D1934, "Standard Test Method for Oxidative Aging of Electrical Insulating Liquids by Open-Beaker Method", 2020.

[150]. IEC 60156, "Insulating liquids - Determination of the breakdown voltage at power frequency - Test method", 2018.

[151]. ASTM D6871, "Standard Specification for Natural (Vegetable Oil) Ester Fluids Used in Electrical Apparatus", 2017.

[152]. ASTM D5555, "Standard Test Method for Determination of Free Fatty Acids Contained in Animal, Marine, and Vegetable Fats and Oils Used in Fat Liquors and Stuffing Compounds", 2017.

TH-2868_156302003

TH-2868_156302003

List of Publications

Patent

1. M. M. Bordeori, M. Maharana, **N. Baruah**, S. K. Nayak, N. Sahoo, "Design and development of an automated open beaker oxidative ageing assessment apparatus," Indian patent – Application No. 201731047043 A, Date of publication: 05/01/2018, Filing date: 28/12/2017 (Examiner's report submitted).

Book Chapter

1. **N. Baruah**, R. Sangineni, M. Maharana, S. K. Nayak, "Processing and evaluation of natural esters," in *Alternative Liquid Dielectrics for High Voltage Transformer Insulation Systems: Performance Analysis and Applications*, IEEE Wiley, 2022.

Journals publications

1. **N. Baruah,** S. K. Nayak, S. K. Pratihar, "Quantitative Effect of Ageing Duration on Dielectric Parameters based on Frequency Response," *IEEE Transactions on Instrumentation & Measurement*, 2021, DOI: 10.1109/TIM.2021.3127306.

2. **N. Baruah**, S. S. Dey, S. K. Nayak, "Evaluation of dissolved gas analysis and long-term performance of non-edible natural ester," *IEEE Trans. Dielectr. Electr. Insul.*, vol. 27, no. 5, pp. 1561-1569, 2020.

3. **N. Baruah**, M. Maharana, S. K. Nayak, "Performance analysis of vegetable oil based nanofluids used in transformers," *IET Sci. Meas. Technol.*, vol. 13, No. 7, pp. 995-1002, 2019.

4. **N. Baruah**, R. Sangineni, M. Chakraborty, S. K. Nayak, "Investigation of natural ester based insulating liquid using statistical hypothesis testing," *IEEJ Trans. on Fundamentals and Materials*, vol. 121, no. 10, 2021.

5. M. Maharana, **N. Baruah**, S. K. Nayak, N. Sahoo, "Effect of oxidative ageing on the thermophysical and electrical properties of the nanofluid with statistical analysis of AC breakdown voltage," *IET Science, Measurement & Technology*, vol. 12, no. 8, pp. 1074-1081, 11 2018.

6. M. Maharana, **N. Baruah**, S. K. Nayak, N. Meher, P. K. Iyer, "Condition assessment of aged ester based nanofluid through physicochemical and spectroscopic measurement," *IEEE Trans. Instrum. Meas.*, vol. 68, No. 12, pp. 4853-4863, 2019.

TH-2868_156302003

7. R. Sangineni, **N. Baruah**, S. K. Nayak, "Analysis of electric field in liquid dielectric on addition of nanoparticles," *Materials Today: Proceedings*, vol.43, no.6, pp. 3603-3609, 2021.

Conferences publications

1. **N. Baruah**, R. Sangineni, C. Saha, D. Kanumuri, M. Chakraborty, S. K. Nayak, "Supervised machine learning model for predictive analysis of dielectric response of insulating liquids," in *IEEE Conference on Electrical Insulation and Dielectric Phenomena (CEIDP)*, 12-15 December, (2021), Vancouver, Canada.

2. **N. Baruah**, R. Sangineni, M. Chakraborty, S. K. Nayak, "Estimation of dielectric parameters of aged natural ester based insulating liquid using open beaker oxidative ageing technique," *12th International Conference on Electrical and Electromechanical Energy Conversion – ECCE Asia (Energy Conversion Congress and Exposition – Asia, 2021)*, online from 24th-27th May, (2021), Singapore.

3. **N. Baruah**, R. Sangineni, M. Chakraborty, S. K. Nayak, "Data driven analysis of aged insulating oils by UV-Vis spectroscopy and principal component analysis (PCA)," *IEEE Conference on Electrical Insulation and Dielectric Phenomena (CEIDP)*, 18-30 October, (2020), East Rutherford, New Jersey, USA.

4. **N. Baruah**, R. Sangineni, M. Chakraborty, S. K. Nayak, "Statistical analysis of natural ester based insulating liquid using hypothesis testing," *9th IEEE International Symposium on Electrical Insulating Materials (ISEIM)*, 13-17 September, (2020), Tokyo, Japan.

5. **N. Baruah**, M. Maharana, S. S. Dey, S. K. Nayak, "Behavioural assessment of aged natural ester based nanofluid using statistical technique," in *IEEE Conference on Electrical Insulation and Dielectric Phenomena (CEIDP)*, 20-23 October, (2019), Richland, Washington, USA.

6. **N. Baruah**, M. Maharana, S. S. Dey, S. K. Nayak, "Nanoparticle polarization effect on the permittivity of the dielectric liquid," in *20th IEEE International Conference on Dielectric Liquids (ICDL)*, 23-27 June, (2019), Rome, Italy.

7. **N. Baruah**, M. Maharana, S. S. Dey, S. K. Nayak, "Enhancement of heat transfer property in insulating fluids using nanoparticles," in *8th IEEE Power India International Conference (PIICON)*, 10-12 December, (2018), Kurukshetra, India.

8. **N. Baruah**, M. Maharana, S. K. Nayak, "Investigation of the electric field variation on surface of nanoparticle added to transformer oil," in *10th IEEE PES Asia-Pacific Power and Energy Engineering Conference 2018 (APPEEC)*, 7-10 October, (2018), Sabah, Malaysia.

TH-2868_156302003

9. **N. Baruah**, M. Maharana, S. K. Nayak, "An electrode model to ascertain the effects of voltage and tip radius with gap distance on electric field of transformer oil," in *2nd IEEE International Conference on Energy, Power and Environment 2018 (ICEPE 2018),* 1-2 June, (2018), Shillong, Meghalaya, India.

10. R. Sangineni, D. Kanumuri, **N. Baruah**, S. K. Nayak, "Non Isothermal Thermo Gravimetric Analysis (TGA) Measurements of Oxidative Aged Solid Insulation," in *IEEE 5th International Conference on Condition Assessment Techniques in Electrical Systems (CATCON),* December, (2021), India.

11. R. Sangineni, **N. Baruah**, S. K. Nayak, "Influence of Concentration of Nanoparticles on the Dielectric Frequency Response of an Insulating Nanofluid," in *IEEE Conference on Electrical Insulation and Dielectric Phenomena (CEIDP),* 12-15 December, (2021), Vancouver, Canada.

12. C. Saha, **N. Baruah**, S. K. Nayak, "Implementation of Self-Organizing Map and Logistic Regression in Dissolved Gas Analysis of Transformer oils," in *2021 IEEE International Conference on the Properties and Applications of Dielectric Materials (ICPADM),* 12-14 July, (2021), Malaysia.

13. M. Chakraborty, **N. Baruah**, S. K. Nayak, P. K. Maiti, "Correlating UV Visible Spectral Response and Thermal Ageing of Blended Transformer Oil," in *2021 IEEE International Conference on the Properties and Applications of Dielectric Materials (ICPADM),* 12-14 July, (2021), Malaysia.

14. S. S. Dey, R. Sangineni, **N. Baruah**, S. K. Nayak, "Study of Heat Transfer Property of the Transformer Oils on Addition of CuO Nanoparticles," in *2021 IEEE International Conference on the Properties and Applications of Dielectric Materials (ICPADM),* 12-14 July, (2021), Malaysia.

15. D. Kanumuri, R. Sangineni, **N. Baruah**, S. K. Nayak, "Study of magnetic properties of mineral oil based nanofluids," in *2021 IEEE International Conference on the Properties and Applications of Dielectric Materials (ICPADM),* 12-14 July, (2021), Malaysia.

16. R. Sangineni, **N. Baruah**, D. Kanumuri, S. K. Nayak, "Comparison of magnetic nature of vegetable oil based nanofluids," in *39th Electrical Insulation Conference (EIC),* online from 7-20 June, (2021), USA.

17. R. Sangineni, **N. Baruah**, M. Chakraborty, S. K. Nayak, "Effect of magnetic properties of liquid dielectric on the leakage flux of power transformer," in *IEEE Conference on Electrical Insulation and Dielectric Phenomena (CEIDP),* 18-30 October, (2020), East Rutherford, New Jersey, USA.

TH-2868_156302003

18. M. Chakraborty, **N. Baruah**, R. Sangineni, S. K. Nayak, "Dissolve gas analysis (DGA) of thermally aged blended transformer oil," in *IEEE Conference on Electrical Insulation and Dielectric Phenomena (CEIDP)*, 18-30 October, (2020), East Rutherford, New Jersey, USA.

19. M. Maharana, **N. Baruah**, S. K. Nayak, K. Wu, "Insulation monitoring of oxidative aged nonedible ester based dielectric fluid by suitable dissolved gas analysis," in *IEEE Conference on Electrical Insulation and Dielectric Phenomena (CEIDP)*, 20-23 October, (2019), Richland, Washington, USA.

20. M. Maharana, **N. Baruah**, S. K. Nayak, N. Sahoo, M. Chakraborty, "Investigation of AC breakdown strength and frequency varied dielectric response of the non-conventional vegetable oil," in *IEEE International Conference on Dielectric Liquids (ICDL)*, 23-27 June, (2019), Rome, Italy.

21. S. S. Dey, R. Sangineni, **N. Baruah**, M. Maharana, S. K. Nayak, "Investigation of thermal conductivity of semiconducting nanofluid for transformer," in *IEEE Conference on Electrical Insulation and Dielectric Phenomena (CEIDP)*, 20-23 October, (2019), Richland, Washington, USA.

22. M. Maharana, **N. Baruah**, S. K. Nayak, N. Sahoo, "Electro-mechanical and chemical strength analysis of thermally aged nanofluid impregnated kraft paper," in *IEEE Conference on Electrical Insulation and Dielectric Phenomenon (CEIDP)*, Cancun, Oct. 21-24, (2018), Mexico, USA.

23. M. Maharana, **N. Baruah**, S. K. Nayak, N. Sahoo, "Nanofluid and transformer oil impregnated aged kraft paper: analysis of its mechanical strength," in *10^{th} IEEE PES Asia-Pacific Power and Energy Engineering Conference 2018 (APPEEC)*, October 7-10, (2018), Sabah, Malaysia.

24. M. Maharana, **N. Baruah**, S. K. Nayak, N. Sahoo, "Thermoelectrically enhanced nanofluid is a suitable replacement for transformer oil," in *36^{th} IEEE Electrical Insulation Conference (EIC)*, 11-14 June, (2018), San Antonio, Texas, USA, ID 247.

25. M. Maharana, **N. Baruah**, S. K. Nayak, N. Sahoo, "Comparative study of mechanical and electrical strength of kraft paper in nanofluid based transformer oil and mineral oil," in *8^{th} IEEE International Symposium on Electrical Insulating Materials (ISEIM)*, 12-15 September, (2017), Toyohashi, Japan.

TH-2868_156302003

Awards and Grants

1. Recipient of the Young Presenter award for presentation at the 9th IEEE International Symposium on Electrical Insulating Materials (ISEIM) held online from 13th-17th September 2020, Tokyo, Japan.

2. Recipient of the DST International Travel Grant to attend and present at the IEEE Conference on Electrical Insulation and Dielectric Phenomena (CEIDP) held from 20th-23rd October, (2019), Richland, Washington, USA. Department of Science and Technology, India. 2019.

3. Recipient of the Student travel grant from IEEE PES to attend the 10th IEEE PES Asia-Pacific Power and Energy Engineering Conference 2018 (APPEEC) held at Sabah, Malaysia from 7th-10th October, 2018.

TH-2868_156302003

TH-2868_156302003